CHAPTER 8
Brain Imaging

Patrick D. Barnes

The central nervous system (CNS) consists of the skull, brain, spine, and spinal cord. The head and neck region contains the face, eye and orbit, nasal cavity and paranasal sinuses, ear and temporal bone, oral cavity, jaw, and neck. Modalities used for the imaging of the pediatric CNS and head and neck region include plain film/computerized radiography (PF/CR), ultrasonography (US), computed tomography (CT), magnetic resonance imaging (MRI), radionuclide imaging (RI), catheter angiography, and myelography. Imaging modalities may be classified as structural or functional. Structural imaging modalities provide spatial resolution primarily on the basis of anatomic or morphologic data (e.g., CT). Functional imaging modalities (including molecular imaging) provide spatial resolution on the basis of physiologic, metabolic, or biologic data or markers (e.g., positron emission tomography [PET]). Some modalities may actually be regarded as providing both structural and functional information (e.g., MRI, PET-CT). The technical and procedural descriptions of angiography, myelography, and other invasive and interventional modalities are detailed in other texts. In this presentation, guidelines for their utilization are presented by region and modality.

BRAIN IMAGING GUIDELINES

Skull Plain Films and Computerized Radiography

Skull PF/CR is most often obtained for trauma (e.g., fracture) or craniofacial anomalies (e.g., craniosynostosis), or to evaluate a lump or bump. It may also clarify cranial findings suggested by CT or MRI. PF and CR are x-ray–based techniques that are being increasingly displaced, or replaced, by the other modalities, especially CT; they are best used in a limited and selective manner to minimize radiation exposure.

Ultrasonography

US is readily accessible, portable, fast, and multiplanar, and provides real-time images. It is less expensive than other cross-sectional imaging modalities and relatively noninvasive (nonionizing radiation). It requires no contrast agent and infrequently needs patient sedation. The resolving power of US is based on variations in acoustic reflectance of tissues. Its diagnostic effectiveness, however, depends primarily on the skill and experience of the operator and interpreter. Also, US requires a window or path unimpeded by bone or air.

Probably the most important uses of US are (1) fetal and neonatal screening; (2) screening of the infant who cannot be examined in the radiology department (e.g., because of prematurity [neonate], use of extracorporeal membrane oxygenation [ECMO], or need for intraoperative imaging); (3) when important adjunctive information is quickly needed (e.g., cystic versus solid, vascularity, vascular flow, or increased intracranial pressure); and (4) for real-time guidance and monitoring of invasive diagnostic or therapeutic surgical and interventional procedures. Brain US is principally used as a screening procedure to evaluate and follow up on premature infants with intracranial hemorrhage or periventricular leukomalacia. Other common indications are screening for the sequelae of hypoxia-ischemia in the term infant and searching for hemorrhage or infarction in infants undergoing ECMO. Doppler US is often used to specifically evaluate intracranial arterial and venous abnormalities in these infants. Any lesion (particularly a cystic one) identified by US should be evaluated by Doppler US to determine its vascularity (e.g., galenic vascular malformation). Although intracerebral mass lesions (cystic or solid) may be detected by real-time US, CT or MRI is often necessary to characterize and determine the extent of disease.

Computed Tomography

Although it uses ionizing radiation, current-generation CT effectively collimates and restricts the exposure to the immediate volume of interest. This applies to the more advanced multidetector/multislice CT (MDCT) technology, which provides ultrafast, high-resolution imaging with direct acquisition in the axial plane and retrospective isotropic multiplanar reformatted or three-dimensional (3D) reconstructions using a variety of soft tissue, bone, vascular, and other high-resolution spatial or temporal algorithms. MDCT is now the preferred method for CT imaging of the pediatric CNS and head and neck region. In fact, MDCT is becoming the standard for the emergency evaluation of trauma. The reasons are its speed and its obviation of the necessity for, and potential risk of, repositioning for direct coronal imaging. As a result, the need for sedation or anesthesia has been dramatically reduced. Also, as previously mentioned, MDCT employs algorithms that are specific to patient age, size, and region in order to minimize radiation exposure. Projection scout images in the frontal or lateral plane are used to plan image acquisition and may provide information similar to that provided by PF/CR but with less spatial resolution. CT requires sedation in infants and young children more often than US but less often than MRI. CT occasionally needs intravenous (IV) contrast enhancement, and sometimes opacification of the cerebrospinal fluid (CSF) with contrast material.

High-resolution bone and soft tissue algorithms are important for demonstrating fine anatomy (e.g., skull base). The bone algorithm is also important for delineating the sutures as an indicator of normal versus deficient brain growth, increased intracranial pressure, and dysplastic versus metabolic bone conditions. Advances in computer display technology include image fusion (e.g., MRI/single-photon emission CT [SPECT], CT/PET), two-dimensional reformatting, 3D volumetric and reconstruction methods, segmentation, and surface rendering techniques. These high-resolution display techniques are used for CT angiography (CTA) and venography (CTV) and in the planning and image guidance of stereotactic neurosurgery and head and neck surgery, radiotherapy, radiosurgery, craniofacial reconstructive surgery; to aid in the surgical stabilization of craniocervical anomalies and scoliosis; and to provide real-time or stereotactic image guidance for interventional and neurosurgical procedures. The surface 3D reconstructions can also assist in differentiating accessory sutures and fissures from fractures.

Contraindications to CT in childhood are unusual, particularly with the proper application of radiation protection, dose reduction, and dosage monitoring in compliance with the "as low as reasonably achievable" (ALARA) principle, the appropriate use of non-ionic contrast agents, the proper administration of sedation or anesthesia, and the use of vital monitoring and support technology when indicated.

The role of CT has been redefined in the context of accessible and reliable US and MRI. US is the procedure of choice for primary imaging or screening of the brain, neck, and spinal neuraxis in the fetus, neonate, and young infant. When US does

not satisfy the clinical inquiry or an acoustic window is not available, CT becomes the primary postnatal modality for brain imaging in children, especially in acute or emergency presentations. Its use is especially important for acute trauma, acute neurologic deficit, encephalopathy, increased intracranial pressure, macrocephaly, headache, unexplained or complicated acute episodic disorder (e.g., seizure, apnea), visual symptoms or signs, suspected CNS infection, shunted hydrocephalus with suspected shunt malfunction, and suspected postoperative complication. In these situations, CT is used primarily to screen for acute or subacute hemorrhage, edema, herniation, fractures, hypoxic-ischemic injury, focal infarction, hydrocephalus, tumor mass, or abnormal collection (e.g., pneumocephalus, abscess, empyema). It may be particularly important to rule out an intracranial mass or collection as a potential source for herniation in a child who must undergo lumbar puncture for diagnostic collection of CSF (e.g., in suspected infection). Another primary indication for CT is the evaluation of bony or airspace abnormalities of the head and neck region, including the skull base, cranial vault, orbit, paranasal sinuses, facial bones, and the temporal bone, especially for trauma and infection (see later). Additionally, CT is the definitive procedure for detection and confirmation of calcification. Secondary indications for CT are often primary indications for MRI (see later); although preferred to CT, MRI is sometimes not readily available or feasible. In these situations, CT is clearly less desirable than MRI.

When CT is used, IV enhancement for blood pool effect (e.g., CTA), blood-brain barrier disruption, or abnormal vascular permeability is additionally recommended for the evaluation of suspected or known vascular malformation, infarction, neoplasm, abscess, or empyema. Enhanced CT may help evaluate a mass or hemorrhage of unknown etiology and identify the membrane of a chronic subdural collection. By identifying the cortical veins, enhanced CT may distinguish prominent low-density subarachnoid collections (benign extracerebral collections or benign external hydrocephalus of infancy) from low-density subdural collections (e.g., chronic subdural hematomas or hygromas). It also may help differentiate infarction from neoplasm or abscess, serve as an indicator of disease activity, for example, in degenerative or inflammatory disease and vasculitis, or provide a high-yield guide for stereotactic or open biopsy (e.g., tumor core). Ventricular or subarachnoid CSF contrast opacification may further assist in evaluating or confirming CSF compartment lesions or communication (e.g., arachnoid cyst, ventricular encystment, CSF leak) or may be used for myelographic evaluation in patients unable to undergo MRI or in whom diagnostic-quality MRI cannot be obtained (e.g., because of an electronic implant or metallic instrumentation). As a rule, and with the possible exception of suppurative infection, MRI is the preferred alternative to CT using IV or CSF contrast administration in the circumstances just enumerated.

CTA and CTV provide vascular spatial and temporal resolution equal or superior to that of MRI; the contrast agent may be administered by rapid hand injection in infants or by power injection in older children. Such dynamic techniques are particularly expedient in the evaluation of acute traumatic vascular injuries (e.g., carotid dissection or transection), hemorrhage due to vascular anomalies (e.g., aneurysm, vascular malformation), for acute vascular occlusive disease (e.g., carotid or vertebrobasilar occlusion, dural sinus or venous thrombosis), including CT perfusion imaging, and for vascular mapping for surgical or radiotherapy planning (e.g., arteriovenous malformation [AVM]).

Radionuclide Imaging

PET has the unique ability to provide specific metabolic tracers (e.g., oxygen utilization and glucose metabolism). The wider availability and relative simplicity of SPECT allows more practical functional assessment of the pediatric CNS. Clinical and investigative applications of SPECT and PET at this time include the assessment of brain development and maturation, focus localization in refractory childhood epilepsy, assessment of tumor progression versus treatment effects in childhood CNS neoplasia, the evaluation of occlusive cerebrovascular disease for surgical revascularization (e.g., moyamoya disease), the diagnosis of brain death, the use of brain activation techniques in the elucidation of childhood cognitive disorders, and the assessment of CSF kinetics (e.g., in hydrocephalus, CSF leaks).

Magnetic Resonance Imaging

MRI is one of the less invasive or relatively noninvasive imaging technologies. Furthermore, the MRI signal is exponentially derived from multiple parameters. MRI also employs many more basic imaging techniques than other modalities. Advancing MRI capabilities have further improved its sensitivity, specificity, and efficiency. They include the fluid attenuation inversion recovery (FLAIR) technique, fat-suppression short T1 inversion recovery (STIR) imaging, gradient recalled echo (GRE) sequence, magnetization transfer imaging (MTI), and vascular gadolinium enhancement for increased structural resolution. IV gadolinium is administered to provide enhancement for blood pool effects, blood-brain barrier disruption, and abnormal vascular permeability. It is recommended for the evaluation of suspected or known vascular malformation, infarction, neoplasm, abscess, or empyema. Fast and ultrafast MRI techniques (fast spin echo, fast gradient echo, echo planar imaging [EPI]) have also been developed to reduce imaging times, improve structural resolution, and provide functional resolution. Important applications include MR vascular imaging (MR angiography [MRA] and MR venography [MRV]) and perfusion MRI (PMRI), diffusion-weighted and diffusion tensor MRI (DWI and DTI), CSF flow and brain/cord motion imaging, brain activation techniques (functional MRI [fMRI]), and MR spectroscopy (MRS). Fast and ultrafast imaging techniques are also being used for fetal imaging, morphometrics, treatment planning, and "real-time" MRI-guided surgical and interventional procedures.

The role of MRI in imaging of the pediatric CNS and head and neck region is defined by its superior sensitivity and specificity in a number of areas in comparison with US and CT. MRI has also redefined the roles of invasive procedures like myelography, ventriculography, cisternography, and angiography. MRI provides multiplanar imaging with equivalent resolution in all planes without repositioning of the patient. Bone does not interfere with soft tissue resolution, although metallic objects often produce signal void or field distortion artifacts. Some ferromagnetic or electronic devices (e.g., pacemakers) pose a hazard, and MRI is usually contraindicated in the presence of such devices. MRI is not as fast as US or CT, and sedation or anesthesia is required in most infants and younger children, because image quality is easily compromised by motion. MRI may not be as readily accessible to the pediatric patient as US or CT, particularly in emergencies or for intensive care cases, although magnet-compatible vital monitoring and support technology are now widely available for these patients.

The FLAIR sequence attenuates the signal from flowing water (i.e., CSF) and increases the conspicuity of nonfluid water-containing lesions lying in close approximation to the CSF-filled subarachnoid and ventricular spaces. The STIR technique suppresses fat signal to provide improved conspicuity of water-containing lesions in regions where fat dominates (e.g., orbit, head and neck, spine). The GRE sequence is used to enhance magnetic susceptibility (T2*) effects to detect iron, calcium, or hemorrhage. The MTI method suppresses background tissues and increases conspicuity for vascular flow enhancement (e.g., MRA) and gadolinium enhancement (e.g., tumor seeding). Diffusion MRI (DWI/DTI), as provided by EPI or line-scan spin echo imaging techniques, generates images based on differences in the rate of diffusion of water molecules and is especially sensitive to intracellular changes. This is particularly true for primary or secondary derangements of cellular energy metabolism. The classic examples

are hypoxia and ischemia; other examples are hypoglycemia, other metabolic disorders (e.g., mitochondrial), viral encephalitis, and status epilepticus. The rate of diffusion, or apparent diffusion coefficient (ADC), is higher for free or pure water (e.g., CSF) than for macromolecular bound water (e.g., gray matter and white matter). Fractional anisotropy, as provided by DTI, addresses the differences in directionality of ADC (e.g., along white matter fiber tracts). The ADC and fractional anisotropy vary according to the microstructural or physiologic state of a tissue, including the level of maturation. Current clinical applications include the assessment of brain maturation, the evaluation of ischemia, and the characterization of tumors. A particularly important application of DWI is in the early detection of diffuse and focal ischemic injury. The ADC of water is reduced within minutes of an ischemic insult and is progressive within the first hour. High intensity is demonstrated on DWI (low intensity on ADC maps) at a time when conventional MRI findings are negative and likely reflects cytotoxic edema. Further investigation is under way regarding the roles of DWI, PMRI, and MRS in the early diagnosis and treatment of potentially reversible ischemic injury. An emerging application of DTI is the assessment of microstructural injury in the neonate as a predictor of neurodevelopmental outcome. Such early indicators may become the basis for interventional trials that may improve outcomes (e.g., in at-risk premature infants). The line-scan technique may be a more useful method for imaging of the spine and spinal cord.

PMRI is currently being used to evaluate cerebral perfusion dynamics through the application of a dynamic gadolinium-enhanced T2*-weighted MRI technique. This new technique is undergoing further development to qualitate and quantitate normal and abnormal cerebrovascular dynamics of the developing brain by analyzing hemodynamic parameters, including relative cerebral blood volume, relative cerebral blood flow, and mean transit time, all as complementary to conventional MRI, MRA, and gadolinium-enhanced MRA. Current applications of this and noncontrast-enhanced methods of PMRI—for example, arterial spin labeling (ASL), flow-sensitive alternating inversion recovery (FAIR), and blood oxygen level–dependent (BOLD)—include the evaluation of ischemic cerebrovascular disease (e.g., hypoxia-ischemia, moyamoya, sickle cell disease), the differentiation of tumor progression from treatment effects, and fMRI. One of the most active areas of research is fMRI for the localization of brain activity. *Functional MRI* is the term often applied to brain activation imaging in which local or regional changes in cerebral blood flow are displayed that accompany stimulation or activation of sensory (e.g., visual, auditory), motor, or cognitive centers. fMRI is providing important information about cognitive and behavioral disorders. Also, it may serve as a guide for safer and more effective tumor resection, AVM resection, and seizure ablation.

MR spectroscopy offers a noninvasive in vivo approach to biochemical analysis. Furthermore, this modality provides additional quantitative information regarding cellular metabolites, because signal intensity is linearly related to steady-state metabolite concentration. MRS can detect cellular biochemical changes prior to the detection of morphologic changes by MRI or other imaging modalities. MRS may therefore provide further insight into both follow-up assessment and prognosis. With advances in instrumentation and methodology and utilization of the high inherent sensitivity of hydrogen-1, single-voxel and multivoxel proton MRS is now carried out with relatively short acquisitions to detect low-concentration metabolites in healthy and diseased tissues. Phosphorus 31 (P-31) spectroscopy has also been developed for pediatric use. Currently, MRS has been used primarily in the assessment of brain development and maturation, perinatal brain injury, childhood CNS neoplasia versus treatment effects, and metabolic and neurodegenerative disorders.

Motion-sensitive MRI techniques not only are used to evaluate vascular flow (e.g., MRA) and perfusion but also may be used to demonstrate the effect of pulsatile cardiovascular flow on other fluid tissues (e.g., CSF) and on nonfluid tissues such as the brain and spinal cord. With the utilization of cardiac or pulse gating, these MRI techniques may be used for preoperative and postoperative evaluation of abnormalities of CSF dynamics (e.g., hydrocephalus, hydrosyringomyelia) as well as abnormalities of brain motion (e.g., Chiari malformation) and spinal cord motion (e.g., tethered cord syndrome).

Brain MRI is the imaging modality of choice in a number of clinical situations. These include developmental delay (e.g., static encephalopathy vs. neurodegenerative disease); unexplained seizures (especially focal), unexplained neuroendocrine disorder, or unexplained hydrocephalus; the pretreatment evaluation of neoplastic processes and the follow-up of tumor response and treatment effects; suspected infectious, postinfectious, and other inflammatory or noninflammatory encephalitides (e.g., encephalitis, postinfectious demyelination, vasculitis); migrational and other submacroscopic dysgeneses (e.g., cortical dysplasia); neurocutaneous syndromes (e.g., neurofibromatosis 1 [NF-1], tuberous sclerosis); intractable or refractory epilepsy; and vascular diseases, hemorrhage, and the sequelae of trauma. A basic, but comprehensive, screening whole-brain MRI protocol, for example, includes the following images:

- Sagittal T1-weighted imaging
- Axial T2-weighted imaging
- Axial FLAIR imaging
- Axial GRE imaging
- Angled coronal STIR imaging
- Axial DWI

Depending on the clinical indication or the results of this basic protocol, other sequences may be prospectively added to the protocol or retrospectively obtained, including use of gadolinium enhancement, MRA/MRV, MRS, PMRI, and higher-resolution regional examination. Real-time radiologist monitoring of these procedures, especially in children requiring sedation, anesthesia, or intensive care or in emergencies, facilitates the process.

MRI frequently offers greater diagnostic specificity than CT or US for delineating vascular and hemorrhagic processes. Advantages include the clear depiction of vascular structures and abnormalities based on proton flow parameters and software enhancements not requiring the injection of contrast agents (e.g., MRA/MRV). MRI with angiography or venography can be used to differentiate arterial from venous occlusive disease. Using magnetic susceptibility sequences, MRI also provides more specific identification and staging of hemorrhage and clot formation according to the evolution of hemoglobin breakdown using T1-weighted, T2-weighted, and GRE sequences. MRI is often reserved for more definitive evaluation of hemorrhage and as an indicator or guide for angiography in a number of special situations. MRI may be used to evaluate an atypical or unexplained intracranial hemorrhage by distinguishing hemorrhagic infarction from hematoma and by distinguishing among the types of vascular malformations (e.g., cavernous malformation vs. AVM). MRA may obviate the need, in some cases of vascular malformation, for conventional angiography during follow-up after surgery, interventional treatment, or radiosurgery.

In the evaluation of intracranial vascular anomalies (e.g., vascular malformation, aneurysm), MRI may identify otherwise unsuspected prior hemorrhage (i.e., hemosiderin). When CT demonstrates a nonspecific focal high density (calcification vs. hemorrhage), MRI may provide further specificity, for example, by distinguishing an occult vascular malformation (e.g., cavernous malformation) from a neoplasm (e.g., glioma). It may further assist US or CT in differentiating benign infantile extracerebral subarachnoid collections from subdural hematomas.

NORMAL DEVELOPMENT

Morphologic CNS development during the embryonic and fetal stages may be subdivided into two basic phases, formation and maturation. More recently, genetic and molecular principles of CNS development have been elucidated. Early formation involves

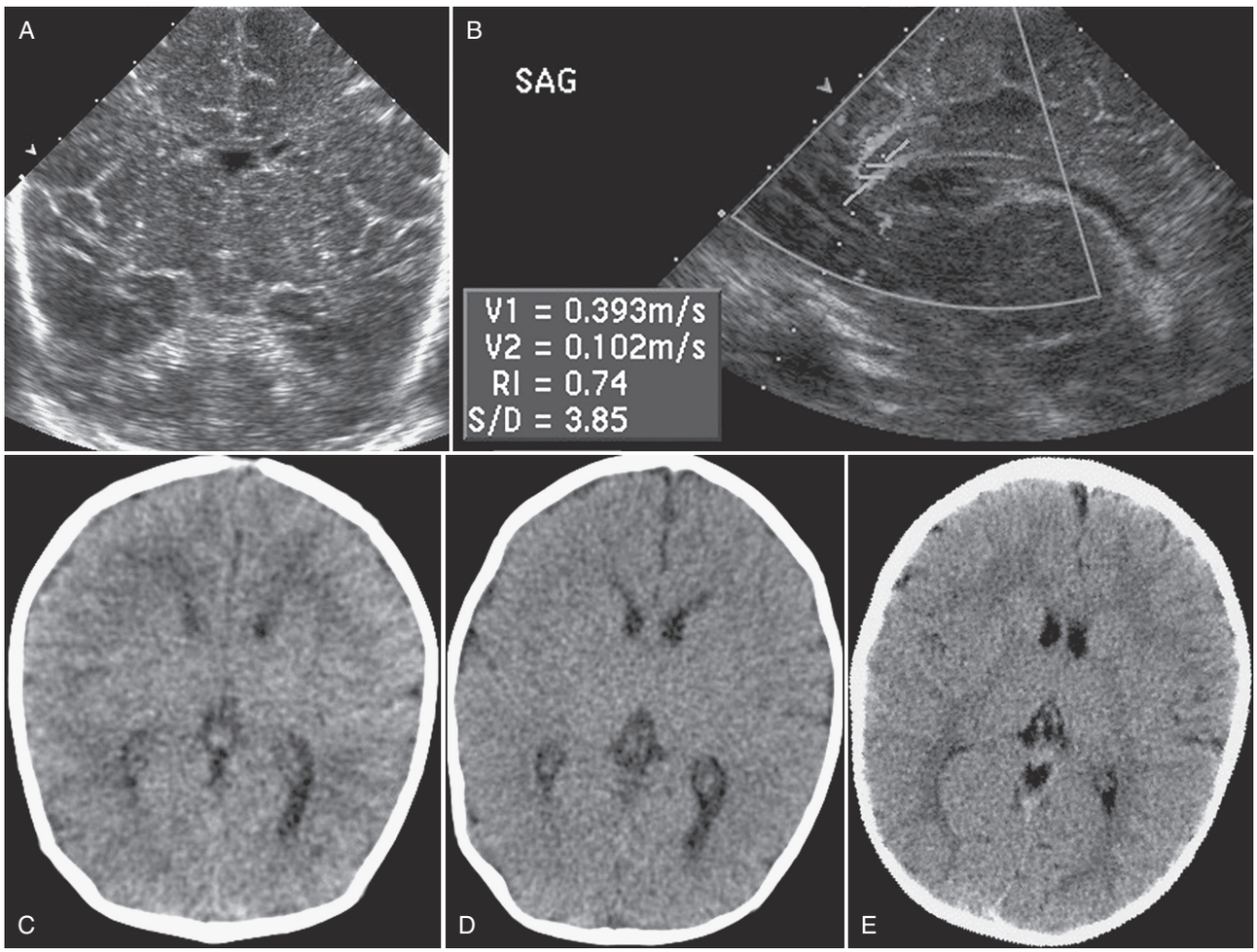

FIGURE 8-1. Normal infant and child brain. **A** and **B,** Coronal US scan (**A**) and sagittal US plus Doppler scan (**B**) with resistive indices (RI) in a term infant. **C** to **E,** CT scans of a term neonate (**C**), a 2-month-old infant (**D**), and a 2-year-old child (**E**) show progress of maturation, including myelination.

neural tube development (0-10 weeks) from the neuroectoderm as induced by the notochord. This development includes dorsal and ventral neural tube closure to form the brain, face, and spinal cord. Later formation involves neuronal, glial, and mesenchymal development (2-6 months) during the stages of proliferation, differentiation, histogenesis, migration, and cortical organization. The result is the formation of the gray and white matter structures, the glia, and the vascular, meningeal, CSF, and supportive musculoskeletal (i.e., skull and spinal column) structures.

Subsequently the CNS primarily undergoes maturational changes, including myelination, cortical maturation, and further connectivity (i.e., synaptogenesis, neuroplasticity). A fundamental understanding of normal development and its variants is necessary for the accurate interpretation of imaging of the CNS in the child. More detailed descriptions of CNS embryology and development are covered in other texts. Knowledge of the normal skull and brain, and their variations of normal, according to stage of development and maturation, is important for proper image interpretation using PF/CR, US, CT, and MRI (Fig. 8-1). This subject is also covered in greater detail elsewhere.

CONGENITAL AND DEVELOPMENTAL ABNORMALITIES

Congenital and developmental abnormalities of the CNS have been classified by van der Knaap and Valk according to the timing (i.e., weeks of gestational age—WGA) of the disorder, rather than the etiology, as the major determinant of the type of malformation (Table 8-1). CNS malformations are also a major cause of childhood hydrocephalus (Table 8-2).

Disorders of Dorsal Induction

Dorsal induction is the process whereby the notochord induces the adjacent ectoderm to form the neural plate. Neural folds develop from the plate to form the primitive neural tube (i.e., primary neurulation), which gives rise to the brain and spinal cord. Malformations associated with disorders of dorsal induction have their origin within the embryonic period (0-4 WGA) and include anencephaly, cephaloceles, Chiari malformations, dermal sinus, spinal dysraphism, and hydrosyringomyelia. The last three malformations are discussed in Chapter 9.

Anencephaly

Anencephaly is due to failure of early cephalic neural tube closure and results in complete absence of the cranium and brain above the brainstem. It is fatal, is associated with elevated alpha-fetoprotein concentrations, and is readily detected by fetal US.

Cephalocele

Cephaloceles are extensions of intracranial tissues through a skull defect. They are classified, according to content and location,

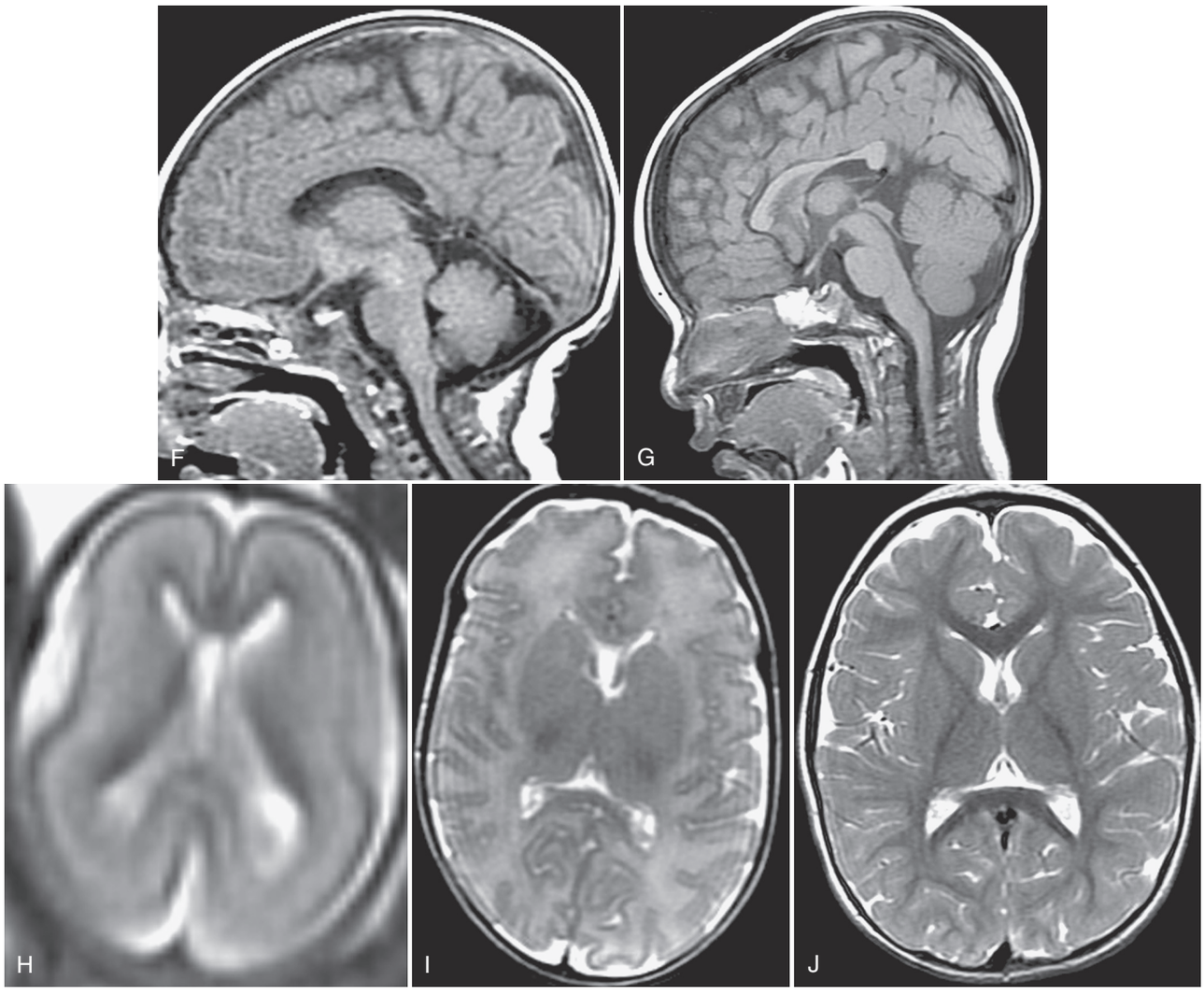

FIGURE 8-1.—CONT'D **F** and **G**, Sagittal T1-weighted MR images of a term neonate (**F**) and a 1-year-old infant (**G**) show progress in brain growth, myelination of the corpus callosum, and pituitary maturation. **H** to **J**, T2-weighted MR images of a 20-week fetus (**H**), a term neonate (**I**), and a 2-year-old child (**J**) show progress in maturation, i.e., decreasing water content along with increasing myelination and cortication.

as meningoceles (meninges only), encephaloceles (brain tissue), and encephalocystomeningoceles (meninges, brain, and ventricles). Cephaloceles may extend through either the calvarium or the skull base. Occipital cephaloceles are most common in western European and North American cultures (Fig. 8-2). They may occur with the Dandy-Walker spectrum of malformations or the Meckel-Gruber syndrome. Occipital cephaloceles often contain dysplastic occipital lobe or cerebellar tissue, and anomalies of the venous sinuses are common. MRI (e.g., in the lateral decubitus position) is best for delineating the contents of cephaloceles as well as venous or dural sinus anomalies or involvement, associated CNS anomalies, and hydrocephalus. Cervico-occipital cephalocele is a component of the Chiari III malformation.

Frontoethmoid cephaloceles are most common in Southeast Asian populations. They are subcategorized as nasoethmoidal, nasofrontal, naso-orbital, and interfrontal. Frontoethmoidal encephaloceles may manifest as hypertelorism or as a glabellar mass. Associated anomalies include corpus callosal hypogenesis, holoprosencephaly, migrational disorder, and hydrocephalus. Failure of closure at the foramen cecum or persistence of the dural projection at that level may result in nasofrontal cephalocele, dermoid-epidermoid, or nasal "glioma" (i.e., isolated ectopic and dysplastic brain tissue; Fig. 8-3). Sphenoidal cephaloceles occur through defects of the sella turcica and sphenoid body (Fig. 8-4). There is potential herniation of the pituitary stalk, third ventricle, and optic apparatus into the sphenoid, ethmoid, or nasopharynx. Associated anomalies include corpus callosum hypogenesis, hypertelorism, and midline facial clefts. Sphenoid wing cephaloceles are usually associated with NF-1.

Parietal cephaloceles occur at the vertex near the posterior fontanelle and are often atretic (Fig. 8-5). The straight sinus is often replaced by an anomalous falcine vein that extends to the defect. Also, emissary veins or the superior sagittal sinus may traverse the defect. Possible associated anomalies are the Dandy-Walker spectrum, callosal hypogenesis, holoprosencephaly, and Chiari II malformation.

Chiari Malformations

The *Chiari I malformation* is defined as an extension of the cerebellar tonsils below the foramen magnum (e.g., > 3-5 mm). It may be associated with hydrocephalus, craniocervical junction anomalies, basilar invagination, scoliosis, or hydrosyringomyelia, or with intracranial hypotension (e.g., spinal CSF leak). Other

TABLE 8-1. Classification of Central Nervous System Malformations by Gestational Timing

I. Disorders of dorsal neural tube development	3-4 weeks	Anencephaly Cephaloceles Dermal sinus Chiari malformations Spinal dysraphism Hydrosyringomyelia
II. Disorders of ventral neural tube development	5-10 weeks	Holoprosencephalies Agenesis of the septum pellucidum Optic and olfactory hypoplasia/aplasia Pituitary-hypothalamic hypoplasia/aplasia Cerebellar hypoplasia/aplasia Dandy-Walker spectrum Craniosynostosis
III. Disorders of migration and cortical organization	2-5 months	Schizencephaly Neuronal heterotopia Agyria/pachygyria Lissencephaly Polymicrogyria Agenesis of the corpus callosum
IV. Disorders of neuronal, glial, and mesenchymal proliferation, differentiation, and histogenesis	2-6 months	Micrencephaly Megalencephaly Hemimegalencephaly Aqueductal anomalies Colpocephaly Cortical dysplasias Neurocutaneous syndromes Vascular anomalies Malformative tumors Arachnoid cysts
V. Encephaloclastic processes	>5-6 months	Hydranencephaly Porencephaly Multicystic encephalopathy Encephalomalacia Leukomalacia Hemiatrophy Hydrocephalus Hemorrhage Infarction
VI. Disorders of maturation	7 mo-2 yr	Hypomyelination Delayed myelination Dysmyelination Demyelination Cortical dysmaturity

TABLE 8-2. Childhood Hydrocephalus

Developmental	Chiari II malformation Aqueductal anomalies Congenital cysts Encephalocele Hydranencephaly Craniosynostosis Skull base anomalies Foraminal atresia Immature arachnoid villi Vein of Galen malformation
Acquired	Posthemorrhage Postinfection Posterior fossa tumors Tumors about the third ventricle Cerebral hemispheric tumors

intracranial anomalies are rarely present. Hydrosyringomyelia is commonly associated with Chiari I malformation in childhood (see Chapter 9).

Chiari II malformations are complex congenital anomalies affecting the craniospinal neuraxis (Fig. 8-6). This primary hindbrain anomaly is characterized by a variable spectrum including caudal displacement of a dysplastic cerebellum and brainstem from a small posterior fossa into an enlarged foramen magnum and upper cervical canal. It is almost always associated with myelomeningocele (see Chapter 9). There are a small fourth ventricle, an elongated medulla, and a cervicomedullary "kink." Hydrocephalus commonly occurs at birth or following surgery for the myelomeningocele. Associated anomalies include callosal hypogenesis, colpocephaly, stenogyria, fenestrated falx with gyral interdigitation, large massa intermedia, tectal "beaking," aqueductal anomalies (e.g., stenosis), heterotopias, persistent or accentuated Lückenschädel (i.e., lacunar) skull, and petrous temporal scalloping. New or progressive neurologic impairment following surgery often requires imaging to evaluate for hydrocephalus, shunt malfunction, encysted or entrapped fourth ventricle, craniocervical compromise (e.g., stenosis), hydrosyringomyelia, or spinal cord "retethering" at the surgical site. A *Chiari III malformation* is a rare disorder in which a cervico-occipital cephalocele contains cerebellum and sometimes brainstem (see Fig. 8-2).

Disorders of Ventral Induction

During ventral induction (4-10 WGA) the cephalic neural tube expands to form the brain, and the notochordal mesoderm induces the overlying ectoderm to form the facial structures.

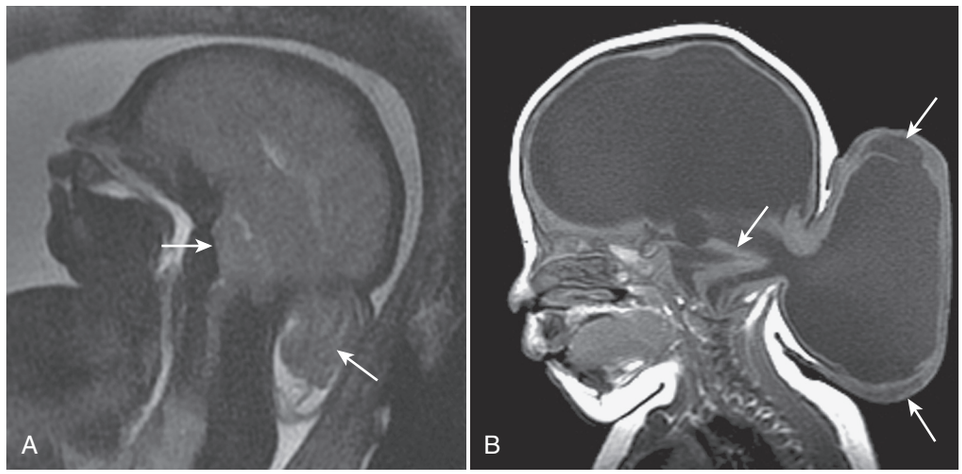

FIGURE 8-2. **A,** Fetal sagittal T2-weighted MR image showing a cervico-occipital cephalocele (*posterior arrow*), Chiari III malformation (*anterior arrow*), and microcephaly. **B,** Neonatal sagittal T1-weighted MR image shows an occipital cephalocele (*posterior arrows*) with a kinked brainstem (*anterior arrow*).

FIGURE 8-3. Nasoethmoidal cephalocele—nasal "glioma" (*arrow*) on a sagittal T2-weighted MR image.

FIGURE 8-4. Sphenoidal cephalocele (*lower arrows*) and hypogenesis corpus callosum (*upper arrow*) on a sagittal T1-weighted MR image.

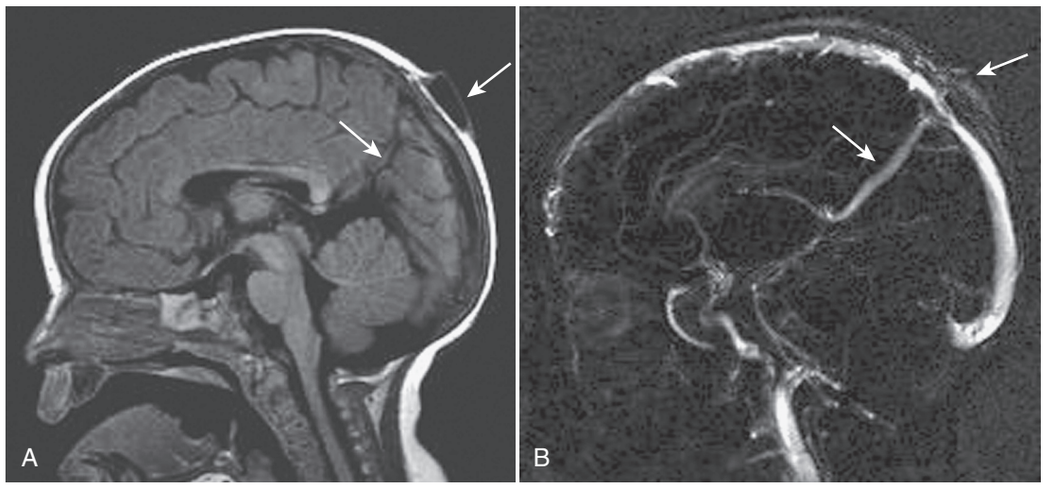

FIGURE 8-5. Parietal cephalocele (*upper arrow*) and transfalcine vein (*lower arrow*) on a sagittal T1-weighted MR image (**A**) and an MR venogram (**B**).

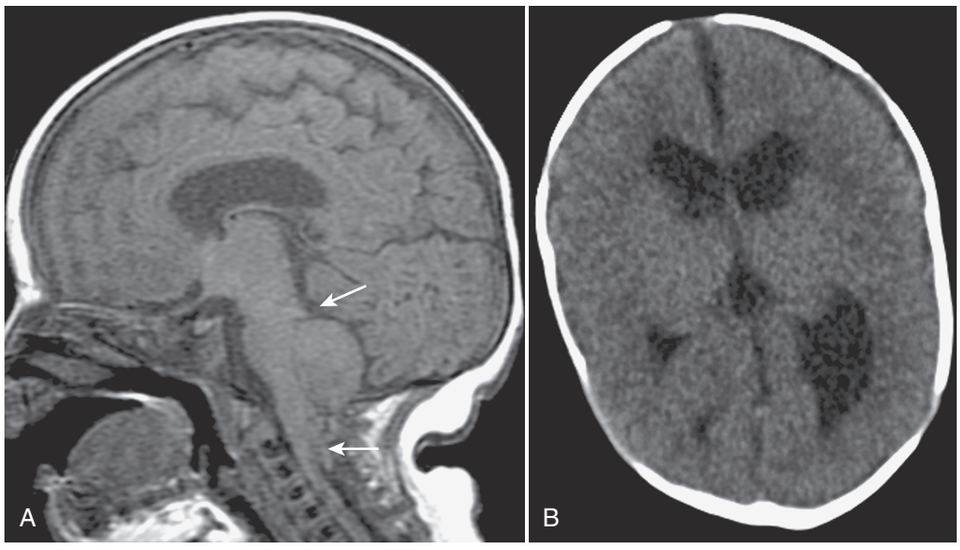

FIGURE 8-6. A, Chiari II malformation (*arrows*) on a sagittal T1-weighted MR image. **B,** Ventriculomegaly on CT.

Diverticulation results in formation of the prosencephalon (forebrain), the mesencephalon (midbrain), and the rhombencephalon (hindbrain). Disorders in this category include the holoprosencephalies, absence of the septum pellucidum, craniosynostosis, and the Dandy-Walker spectrum of malformations.

Holoprosencephaly

The holoprosencephalies (HPEs) are a spectrum of disorders resulting from lack of normal cleavage of the telencephalon into two cerebral hemispheres and lack of separation of the telencephalon from the diencephalon (Fig. 8-7). Associated facial anomalies include cyclopia, ethmocephaly, cebocephaly, and hypotelorism. Alobar HPE, the most severe form, is often fatal (Fig. 8-7A). It is composed of microcephaly, a common hemisphere, a monoventricle with dorsal cyst, thalamic fusion, absence of the falx and septum pellucidum, corpus callosum agenesis, and absence of olfactory apparatus. There is an azygous (single) anterior cerebral artery with absence of the superior sagittal sinus, straight sinus, and internal cerebral veins. Semilobar HPE is an intermediate form (Fig. 8-7B). Facial features are less common and less severe. It consists of microcephaly, partial posterior cleaving of the cerebral hemispheres, absence of the septum pellucidum and of anterior portions of the corpus callosum, partial separation of the thalami, partially formed temporal horns, and a posterior falx and interhemispheric fissure. Lobar HPE is the third classic form (usually no facial anomalies) along with the middle interhemispheric subtype (Fig. 8-7C and D). There is failure of cleavage of the cerebral hemispheres frontally or parietally. The septum pellucidum is absent, and the corpus callosum may be incomplete or dysplastic.

Absence of the Septum Pellucidum

Absence of the septum pellucidum is characterized by complete or partial absence of the leaflets of the septum pellucidum (Fig. 8-8). Septo-optic dysplasia (de Morsier syndrome) includes hypoplasia of the optic nerves. Schizencephaly or heterotopias are present in half the cases. Pituitary-hypothalamic dysfunction occurs in most (e.g., growth hormone or thyroid-stimulating hormone deficiencies), including ectopia of the posterior pituitary bright spot. In some patients there is complete absence of the septum pellucidum and hypoplasia of the cerebral white matter without other anomalies. Absence of the septum pellucidum may also occur with Chiari II malformation, holoprosencephaly, callosal agenesis, and severe hydrocephalus.

Posterior Fossa Cystic Malformations

Posterior fossa cystic malformations are subdivided along a continuum that includes the Dandy-Walker malformation, Dandy-Walker variant, mega cisterna magna, and Blake's pouch or arachnoid cyst. The classic *Dandy-Walker malformation* is characterized by complete or partial vermian agenesis (especially of the inferior vermis), a large retrocerebellar cyst communicating with the fourth ventricle, an enlarged posterior fossa, elevation of the torcular above the lambda, and absence of the falx cerebelli (Fig. 8-9). Associated CNS and systemic anomalies are common, including corpus callosum hypogenesis, polymicrogyria, heterotopias, cephalocele, and holoprosencephaly. Macrocephaly and hydrocephalus are common. Evaluation of aqueductal patency is important before surgery for ventricular or cyst shunting.

In *Dandy-Walker variant*, the cerebellar vermis is hypogenetic (i.e., inferior vermis), the posterior fossa is usually of normal size, and there is separation of the fourth ventricle from a smaller retrocerebellar space (Fig. 8-10A). If the cerebellar vermis is completely formed and an enlarged retrocerebellar CSF space is present, the anomaly is usually designated *mega cisterna magna* (Fig. 8-10B). If the retrocerebellar CSF collection exerts mass effect on a completely formed cerebellum, then *Blake's pouch or arachnoid cyst* may be diagnosed, especially if there is hydrocephalus (Fig. 8-11). Other CNS or systemic anomalies are uncommon in Dandy-Walker variant, mega cisterna magna, and Blake's pouch or arachnoid cyst. The cystic posterior fossa anomalies are to be distinguished from cerebellar hypoplasia (formed but small cerebellum without cyst), pontocerebellar hypoplasia (formed but small pons and cerebellum), Joubert syndrome (superior or total vermian hypogenesis), rhombencephalosynapsis (absence of vermis with fused hemispheres), and cerebellar atrophy or degeneration (small cerebellum with prominent fissures).

Craniosynostosis

Craniosynostosis (premature fusion of the sutures) may be primary or secondary. Primary synostosis is probably related to an anomaly of skull base development. Secondary synostosis may be due to external compression of the calvarium, metabolic abnormalities, or failure of brain growth. Primary craniosynostosis may also be syndromic. Examples are Apert, Crouzon, and Pfeiffer syndromes (see Chapter 10). Sutural synostosis may be identified on PF/CR or CT as bony bridging of the affected suture. 3DCT is the best procedure for surgical planning. Sagittal synostosis produces elongation of the skull (dolichocephaly)

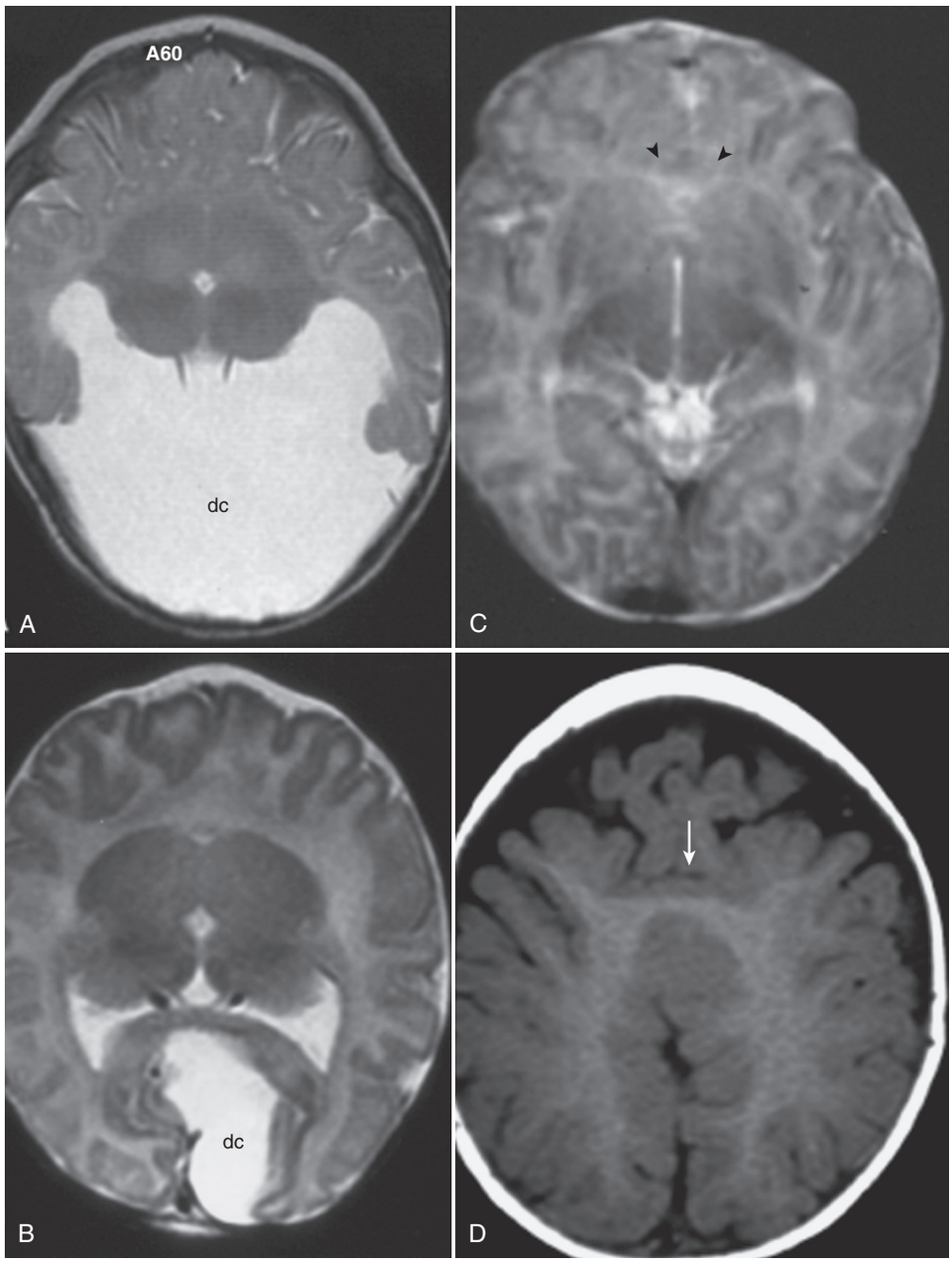

FIGURE 8-7. The spectrum of holoprosencephaly (HPE) on MR images. **A,** Alobar HPE on an axial T2-weighted image; dc, dorsal cyst. **B,** Semilobar HPE on an axial T2-weighted image. **C,** Lobar HPE on an axial T2-weighted image. **D,** Middle interhemispheric subtype of HPE on an axial T1-weighted image; *arrowheads* (**C**) and *arrow* (**D**) indicate midline fusion.

(Fig. 8-12A and B). Coronal synostosis results in anterior plagiocephaly (unilateral) or brachycephaly (bilateral) with elevation of the ipsilateral orbit yielding a "harlequin eye" appearance (Fig. 8-12C and D). Metopic synostosis produces trigonocephaly. Lambdoidal synostosis results in posterior plagiocephaly (unilateral) or brachycephaly (bilateral). The latter is to be distinguished from the more common deformational plagiocephaly or brachycephaly resulting from intrauterine or postnatal molding. Fusion of the sagittal, coronal, and lambdoid sutures produces a cloverleaf skull (kleeblattschädel), which may be seen in thanatophoric dwarfism.

Disorders of Neuronal Proliferation and Differentiation

Micrencephaly, megalencephaly, aqueductal abnormalities, and arachnoid cysts are discussed here. Other anomalies often included in the category "disorders of neuronal proliferation and differentiation" are colpocephaly, neurocutaneous syndromes, vascular anomalies, and malformative tumors; the last three are discussed in later sections.

Micrencephaly

Micrencephaly (smaller than normal brain mass) is a primary form of microcephaly (small head) that is often genetic. The brain is small but may be morphologically normal on imaging. This is contrasted with microcephaly related to other malformations (e.g., lissencephaly) or to acquired conditions (e.g., post-infection). In these cases, the brain is morphologically abnormal (see Fig. 8-2).

Megalencephaly

Megalencephaly (larger than normal brain mass) may be bilateral or unilateral. The bilateral form is most commonly familial but also occurs in other conditions, such as cerebral gigantism, the phakomatoses, and Beckwith-Weidemann syndrome. Unilateral

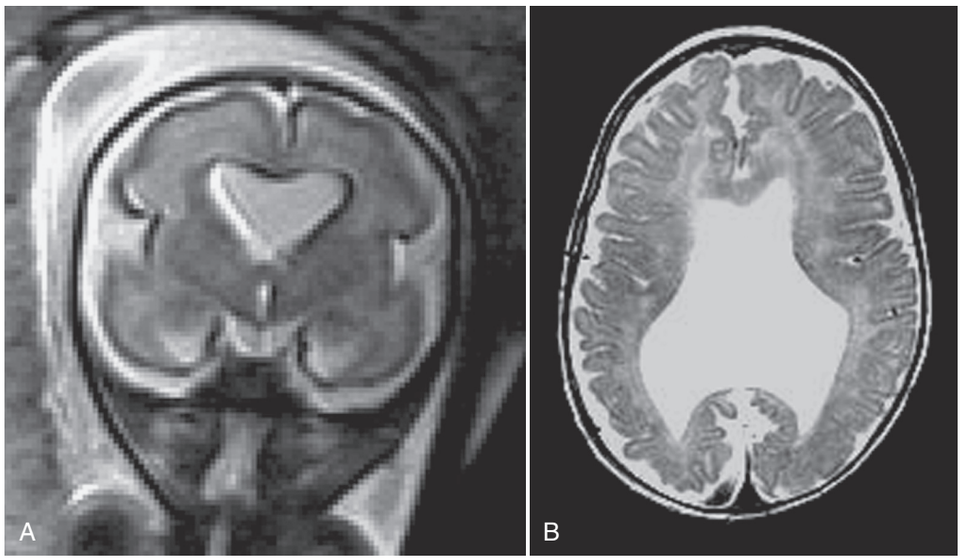

FIGURE 8-8. Absence of the septum pellucidum on a fetal coronal T2-weighted MR image (**A**) and a postnatal axial T2-weighted MR image (**B**).

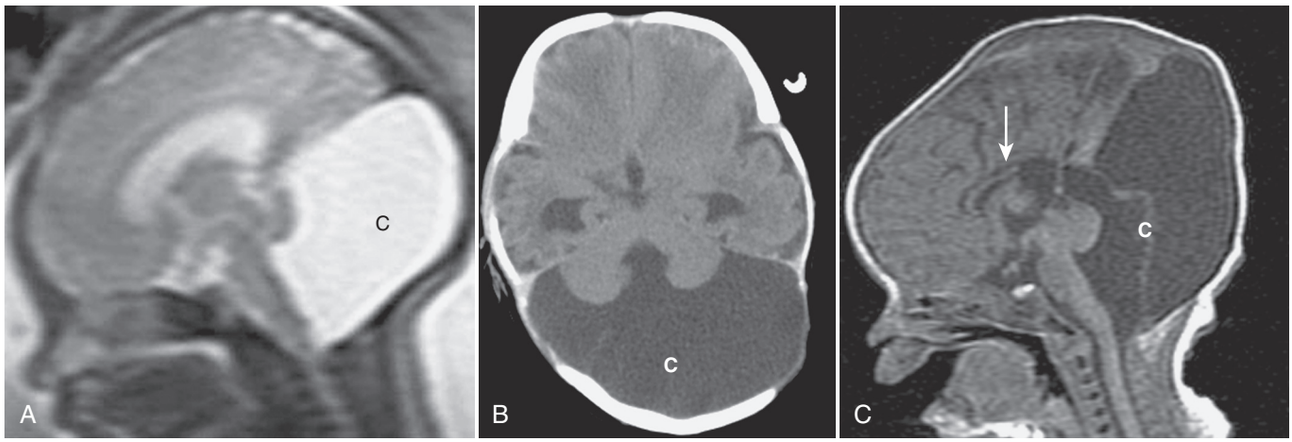

FIGURE 8-9. Dandy-Walker cyst (c) on a fetal sagittal T2-weighted MR image (**A**), a neonatal axial CT scan (**B**), and a sagittal T1-weighted MR image, which also shows hypogenesis of the corpus callosum (*arrow*).

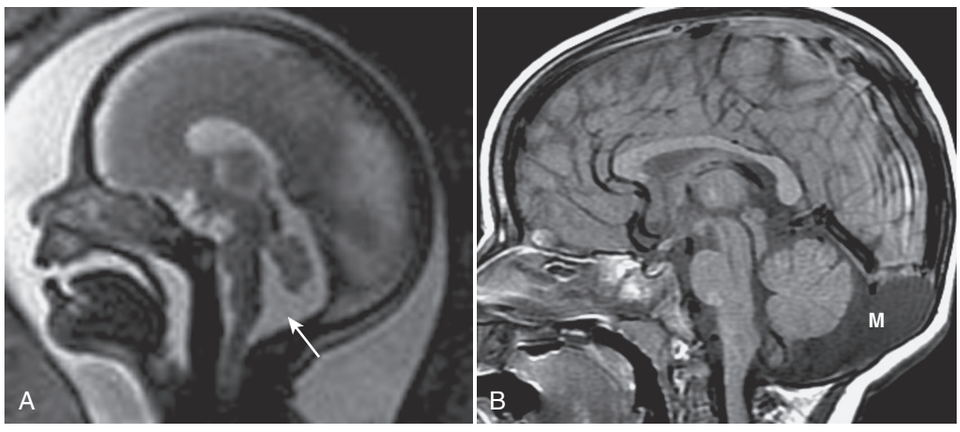

FIGURE 8-10. A, Dandy-Walker variant (*arrow*) on a fetal sagittal T2-weighted MR image. **B,** Mega cisterna magna (M) on a sagittal T1-weighted MR image.

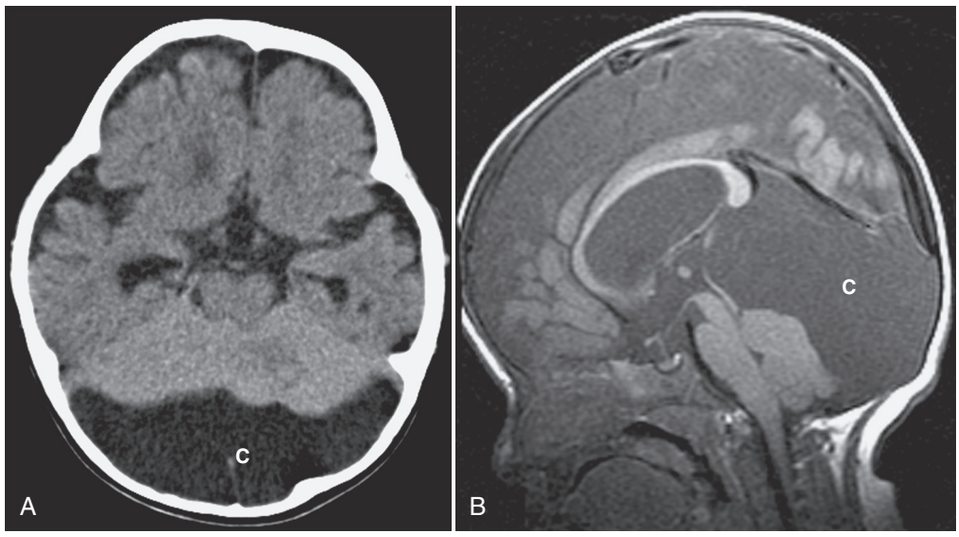

FIGURE 8-11. Retrocerebellar arachnoid cyst (c) and hydrocephalus on a CT scan (**A**) and a sagittal T1-weighted MR image (**B**).

megalencephaly is a hamartomatous cerebral overgrowth that may be isolated or may occur with ipsilateral hemihypertrophy of the body, linear sebaceous nevus syndrome, NF-1, and hypomelanosis of Ito. Intractable seizures, developmental delay, or hemiparesis is common. On imaging there is unilateral cortical thickening with polymicrogyria, pachygyria, or agyria (Fig. 8-13). Enlargement of the lateral ventricle and abnormal white matter densities/intensities are common. A more localized cortical form of this disorder may be seen as one of the focal cortical dysplasias that characteristically manifests as seizures (Fig. 8-14). This form may have a similar appearance to an isolated "tuber" (see tuberous sclerosis) and must be differentiated from other focal cortical lesions that manifest as seizures (see neoplasms).

Aqueductal Abnormalities

Aqueductal narrowing may be primary and maldevelopmental or secondary (acquired). It is a common cause of hydrocephalus (see Table 8-2) and may be isolated or associated with other developmental or acquired conditions. Developmental narrowing may occur in the form of stenosis, gliosis, forking (i.e., fenestration), or a membrane. Hemorrhage, infection, or tumors may lead to acquired aqueductal stenosis. Imaging often shows hydrocephalus with lateral and third ventricular enlargement and a normal-sized or small fourth ventricle (Fig. 8-15). There may be tectal dysplasia with thickening or beaking. This is to be distinguished from tectal glioma (see neoplasm discussion).

Arachnoid Cyst

Arachnoid cysts, which are CSF-containing lesions within an arachnoid membrane, may be primary and malformative. There may be hypogenesis or dysplasia of adjacent brain structures. Arachnoid cysts may expand the cleft of schizencephaly.

Secondary, or acquired, arachnoid cysts are CSF loculations produced by arachnoidal scarring, for example, as a result of inflammation or hemorrhage. Occasionally they are associated with neoplastic invasion of the subarachnoid space (e.g., pilocytic astrocytoma). Common sites include the middle cranial fossa and sylvian fissure, suprasellar, quadrigeminal plate cistern, and posterior fossa. They may be solitary or multiple. Occasionally, they may occur intraventricularly, periventricularly, or along the cerebral convexities. On CT and MRI, arachnoid cysts have CSF density and intensity characteristics, respectively (see Fig. 8-11; Figs. 8-16 and 8-17). The cyst wall may not be visualized, but septations may be present. Calcification or enhancement with contrast agent is not expected unless the cyst is associated with an inflammatory or neoplastic process. Vascular displacement and bony remodeling are often seen. Hydrocephalus may occur, especially with midline cysts (e.g., retrocerebellar, suprasellar). Arachnoid cysts may occasionally be complicated by intracystic, subarachnoid, or subdural hemorrhage (or hygroma).

Disorders of Neuronal Migration and Cortical Organization

Disorders of neuronal migration and cortical organization include lissencephaly, pachygyria, polymicrogyria, heterotopia, schizencephaly, and hypogenesis of the corpus callosum. More localized defects may manifest as congenital hemiparesis or focal seizures, including medically refractory epilepsy that may be amenable to surgery. More extensive defects are often associated with more global neurodevelopmental delay.

Lissencephaly

Lissencephaly may be considered a spectrum of diffuse cortical malformations resulting from faulty migration and including agyria (absence of sulci and gyri), pachygyria (coarse, broad, flat gyri with shallow intervening sulci), or a combination (agyria-pachygyria). Type I (classical lissencephaly; LIS I gene) results from undermigration, which leads to a four-layer cortex with a "smooth" surface, microcephaly, and severe developmental delay. In this group are the Miller-Dieker, X-linked, and isolated forms. Lissencephaly may also result from toxins (e.g., alcohol) or congenital infection (e.g., cytomegalovirus with associated periventricular calcifications). Agyria, pachygyria, or a mixed pattern may be seen (Fig. 8-18) along with abnormal myelination, band heterotopia ("double cortex"), deficient gray matter–white matter interdigitation, abnormal sylvian fissures (incomplete opercularization), ventriculomegaly, or colpocephaly.

Type II (cobblestone) lissencephaly results from overmigration, which leads to an irregular cortex (cobblestone dysplasia, polygyria, or polymicrogyria) with hypomyelination and hindbrain plus ocular anomalies. It occurs with the merosin-positive congenital muscular dystrophies and includes Walker-Warburg syndrome, Fukuyama syndrome, and cerebro-ocular muscular syndrome (Haltia-Santavuori or muscle-eye-brain disease). The prototypical Walker-Warburg syndrome is characterized by a variable combination of cobblestone lissencephaly, hypomyelination, vermian hypogenesis, kinked brainstem, cerebellar polymicrogyria or cysts, cephalocele, callosal hypogenesis, hydrocephalus, and ocular abnormalities (e.g., retinal, optic dysplasia) (Fig. 8-19).

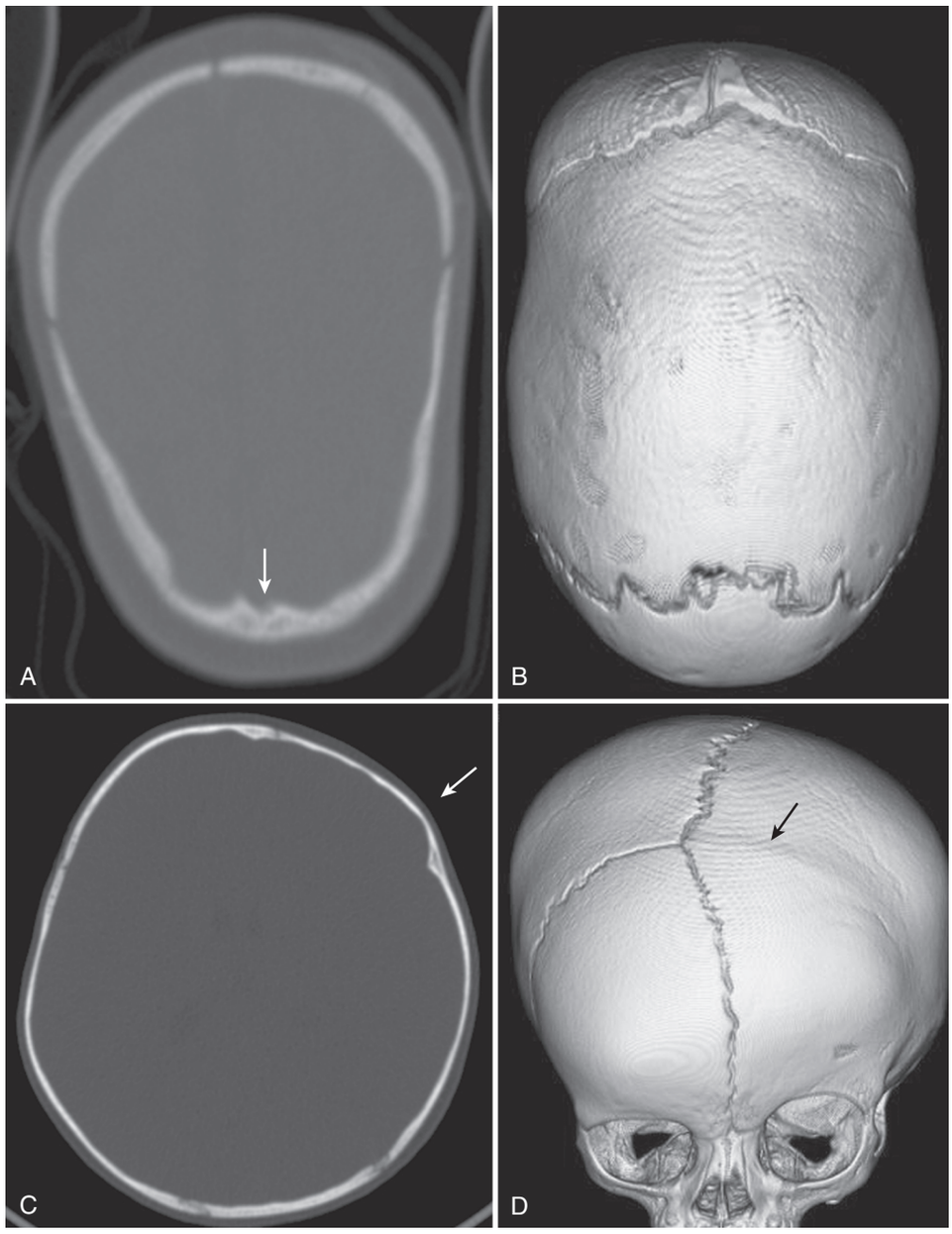

FIGURE 8-12. Craniosynostosis (*arrows):* sagittal type on axial CT (**A**) and top view 3DCT (**B**); coronal type on axial CT (**C**) and front view 3DCT (**D**).

Polymicrogyria

Polymicrogyria (PMG; also known as microgyria) results from a late migrational or post-migrational disorder in which the cortex has an irregular, serrated, or pebble-like appearance. PMG is the major component of a number of focal and diffuse forms of cortical dysgenesis or dysplasia and often occurs with other disorders of migration, differentiation, and proliferation. Early gestational cytomegalovirus (CMV) infection may result in diffuse PMG (Fig. 8-20). The underlying cortex is serrated or thickened and of gray matter intensity on all MRI sequences. PMG lines the complete cleft of a schizencephalic defect and the partial cleft of some forms of focal cortical dysgenesis/dysplasia (Fig. 8-21). Associated white matter hyperintensity on T2-weighted sequences reflects undermyelination. Often there is reduced white matter volume and decreased gray matter–white matter interdigitation. It may be difficult to distinguish PMG from pachygyria in some cases. Occasionally anomalous veins or arachnoidal cysts are associated with the cleft.

Schizencephaly

A migrational anomaly, schizencephaly manifests as a transmantle cleft. It may occur at any site and may be unilateral or bilateral, and symmetric or asymmetric. The cerebral cleft is classically a CSF-containing hemispheric defect that communicates with the lateral ventricle and the subarachnoid space. It is lined by PMG and covered by an ependyma-to-pia membrane. The cleft may be narrow (i.e., closed-lip) or wide (open-lip). Occasionally an incomplete, or partial, cortical cleft is present that does not communicate with the ventricle. Schizencephaly is frequently associated with absence of the septum pellucidum, including septo-optic dysplasia (de Morsier syndrome). On MRI, the cleft is identified

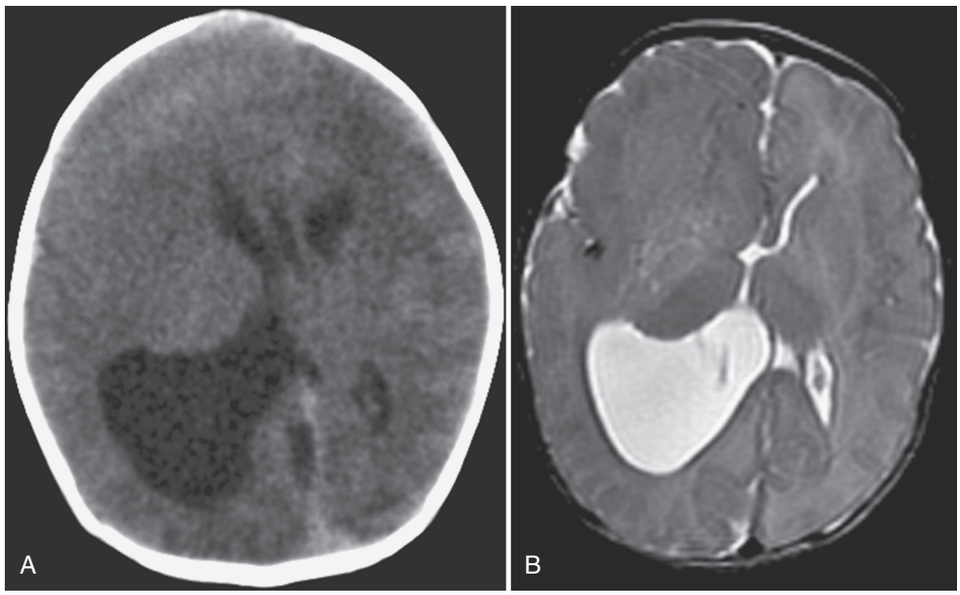

FIGURE 8-13. Hemimegalencephaly and cortical dysplasia on CT scan (**A**) and axial T2-weighted MR image (**B**).

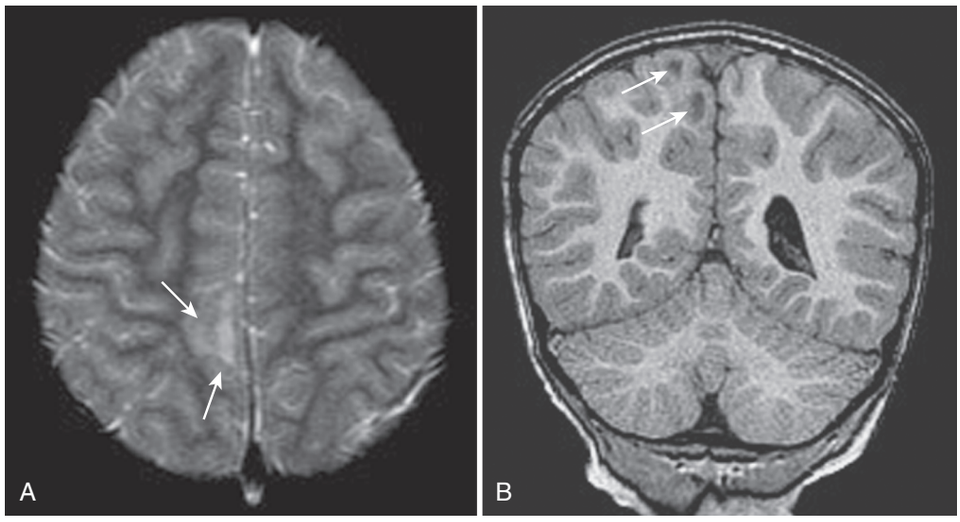

FIGURE 8-14. Focal cortical dysplasia (*arrows*) on axial T2-weighted (**A**) and coronal T1-weighted (**B**) MR images.

as a CSF-intensity defect lined by thickened or irregular gray matter intensities and associated with cortical and ventricular dimples (see Fig. 8-21). This appearance differentiates it from porencephaly, which is encephaloclastic (e.g., post-infarction or post-hemorrhagic) and is a glial-lined defect that extends through both gray and white matter.

Neuronal Heterotopia

Neuronal heterotopias arise as a result of arrested radial neuronal migration from the subependymal germinal matrix zone to the cortical plate. They may be nodular or laminar and single, multiple, or diffuse. They may occur in a cortical, subcortical, periventricular, or transmantle distribution. Neuronal heterotopia may manifest as an isolated anomaly (e.g., nodular type) or may occur in association with other migrational disorders (e.g., laminar or band type in lissencephaly). Isolated heterotopias typically manifest as seizures that may be refractory. Periventricular nodular heterotopia may be associated with the filamin-1 gene mutation. On MRI, neuronal heterotopias are usually of gray matter intensity on all sequences (Fig. 8-22).

Hypogenesis of the Corpus Callosum

The development of the corpus callosum (CC; at 8-20 weeks' gestation) normally proceeds from the genu bidirectionally—that is, posteriorly to the body and the splenium, and anteriorly to the rostrum (see Fig. 8-1). With agenesis, the entire CC is absent. With partial agenesis, the posterior body, splenium, and rostrum are commonly absent. Absence of only the anterior CC may indicate a destructive process. An exception is holoprosencephaly, in which only the splenium and posterior body may be present. CC hypogenesis may be isolated or associated with other anomalies, including the Chiari malformations, the Dandy-Walker malformation spectrum, the HPEs, median cleft face syndromes, encephaloceles, and Aicardi syndrome (female, CC hypogenesis, interhemispheric cyst, lacunar chorioretinopathy, mental retardation, and infantile spasms).

Sagittal MRI best shows the extent of the CC hypogenesis (see Figs. 8-4 and 8-9; Figs. 8-23 and 8-24). The cingulate gyri remain everted, and the cingulate sulcus does not form. As a result, the parasagittal gyri appear to radiate about the roof of the third ventricle. Additionally, the axons, which would normally cross through the CC, are diverted and extend along the medial surface of the lateral ventricles (Probst bundles). The third ventricle is frequently "high-riding." The bodies of the lateral ventricles typically assume a parallel configuration on axial images, and colpocephaly is commonly present. There may be an associated interhemispheric cleft, arachnoid cyst (Fig. 8-24A and B), neuroepithelial cyst, or pericallosal lipoma (Fig. 8-24C and D).

Encephaloclastic Disorders: Secondarily Acquired Injury of Formed Structures

The expression of an intrauterine insult depends on its severity and timing. First-trimester and early second-trimester insults usually result in malformations, whereas later insults more often produce injury to formed structures (i.e., destructive or disruptive). The latter are classified as *encephaloclastic*. Also, these later injuries are more commonly associated with a reactive astroglial response (i.e., gliosis). Some transgestational insults may have both malformative and encephaloclastic features (e.g., CMV infection). The encephaloclastic category includes hydranencephaly, porencephaly, encephalomalacia, leukomalacia, hemiatrophy, hydrocephalus, hemorrhage, and infarction.

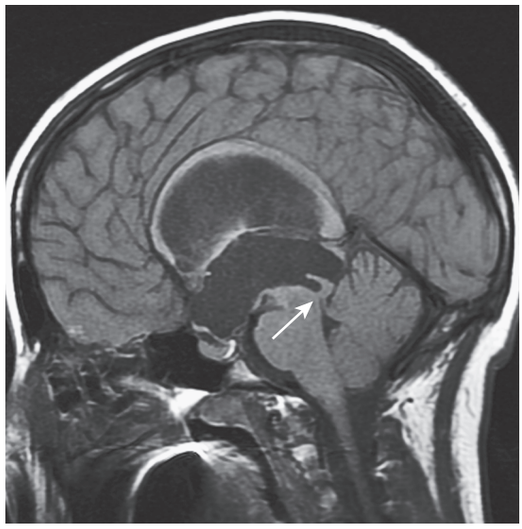

Figure 8-15. Aqueductal stenosis (*arrow*) and hydrocephalus on sagittal T1-weighted MR image.

Hydranencephaly

Hydranencephaly is a condition in which most of the cerebrum in the distribution of the internal carotid arteries is replaced by thin-walled, CSF-filled cavities. There is relative preservation of structures in the vertebrobasilar arterial territories (occipital lobes, inferior temporal lobes, thalami, brainstem, and cerebellum). This pattern implicates bilateral internal carotid arterial occlusions as the cause. Hydranencephaly has also been observed with intrauterine infection (e.g., toxoplasmosis and CMV). The presence of the falx and the separation of paired structures at the midline differentiate hydranencephaly from alobar HPE (Fig. 8-25). However, it may be difficult to distinguish hydranencephaly from severe hydrocephalus associated with marked attenuation of the cerebral mantle. Treatment with CSF shunting is important in both cases in an attempt to preserve tissue and prevent massive macrocephaly.

Porencephaly, Encephalomalacia, Leukomalacia, and Hemiatrophy

The response of the brain to focal, multifocal, or diffuse injury (e.g., ischemia, hemorrhage, infection) changes during gestation. The result of an earlier insult may be one or more thin-walled, CSF-containing cavities known as a porencephaly or multicystic encephalomalacia (Fig. 8-26). The glial-lined cysts often have no septations or associated gliosis. Porencephaly may have a ventricular communication and may be associated with hydrocephalus. Encephalomalacia, leukomalacia, and hemiatrophy, which are due to later insults, may be multicystic, macrocystic, microcystic, or noncystic. Gliosis and septations are commonly present.

Disorders of Maturation

Neuronal and glial proliferation and axonal myelination continue in a predictable pattern during maturation of the developing brain. The process of myelination begins during the fifth month

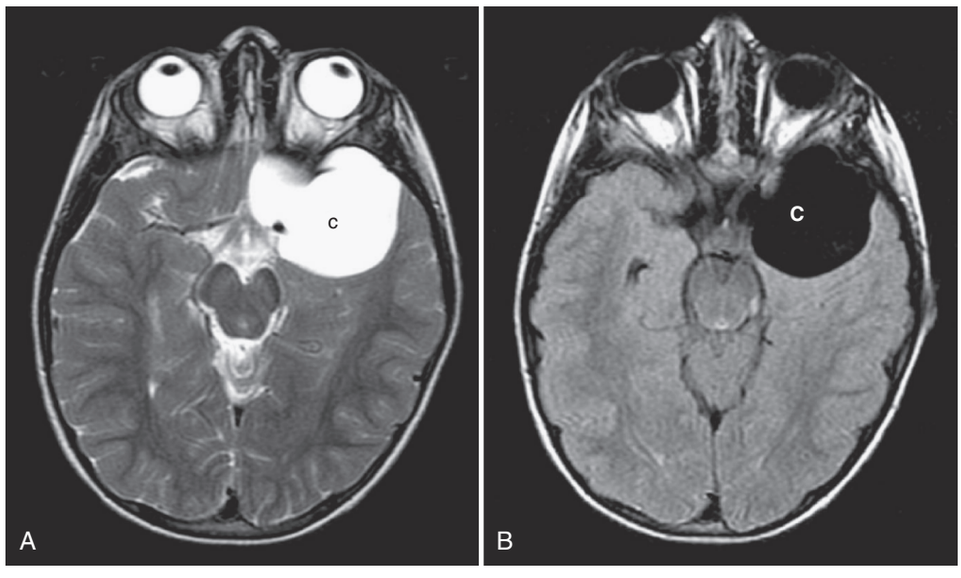

Figure 8-16. Middle cranial fossa/sylvian arachnoid cyst (c) on axial T2-weighted (**A**) and FLAIR (**B**) MR images.

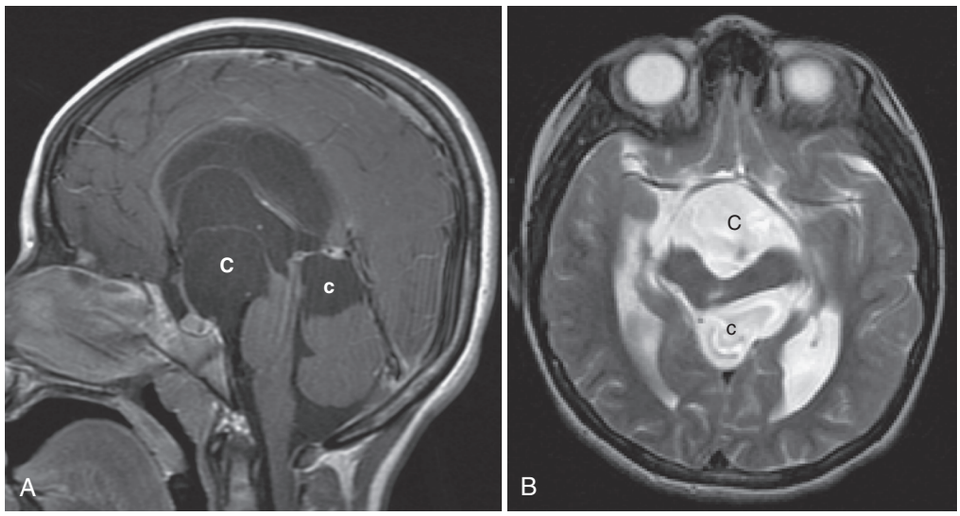

FIGURE 8-17. Suprasellar (**C**) and supracerebellar (c) arachnoid cysts with hydrocephalus on sagittal T1-weighted (**A**) and axial T2-weighted (**B**) MR images.

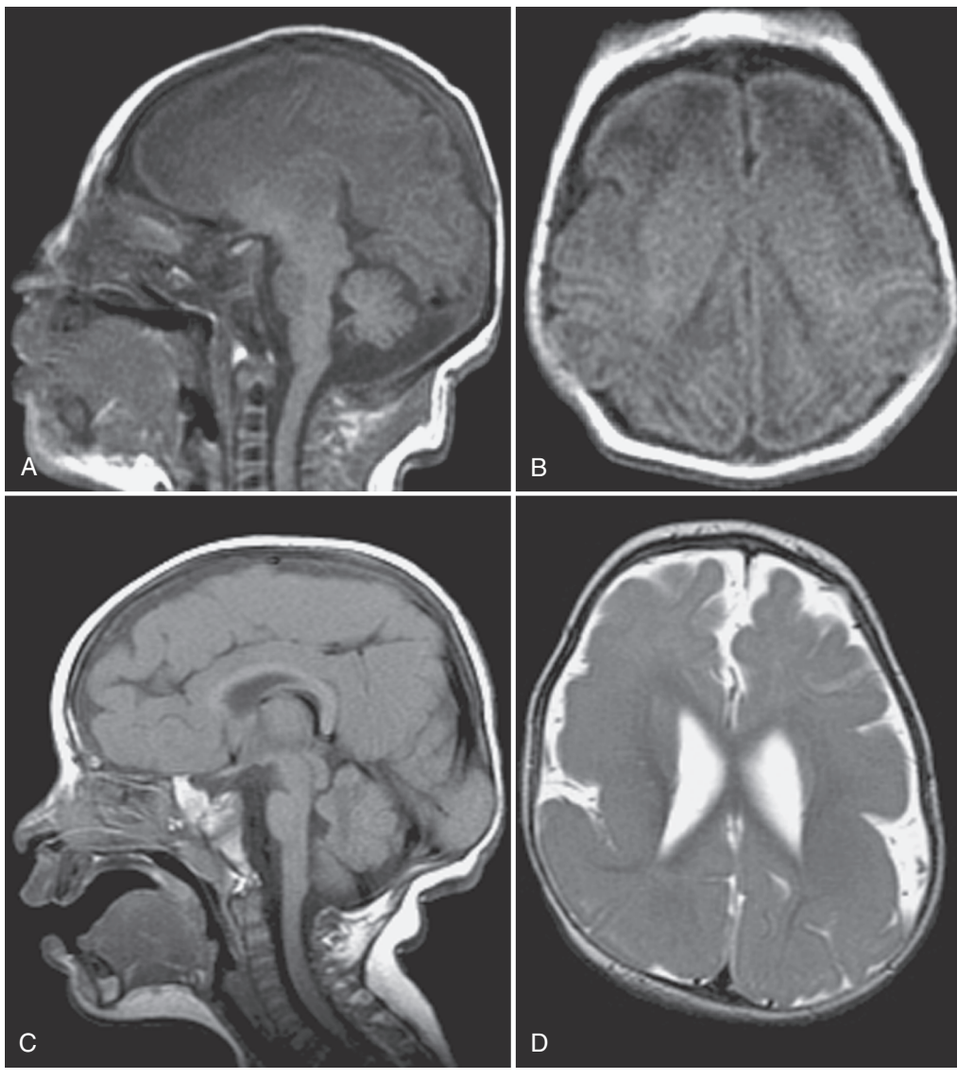

FIGURE 8-18. Agyria (lissencephaly) on sagittal (**A**) and axial (**B**) T1-weighted MR images. Pachygyria on sagittal T1-weighted (**C**) and axial T2-weighted (**D**) MR images.

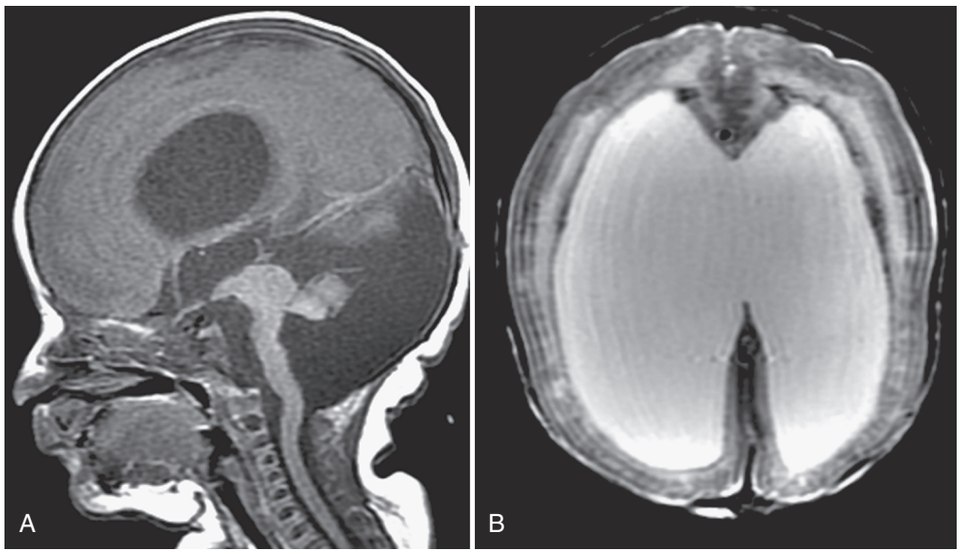

FIGURE 8-19. Cobblestone lissencephaly (Walker-Warburg syndrome) on sagittal T1-weighted (**A**) and axial T2-weighted (**B**) MR images.

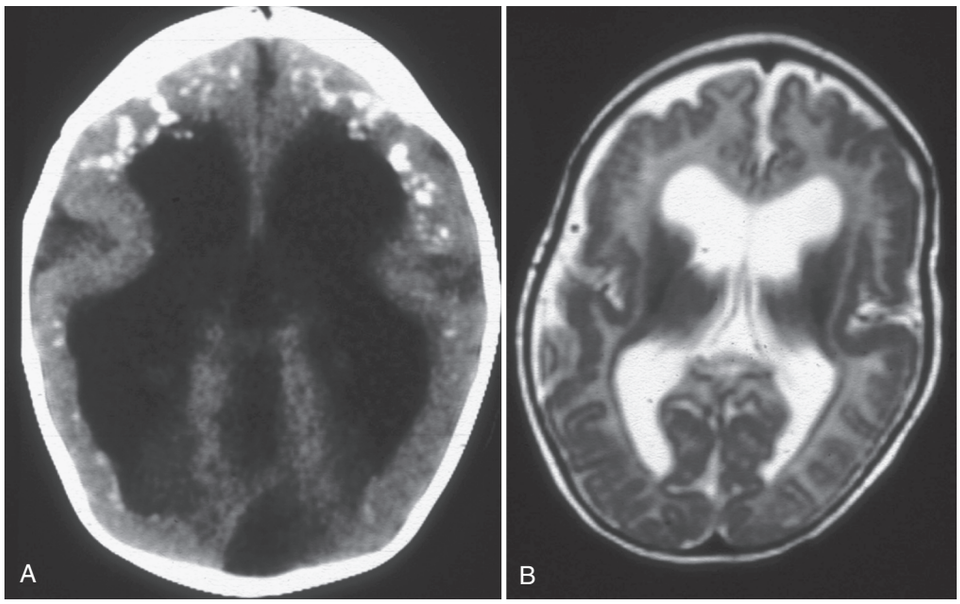

FIGURE 8-20. **A,** Cytomegalovirus infection with calcification on CT scan. **B**, Diffuse polymicrogyria on axial T2-weighted MR image.

of fetal life and continues into adulthood. However, these changes are most dramatic during the first 2 to 3 years of postconceptional life. MRI provides the best assessment of maturation, including evaluation of myelination based on T1 and T2 relaxation (see Fig. 8-1). The watery, unmyelinated white matter of the immature brain is hypointense on T1-weighted imaging (T1-hypointense) and hyperintense on T2-weighted imaging (T2-hyperintense). Myelinated areas appear T1-hyperintense and T2-hypointense, approaching an adult pattern after 18 to 24 months of postnatal age. At the same time, cortical maturation occurs and is manifest as progressive secondary and tertiary gyral and sulcal development along with frontal, temporal, and parietal opercularization about sylvian fissures to cover the insula (see Fig. 8-1).

The ability to diagnose a delay in maturation depends on recognition of the normal pattern at any given age. In general, normal myelination proceeds in a caudal to cephalad direction, which parallels sensory and motor development. CNS myelination first begins within the spinal cord and brainstem and progresses rapidly into the cerebellum, the midbrain, the posterior thalami, the posterior limb of the internal capsule, and deep white matter tracts of the corona radiata and centrum semiovale, leading to the paracentral cortical motor strips by 40 to 44 weeks' gestation. The optic tracts and radiations begin to myelinate early, usually appearing anteriorly within the first 2 to 3 months and extending to involve the calcarine cortex by 4 to 6 months. Myelination of the corpus callosum first begins within the splenium at 2 to 3 months and progresses anteriorly to the genu and rostrum by 6 to 8 months. Myelination of the centrum semiovale extends from a central focus, first posteriorly and finally anteriorly to the frontal cortex.

A number of conditions may result in underdevelopment and undermyelination, including malformative disorders (e.g., genetic), hypoxia-ischemia, infection, trauma, and metabolic diseases. The pattern of abnormal maturation is commonly nonspecific as to the etiology. Distinguishing cortical immaturity from dysmaturity, or delayed myelination from hypomyelination, demyelination,

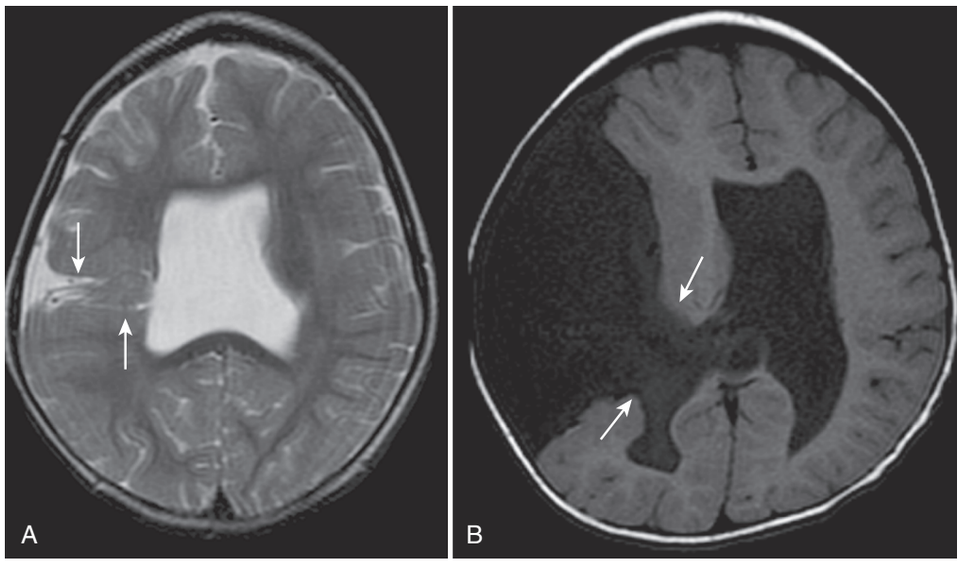

FIGURE 8-21. Schizencephaly (*arrows*) with polymicrogyria and absence of the septum pellucidum on axial MR images. **A,** Closed-lip schizencephaly on a T2-weighted image. **B,** Open-lip schizencephaly on a T1-weighted image.

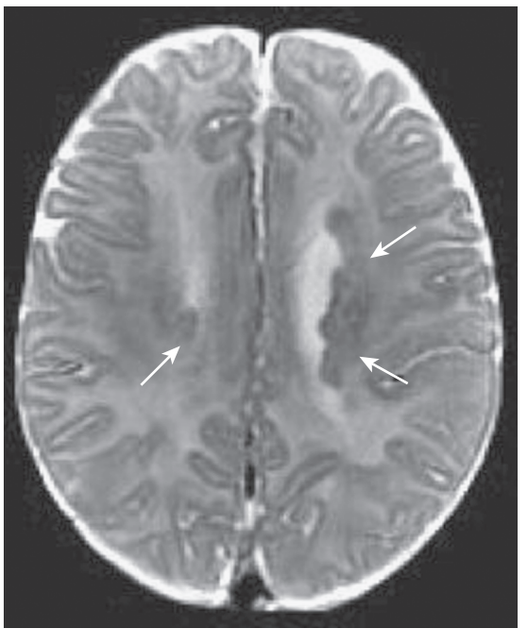

FIGURE 8-22. Neuronal heterotopia (*arrows*) on an axial T2-weighted MR image.

or dysmyelination, is often difficult. Therefore, it may be impossible from a single examination to distinguish an encephaloclastic and static process (e.g., postischemic) from a progressive and degenerative one (e.g., leukodystrophy). This issue may be clarified only by the clinical evaluation and follow-up MRI.

TRAUMA

The immaturity of the skull and brain during infancy is associated with patterns of traumatic injury that are special to this group. With further maturation, the manifestations of trauma in the older child and adolescent are similar to those in the adult. It is often not possible to distinguish accidental from nonaccidental injury (i.e., child abuse) on the basis of imaging findings.

Parturitional and Neonatal Injury

Neonatal extracranial hemorrhage may be associated with labor and delivery, including instrumentation (forceps, vacuum), coagulopathy, or both. These are the caput succedaneum, subgaleal hemorrhage, and cephalohematoma. Caput succedaneum is usually a self-limited subcutaneous hemorrhage. Subgaleal hemorrhage occurs beneath the galea aponeurotica of the occipitofrontalis muscle; the hemorrhage may be very large and extensive within this space and a potential cause of anemia or circulatory compromise (Fig. 8-27). A cephalohematoma is a subperiosteal hemorrhage. The bleeding is usually confined and may occasionally be associated with skull fractures. Over time, the lesion may calcify and may manifest as skull mass, but it usually disappears over a period of months to years.

Neonatal skull fractures are deformational in origin (e.g., impact) and may be linear, buckled, or depressed (Fig. 8-28). Linear fractures most frequently occur in the parietal region and may be associated with cephalohematoma. It may be difficult to distinguish a linear fracture from any of a number of normal skull variants (e.g., fissures, accessory sutures). Depressed fractures occur readily because of the immaturity of the cranial vault (i.e., "ping-pong" fracture). They are best evaluated with CT, especially for planning of surgical intervention. Occasionally, a congenital skull deformation, resulting from intrauterine forces (e.g., amniotic bands), may mimic a depressed fracture (see Fig. 8-28).

The intracranial trauma associated with the birth process (i.e., parturitional and/or coagulopathy) often results in small subarachnoid or subdural hemorrhages, especially along the tentorium and posterior falx (Fig. 8-29) about the dural venous sinuses. Such trauma may be difficult to distinguish from venous sinus thrombosis. Posterior fossa subdural hemorrhage may be associated with tentorial laceration, occipital osteodiastasis, or dural venous sinus injury. If it is massive, there may be brainstem compression or hydrocephalus. Neonatal supratentorial subarachnoid and subdural hemorrhages may be associated with injury to the falx or a superficial cerebral vein. An accompanying fracture may be present. There may be injury to the inferior sagittal sinus with interhemispheric hemorrhage, or tearing of a cortical vein with a convexity hemorrhage. Traumatic intracerebral or intraventricular hemorrhage is unusual, particularly in the absence of extracerebral hemorrhage. Brain injury may be directly or indirectly associated with parturitional trauma.

FIGURE 8-23. Agenesis corpus callosum on MR images: **A,** Fetal axial T2-weighted image. **B,** Neonatal sagittal T1-weighted image. **C,** Axial T2-weighted image showing Probst bundles (*arrows*).

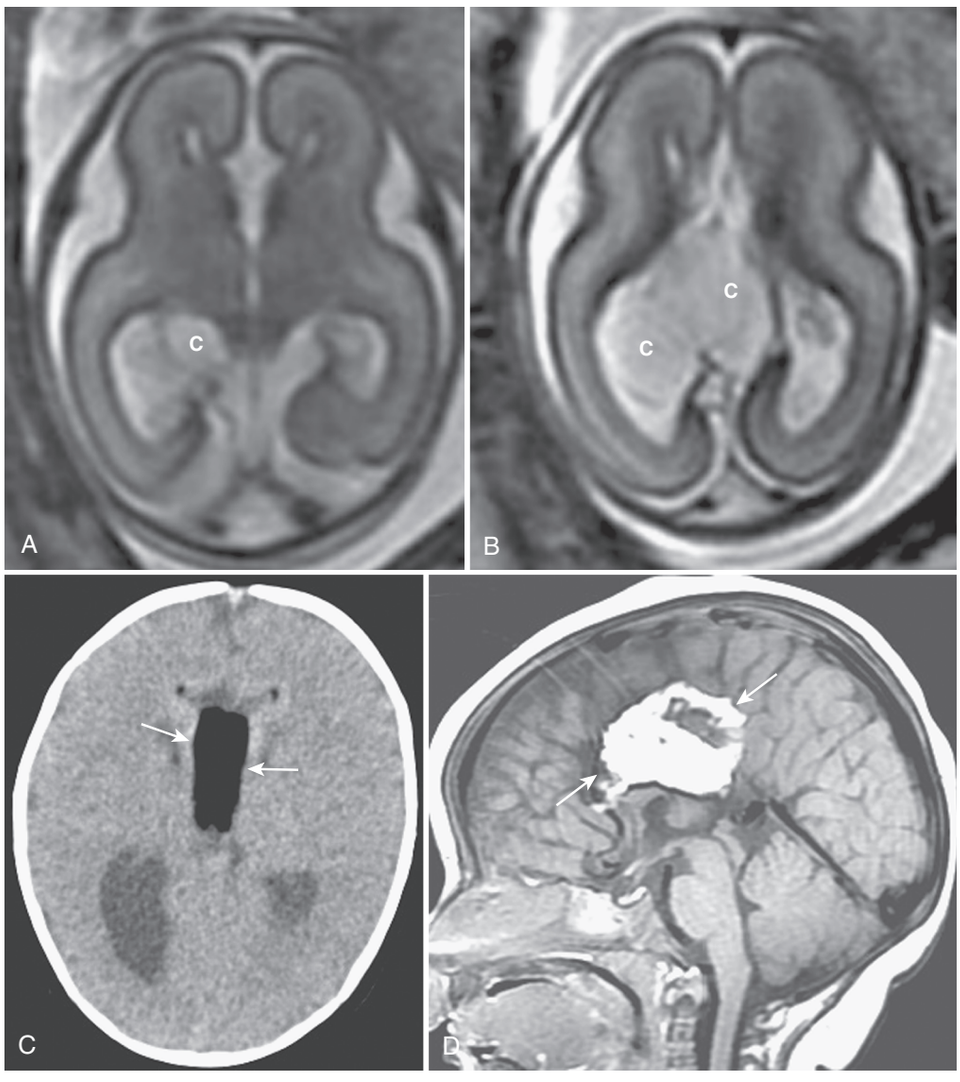

FIGURE 8-24. Agenesis corpus callosum with cyst (c) on fetal axial (**A,B**) T2-weighted MR images. Agenesis corpus callosum with lipoma (*arrows*) on axial CT scan (**C**) and sagittal T1-weighted image (**D**) in another neonate.

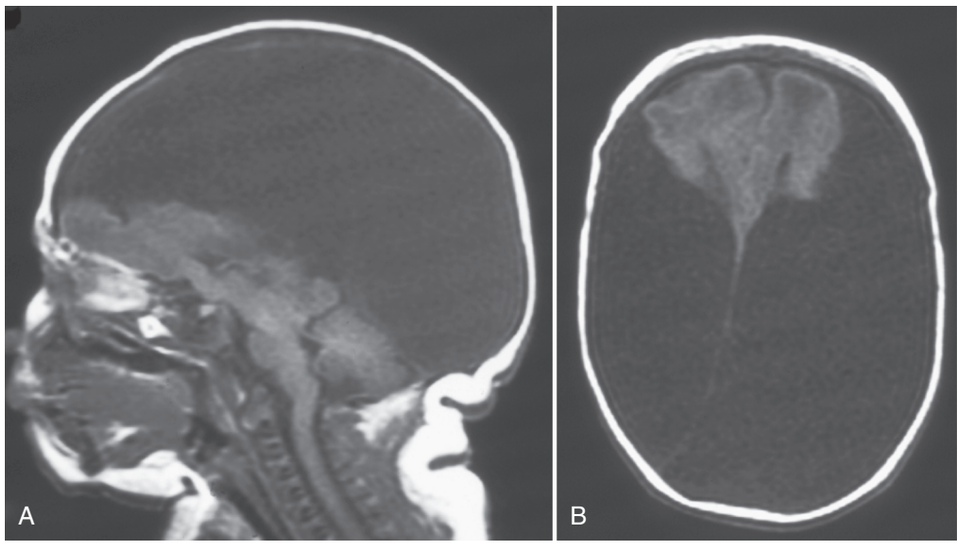

FIGURE 8-25. Hydranencephaly on sagittal (**A**) and axial (**B**) T1-weighted MR images.

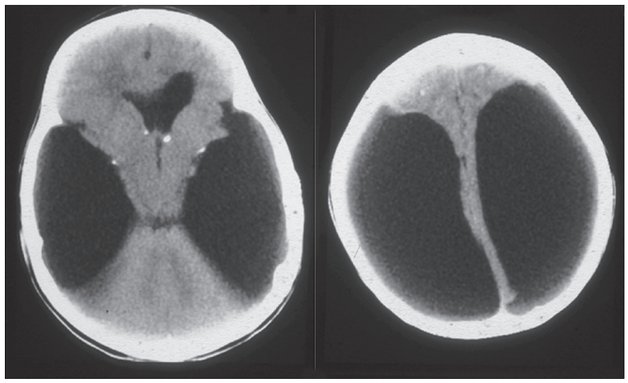

FIGURE 8-26. Congenital toxoplasmosis. CT scans show hydrocephalus, porencephaly, and calcifications.

Injury to the Infant, Child, and Adolescent

Skull Fractures

The dynamics of head trauma in childhood depend on the level of maturity and relate biomechanically to a spectrum from deformation to acceleration-deceleration regarding the relationships of brain tissues, vasculature, CSF, meninges, and skull. Trauma is often associated with deformation (i.e., impact), which may or may not produce a skull fracture. The brain of the infant is surrounded by large amounts of CSF that separate it from the cranial vault and base. Therefore, movement of the brain within the cranium may be considerable. Skull fracture may occur at the site of cranial inbending or as a secondary outbending. Suture diastasis may also be the result of such forces. Skull fractures, including simple fissure fractures and diastatic and/or depressed fractures, are relatively common in pediatric head trauma (see Fig. 8-28). However, skull fracture does not always indicate intracranial injury, nor does the absence of fracture exclude such injury. Multiple comminuted linear fractures may occur in infants without evidence of depression or sutural diastasis. Linear fractures may be straight or irregular. They may also be diastatic without being depressed. Healing of linear fracture in an infant or young child usually occurs over 3 to 6 months; it may require up to a year in older children and teenagers. Dural tears are present in approximately one third of children with depressed or diastatic fractures. There may be concomitant brain damage or an associated subdural or extradural hematoma. Surgical repair depends on the severity of deformity. Failed fracture healing or increasing diastasis—that is, growing fracture—suggests the presence of a leptomeningeal cyst. Often there are associated subgaleal and subdural collections along with underlying encephalomalacia. Occasionally, brain tissue may herniate into the defect or there may be a pseudoaneurysm.

Intracranial Hemorrhage

Hemorrhage is a common finding in acute intracranial injury in children. Extraparenchymal hemorrhages may be categorized by their subarachnoid, subdural, or epidural location. Any or all of the compartments may be involved. Subarachnoid hemorrhage is a common finding with head injury and often accompanies parenchymal trauma. CT demonstrates subarachnoid hemorrhage as an area of high density extending into the sulci or layering along the tentorium (see Fig. 8-29).

Subdural hematomas usually result from a "tear" in the bridging veins. These veins are particularly vulnerable to injury in the infant owing to the relatively soft consistency of the immature brain and the prominent extracerebral subarachnoid spaces. They may be unilateral or bilateral. Imaging often reveals a crescentic collection (Fig. 8-30). In the acute phase, the hemorrhages are hyperdense on CT. Hyperacute hemorrhage (i.e., unclotted) may be isodense to low-density. Isolated or associated traumatic arachnoid tear may produce acute subdural hygromas which may be of CSF density on CT and may follow CSF intensity on MRI. After 7 to 10 days, the subdural hemorrhages usually appear isodense or of low density on CT. It is not possible, in a mixed-density collection, to distinguish a hyperacute-acute hemorrhage from a chronic collection associated with acute rehemorrhage (Figs. 8-30 and 8-31). MRI may provide better precision regarding the timing (Table 8-3).

On occasion it may be difficult to distinguish chronic subdural hematoma from benign extracerebral collection (BEC) in an infant with macrocephaly, particularly on CT (see Fig. 8-30). The differentiation, however, has significant implications because subdural hematoma is often of a traumatic origin and BEC is a self-limited, often familial, condition resulting from immaturity of the arachnoid granulations (decreased CSF absorption rate).

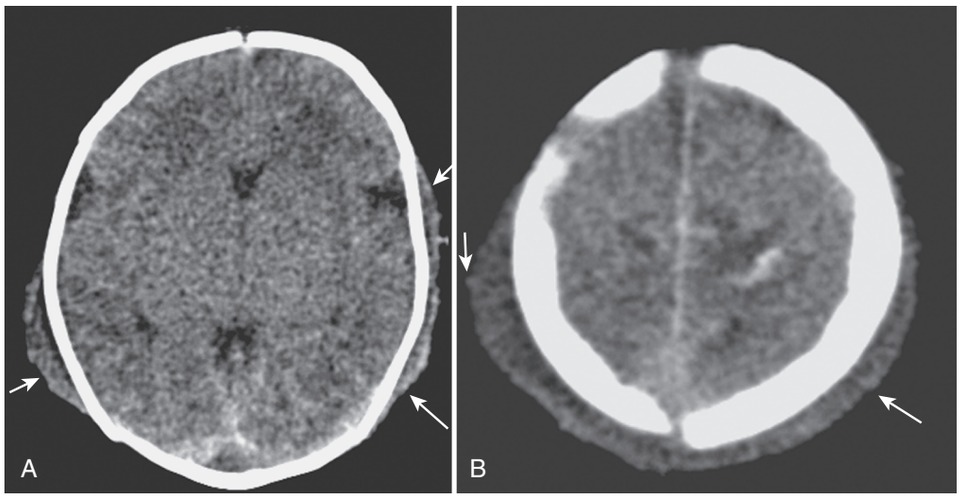

FIGURE 8-27. **A** and **B**, Subgaleal collections (*arrows*) on neonatal CT scans.

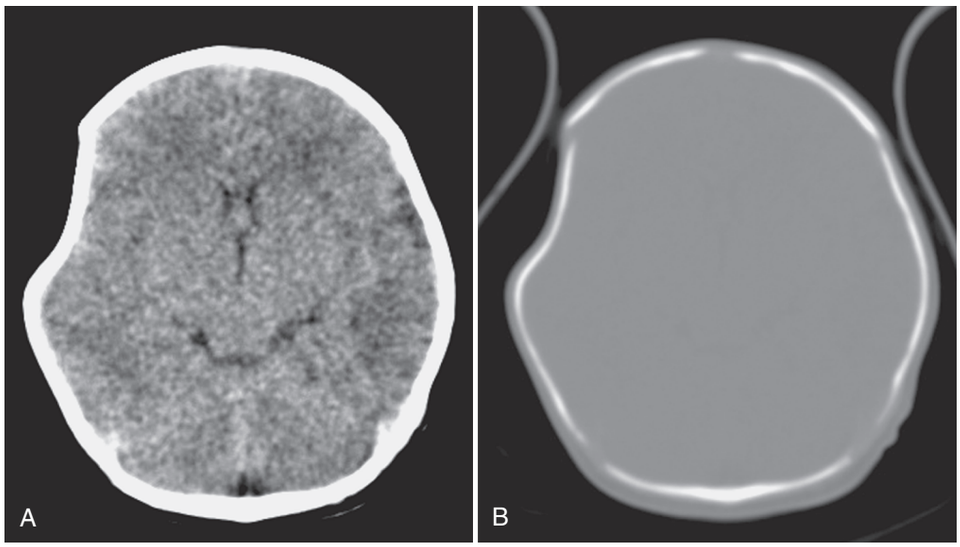

FIGURE 8-28. **A** and **B**, CT scans of cranial depression in a newborn.

The two conditions may coexist on a spontaneous, accidental, or nonaccidental basis (see Fig. 8-30). BEC is usually associated with mild prominence of the ventricular system and extracerebral CSF spaces, especially over the frontal lobes. It typically resolves by 2 years of age. The gyri are not compressed, the fluid follows CSF on all MRI sequences, and the cortical vessels traverse the collections. Chronic subdural hematomas are usually of non-CSF intensity, may compress the gyri, and displace the cortical vessels toward the brain surface.

Subarachnoid hemorrhage is a common finding with head injury and often accompanies parenchymal trauma. CT demonstrates subarachnoid hemorrhage as an area of high density extending into the sulci or layering along the tentorium. Epidural hematoma may be of arterial origin (e.g., middle meningeal artery) or venous origin. Therefore, the presentation may be acute (e.g., arterial) or subacute (e.g., venous). CT usually shows a lentiform, high-density collection that is often confined by the sutures. Low-density appearance or fluid-fluid levels may indicate active hemorrhage (Fig. 8-32). An accompanying fracture is often present. The intensities of the lesion on MRI depend on the age of the hemorrhage at the time of imaging (Table 8-3).

Brain Injury

The range of brain injury includes acute to subacute injuries (e.g., contusion, shear injury, intracerebral hemorrhage, edema, hypoxia-ischemia) and chronic injuries (e.g., atrophy, encephalomalacia, mineralization). Contusions may be hemorrhagic or nonhemorrhagic, typically occur in cortical gray matter along brain surfaces next to hard tissues (e.g., bone, dura), and may appear near or opposite the point of impact (i.e., coup or contrecoup, respectively). Shear injury occurs deeper in the brain within the subcortical and periventricular white matter at gray matter–white matter junctions, is more often nonhemorrhagic than hemorrhagic, and may appear as gross tears or as more subtle axonal injury. This injury has been previously referred to as "diffuse axonal injury" but is more properly termed *multifocal or traumatic axonal injury*, because diffuse axonal injury is more characteristic of hypoxic-ischemic damage.

Edema or swelling may be traumatic, hyperemic, hypoxic-ischemic, or related to other factors (e.g., seizures, metabolic). Traumatic edema is related to direct traumatic effects such as contusion, shear, and vascular injuries (e.g., associated with dissection or herniation). Malignant brain swelling in children with

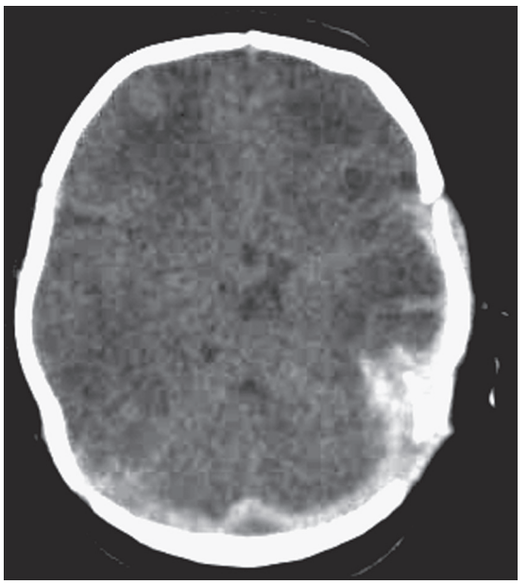

FIGURE 8-29. CT scan showing birth-related high-density hemorrhage along the tentorium and falx in a neonate.

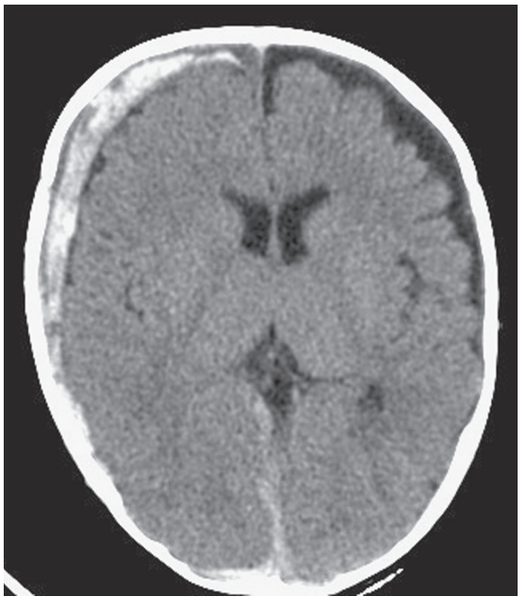

FIGURE 8-30. CT scan demonstrating high-density right subdural hematoma superimposed upon low-density benign extracerebral collections in a premature infant.

head trauma may also occur because of cerebrovascular congestion (i.e., hyperemia) as a vasoreactive or an autoregulatory phenomenon (see Fig. 8-31). Global hypoxia (e.g., apnea, respiratory failure) or ischemia (e.g., cardiovascular failure) is likely a major cause of, or contributor to, brain edema in the child with head trauma. Other contributors to edema or swelling include such complicating factors as seizures (e.g., status epilepticus), fluid-electrolyte imbalance, and other systemic or metabolic derangements (e.g., hypoglycemia). The type (e.g., cytotoxic, vasogenic) and pattern of edema conforms to the nature and distribution of the causative insult. Traumatic edema is often focal or multifocal (e.g., in areas of contusion, shear, or hemorrhage). Hyperemic edema is often diffuse and may appear early as accentuated gray matter–white

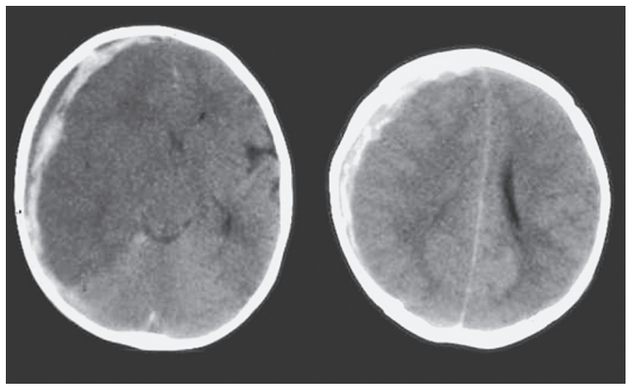

FIGURE 8-31. CT scans of acute-hyperacute right subdural hematoma and cerebral edema in an infant.

matter differentiation. Hypoxic-ischemic injury may have a diffuse appearance acutely with decreased gray-white differentiation throughout the cerebrum (e.g., "white cerebellum" sign; Fig. 8-33) and then evolve to a more specific pattern—for example, border zone or watershed, basal ganglia/thalamic, cerebral white matter necrosis, and reversal sign (reversed gray-white differentiation; Fig. 8-33). The subacute to chronic sequelae of traumatic brain injury include hydrocephalus, atrophy, encephalomalacia, gliosis, mineralization, and chronic extracerebral collections.

Vascular Trauma

Vascular trauma may result in dissection or pseudoaneurysms. The vascular injury may be the result of penetrating or nonpenetrating trauma or may be spontaneous (i.e., no history of significant trauma). Dissection of the internal carotid artery typically involves the cervical or supraclinoid segments. Dissection of the vertebrobasilar system most commonly involves the distal cervical segments of the vertebral artery at the C1 to C2 level. Intracranial or multiple dissections are rare. Dissection often results in distal embolic infarction. Pseudoaneurysms may be associated with hemorrhage. Dissection is demonstrated on MRA, CTA, or angiography as vascular narrowing or occlusion with or without a pseudoaneurysm (Fig. 8-34). A beaded vascular appearance may indicate an underlying arteriopathy (e.g., fibromuscular dysplasia).

Nonaccidental Injury

Intracranial injury is reportedly the leading cause of death and disability in nonaccidental injury (NAI)—that is, inflicted injury or child abuse (also called trauma X). The spectrum of lesions encountered as a result of NAI is similar to those produced by accidental injury (see Figs. 8-28 to 8-34). Fractures, subdural and subarachnoid hemorrhage, cortical contusion, axonal shear injury, and cerebral edema may all result from NAI or accidental trauma. NAI may be suspected when the extent of injury is excessive for the given history or when injuries of varying ages are present. This statement includes injury by strangulation or suffocation. CNS lesions previously reported to be suspicious for NAI are the interhemispheric subdural hematoma, retinal hemorrhages, and subdural hematoma, particularly when associated with characteristic skeletal fractures demonstrated by bone survey. However, such findings may also be seen with accidental trauma and certain medical conditions. "Mimics" of NAI (e.g., dural and retinal hemorrhages) include accidental trauma (e.g., short falls), hypoxia-ischemia (e.g., dysphagic choking), coagulopathies, vascular diseases (e.g., venous thrombosis), infectious or postinfectious conditions (e.g., after vaccination), metabolic disorders, neoplastic diseases, certain therapies, and some congenital and dysplastic disorders (e.g., vitamin C, D, and K deficiencies, osteogenesis imperfecta). CT and MRI both assist with the evaluation of pattern of injury and timing issues. A timely and thorough clinical,

TABLE 8-3. Magnetic Resonance Imaging of Intracranial Hemorrhage and Thrombosis

Stage of Disease	Features and Timing	T1-Weighted Imaging	T2-Weighted Imaging	Biochemical Form(s)
Hyperacute	Edema <24 hours	Isointense-low I	High I	OxyHb
Acute	Edema 1-3 days	Isointense-low I	Low I	DeoxyHb
Early subacute	Edema 3-7 days	High I	Low I	MetHb, intracellular
Late subacute	No edema 1-2 weeks	High I	High I	MetHb, extracellular
Early chronic	No edema >2 weeks	High I	High I	Transferrin
Chronic	Cavity	Isointense-low I	Low I	Ferritin, hemosiderin

Hb, hemoglobin; I, signal intensity.

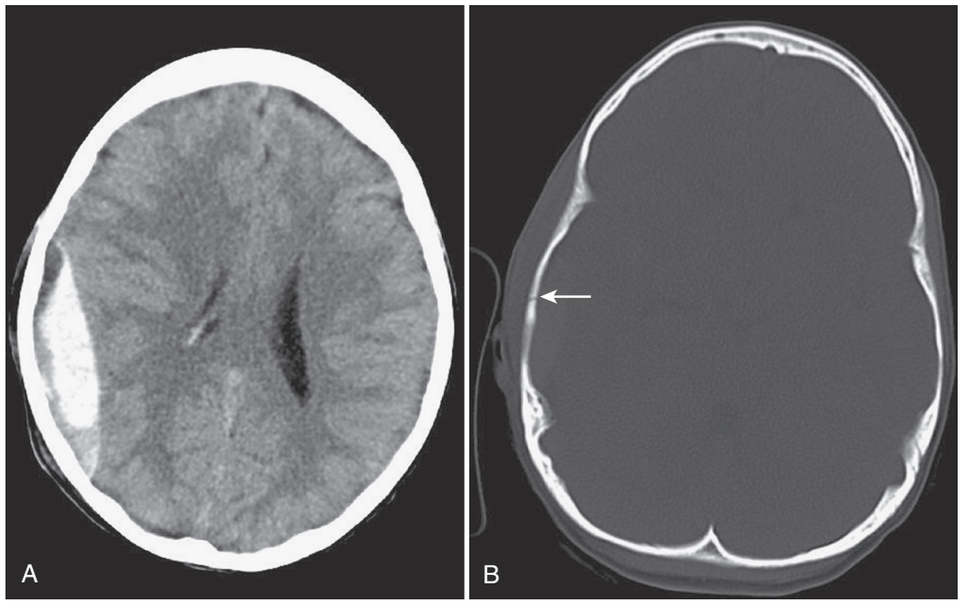

FIGURE 8-32. **A** and **B,** CT scans of linear right temporoparietal skull fracture (*arrow*) with hyperacute epidural hematoma.

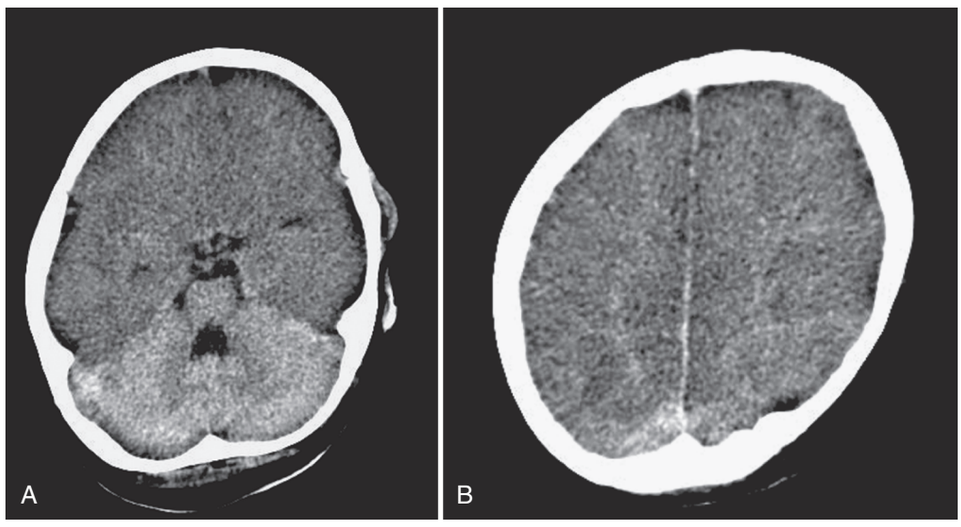

FIGURE 8-33. CT scans of hypoxia-ischemia injury. **A,** The "white cerebellum sign." **B,** The "reversal sign."

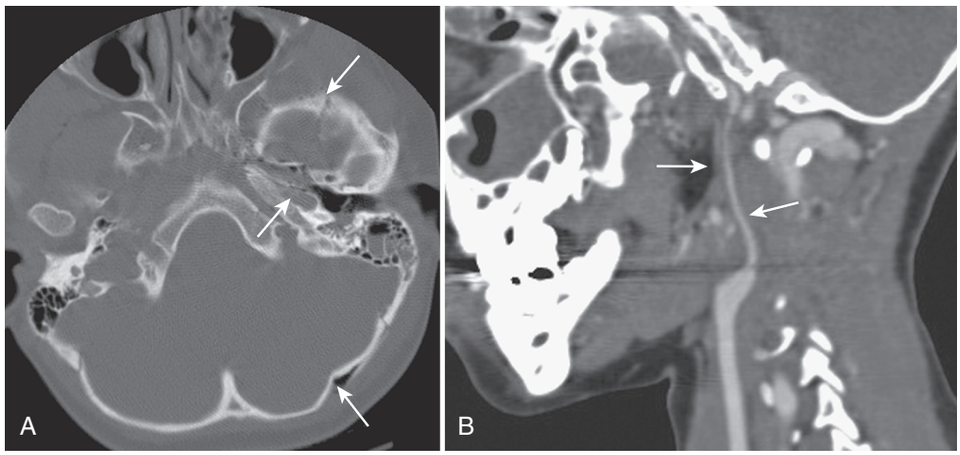

FIGURE 8-34. **A,** CT scan shows skull base fracture (*arrows*) from the occipital bone through the mastoid, petrous, and carotid canal. **B,** Sagittal reformatted CT angiogram shows internal carotid arterial dissection with narrowing (*arrows*).

radiologic, and biomechanical evaluation of childhood CNS trauma and alleged NAI, in addition to the social service assessment, may make the difference between appropriate child protection and an improper breakup of the family or a wrongful indictment and conviction.

INTRACRANIAL INFECTIONS AND INFLAMMATORY DISEASE

Congenital and Neonatal Infections

The most common congenital and neonatal infections involving the CNS are those related to the TORCH agents—that is, toxoplasmosis (TXP), other (e.g., syphilis), rubella, CMV, herpes simplex 2 (HSV-2), human immunodeficiency virus type 1 (HIV-1)—and bacterial infections. TXP, rubella, CMV, and HIV are transmitted to the fetus through the placenta. HSV-2 and bacterial infections are often acquired via the birth canal during parturition. The manifestations of congenital and neonatal infections depend more on the timing than on the agent. Infections in the first trimester and early second trimester (e.g., CMV) commonly result in malformations. Later infections (e.g., TXP) are often associated with encephaloclastic lesions, hydrocephalus, undermyelination, calcification, and gliosis. Transgestational infections (e.g., CMV) may result in combined malformative and destructive lesions. Rarer congenital infections (e.g., congenital lymphocytic choriomeningitis viral syndrome) may mimic the findings of CMV or TXP infection.

Cytomegalovirus

CMV is the most common of the TORCH infections. Clinical manifestations include microcephaly, hearing loss, seizures, chorioretinitis, developmental delay, hepatosplenomegaly, and petechiae. Depending on the timing of the infection, the result is varying degrees of cortical dysgenesis (e.g., lissencephaly, heterotopia, polymicrogyria; see Fig. 8-20), ventriculomegaly, gliosis, delayed myelination, cysts, calcifications, or cerebellar hypoplasia. The calcifications are typically periventricular and are best shown by CT (see Fig. 8-20).

Toxoplasmosis

TXP is an intracellular infection with a parasite (*Toxoplasma gondii*) that usually occurs by maternal ingestion of oocytes from undercooked pork or beef and transplacental spread to the fetus. The second most common TORCH infection, it manifests as seizures, mental retardation, and chorioretinitis. Calcifications are common and more random in distribution, including periventricular, cortical, and basal ganglia. Hydrocephalus often results from the granulomatous meningeal or ependymal reaction, including aqueductal stenosis (see Fig. 8-26). Cortical dysgenesis/dysplasia is infrequent. Occasionally, there is porencephaly or hydranencephaly.

Rubella

Congenital rubella viral infection has decreased in prevalence as the result of maternal screening and immunization. Infections occurring early in pregnancy are more likely to produce disease, including microcephaly, infarctions, chorioretinitis, cataracts, glaucoma, sensorineural hearing loss, and cardiac disease. Imaging often shows calcifications in the basal ganglia and cortex, infarctions, and undermyelination.

Herpes Simplex Virus Type 2

Neonatal HSV-2 infection (sexually acquired form) usually results from maternal genital transmission during parturition. Characteristic manifestations include neonatal cutaneous, ocular, and mucous membrane lesions or jaundice, fever, and respiratory distress. Meningoencephalitis may result in seizures or lethargy. Imaging shows that the involvement tends to be diffuse, multifocal, or asymmetric; the findings include edema, petechial hemorrhages, and enhancement with contrast agent (Fig. 8-35). Restricted diffusion may be seen early. The sequelae include gliosis, undermyelination, and multicystic encephalomalacia.

Syphilis

Fetal syphilis infection (with the spirochete *Treponema pallidum*) is most commonly associated with maternal secondary syphilis. Clinical signs are condylomata, lymphadenopathy, meningitis, periostitis, and osteochondritis. Basal meningitis with perivascular extension occurs and may be associated with hydrocephalus, but parenchymal lesions are uncommon. The meningovascular involvement rarely results in aneurysm and intracranial hemorrhage.

Human Immunodeficiency Virus Type 1

HIV-1 infection is often a congenitally acquired disease. It may also occur through transfusions with infected blood products. The virus is both lymphotropic and neurotropic. Symptoms are variable and usually delayed for a few months after the initial infection. The acquired immunodeficiency syndrome (AIDS) is the most severe form. CNS disease usually results from HIV infection alone (e.g., leukoencephalopathy). Less often there may be associated opportunistic infections (e.g., TXP, CMV, *Mycobacterium avium-intracellulare*, and papovavirus) or neoplasia (e.g., lymphoma). Thromboses and embolization with infarction may result from an aneurysmal arteriopathy of the circle of Willis. Hemorrhage may rarely occur, especially if there is thrombocytopenia. Progressive encephalopathy is common, along with movement disorder, ataxia, developmental delay, and microcephaly. Imaging

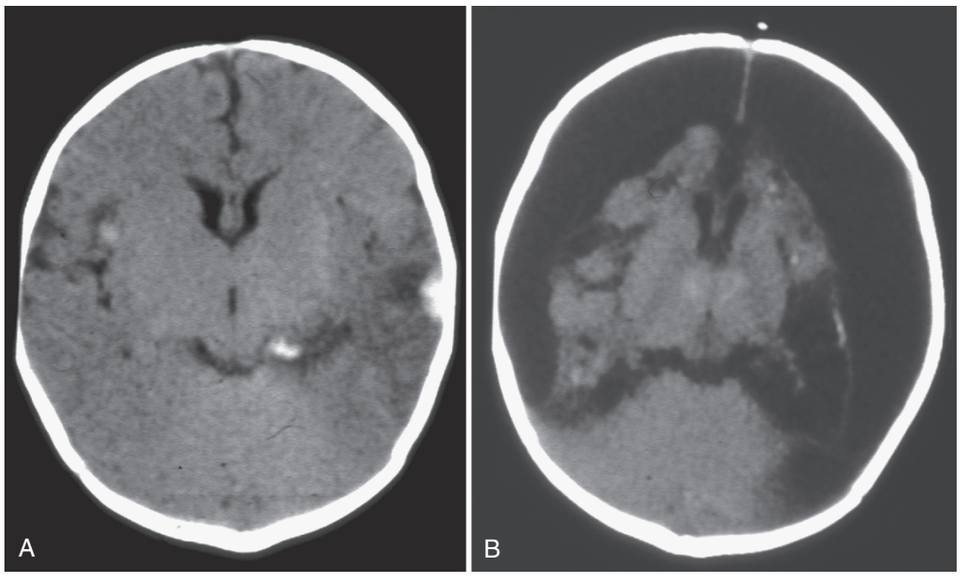

FIGURE 8-35. Herpes simplex virus type 2 encephalitis on CT. **A,** Acute phase including hemorrhages. **B,** Chronic phase with atrophy and calcifications.

shows atrophy, symmetric undermyelination/demyelination, and calcification (e.g., basal ganglia, frontal lobe, cerebellum). Lymphadenopathy and parotid lymphoepithelial cysts are also characteristic. Superimposed infection or tumor occurs less commonly in the childhood form and may produce one or more focal lesions. A ring-enhancing lesion may suggest TXP. A T2-hypointense lesion with marked ring or solid enhancement suggests lymphoma. Areas of asymmetric demyelination may indicate progressive multifocal leukoencephalopathy (PML).

Neonatal Meningitis

Neonatal meningitis is most commonly due to infection with group B streptococcus (GBS), *Escherichia coli*, or *Listeria monocytogenes*. Other bacterial causes include *Staphylococcus*, *Proteus*, and *Pseudomonas*. Newborn meningitis may be related to maternal urogenital infection, premature membrane rupture, or nosocomial conditions. The immaturity of the CNS and immune system predisposes the neonate to severe injury. The clinical onset (e.g., of GBS) may be early postnatal or may be delayed for a few months. Hematogenous infection often produces purulent ventriculitis and arachnoiditis. Venous or arterial occlusions (vasculitis, thrombosis) often result in hemorrhagic or ischemic infarctions. Hydrocephalus is also common. Imaging may show edema, ischemic or hemorrhagic infarction, and ependymal or leptomeningeal enhancement. With ventriculitis, US may show abnormal intraventricular and periventricular echoes plus ventricular wall thickening. In chronic infection, there may be hydrocephalus, ventricular encystment, atrophy, calcification, cavitations, or encephalomalacia. Rim-enhancing necrotic cavitation or abscess may rarely occur (e.g., with *Citrobacter* infection; Fig. 8-36).

Suppurative Infections

Osteomyelitis

Osteomyelitis of the skull is rare in childhood and may be primary (tuberculosis, fungal, syphilis) or secondary (e.g., bacterial from sinusitis, mastoiditis, cellulitis, sepsis, trauma, or surgery). PF/CR or CT may show lytic destruction or soft-tissue swelling. CT or MRI may show associated intracranial suppuration or venous thrombosis (Fig. 8-37). Sclerosis may appear with chronic infection. Radionuclide imaging may be helpful in selected cases.

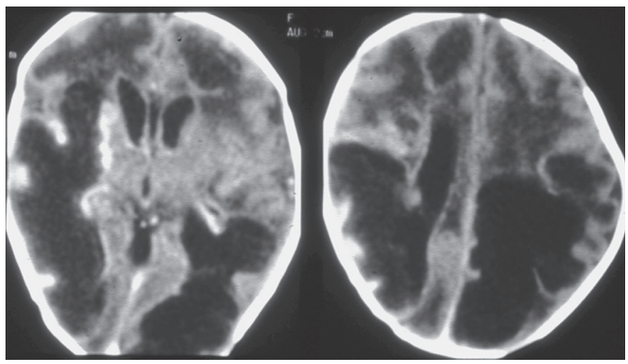

FIGURE 8-36. *Citrobacter* meningitis. CT scans show enhancing abscesses, ventriculitis, and hydrocephalus.

Meningitis

Meningitis may be either bacterial (purulent, suppurative, or septic meningitis) or viral (aseptic meningitis) in origin. Brain involvement results in cerebritis or meningoencephalitis. Meningitis from *Haemophilus influenzae* type B infection in older infants and young children has been reduced in prevalence by immunization. In older children, meningitis is often due to *Streptococcus pneumoniae* or *Neisseria meningitides*. Infections (e.g., *Staphylococcus aureus* or *Staphylococcus epidermidis*) may also be associated with ventricular shunt malfunction or dermal sinus. Meningitis in older children may be hematogenous or due to direct spread from adjacent mastoiditis or sinusitis, CSF leak, congenital or acquired defects, trauma, or surgery. Fever, meningismus, headache, seizures, and photophobia may be present. Vasculitis or thrombosis may produce arterial or venous infarction. Subdural effusions are often small and bilateral but may be asymmetric or unilateral. Surgical intervention may be considered for large or purulent collections.

Recurrent meningitis may suggest a parameningeal focus (e.g., mastoiditis, sinusitis) or abnormal communication (e.g., traumatic fistula, dermal sinus, cephalocele, inner ear anomaly, or primitive neurenteric connection). Noninfectious causes of meningitis in childhood include leukemia and disseminated CNS neoplasia (e.g., medulloblastoma). Imaging findings for meningitis are often

negative in the acute stage. Other findings in purulent meningitis include subarachnoid or ventricular enlargement, subdural effusion, ependymal or leptomeningeal enhancement, and single or multiple focal infarctions (Fig. 8-38). Hemorrhagic infarction may result from cortical venous or dural sinus thrombosis. The sequelae may include atrophy, encephalomalacia, or hydrocephalus.

Cerebritis, Abscess, and Empyema

Suppurative infections are usually bacterial and may be bloodborne (e.g., systemic infection or a remote source) or occur from direct inoculation (e.g., trauma), contiguous infection (e.g., sinusitis), or septic thrombophlebitis of bridging veins (see Fig. 8-37). At-risk children include those with uncorrected or palliated cyanotic heart disease, pulmonary arteriovenous malformations, chronic pulmonary conditions (e.g., cystic fibrosis), and immune-compromised states (oncologic treatment, transplantation). Infecting agents include *S. aureus*, streptococci, gram-negative bacilli, anaerobes, and, rarely, *Nocardia*, *Mycobacterium tuberculosis*, or fungi. If such infections are untreated, the result may be cerebritis, abscess, or empyema.

In cerebritis, there is inflammation, which progresses to tissue necrosis and edema. Without treatment, the inflammation may evolve to abscess (single or multiple) with collagenous encapsulation over 1 to 2 weeks. Antibiotic therapy alone may be ineffective, and surgical drainage or excision may be warranted. In early cerebritis, edema (hypodensity, T2/FLAIR hyperintensity) and irregular enhancement may be present. With evolution, the necrosis and abscess are more defined. The abscess rim becomes T1-hyperintense and then T2-hypointense. The center typically shows restricted diffusion. Intense rim enhancement progresses with chronicity.

Epidural abscess and subdural empyema occur more often in teenagers than in younger children, and more often with sinusitis than with mastoiditis (see Fig. 8-37). The overlying collection may be small or may have a mass effect (Fig. 8-39). Associated brain edema, cerebritis, infarction, or abscess may occur. Imaging demonstrates crescentic or lentiform extracerebral collections with peripheral enhancement and restricted diffusion.

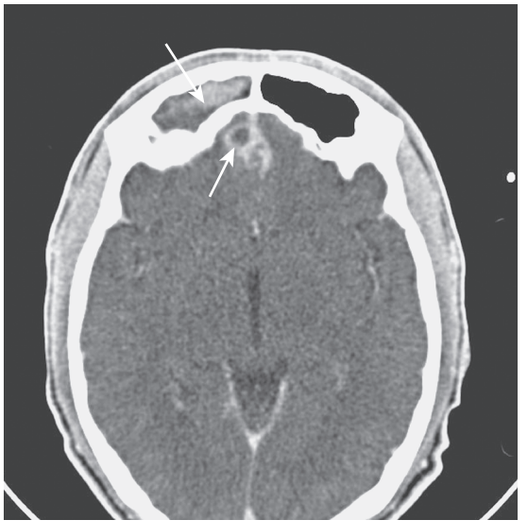

FIGURE 8-37. Frontal sinusitis (*upper arrow*) with subdural empyema and cerebral abscess (*lower arrow*) on enhanced CT scan.

The Encephalitides

Encephalitis, meningoencephalitis, leukoencephalitis, cerebellitis, and encephalomyelitis may be the result of a primary viral infection or an immunologic reaction to prior infection or vaccination (i.e., acute disseminated encephalomyelitis [ADEM]). Viral infection may occur sporadically (e.g., HSV-1, HIV, Ebstein-Barr virus [EBV], *Mycoplasma*) or in epidemics (e.g., spread by ticks, mosquitoes). The major involvement may be meningeal (i.e., aseptic meningitis, due to mumps or coxsackievirus), gray matter (e.g., HSV-1, arboviruses, rabies, Rasmussen encephalitis), or white matter (e.g., eastern and western equine virus, HIV, ADEM, PML, subacute sclerosing panencephalitis [SSPE]). Reye syndrome is an uncommon parainfectious encephalopathy associated with viral illness, salicylate intake, hepatotoxicity, and cerebral edema. Although the clinical and imaging findings in the encephalitides are often nonspecific, some processes may have characteristic features. The differentiation of primary viral encephalitis (usually gray matter involvement) from ADEM (predominant white matter involvement) is important, because the former may require antiviral therapy and the latter may respond only to corticosteroids.

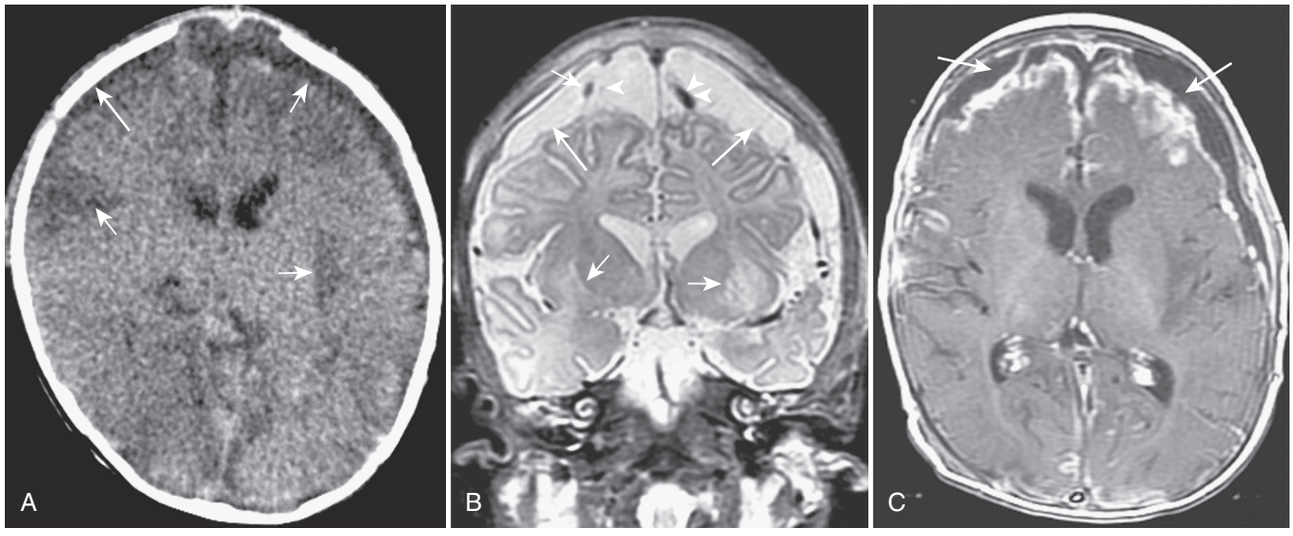

FIGURE 8-38. Pneumococcal meningitis. CT scan (**A**) and coronal T2-weighted (**B**) and gadolinium-enhanced T1-weighted (**C**) MR images demonstrate enhancing subdural collections (**A** to **C,** *top long and short arrows*), venous thromboses (**B,** *top short arrows and arrowheads*), and infarctions (**A** and **B**, *bottom short arrows*).

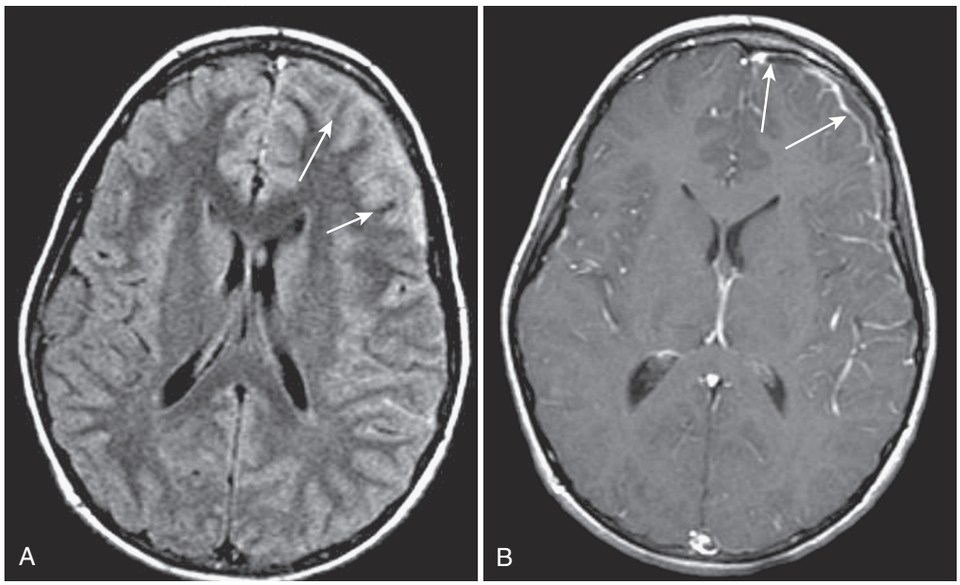

Figure 8-39. Left frontal cerebritis on axial FLAIR MRI (*arrows* in **A**) associated with left frontal subdural empyema on axial gadolinium-enhanced T1-MRI (*arrows* in **B**).

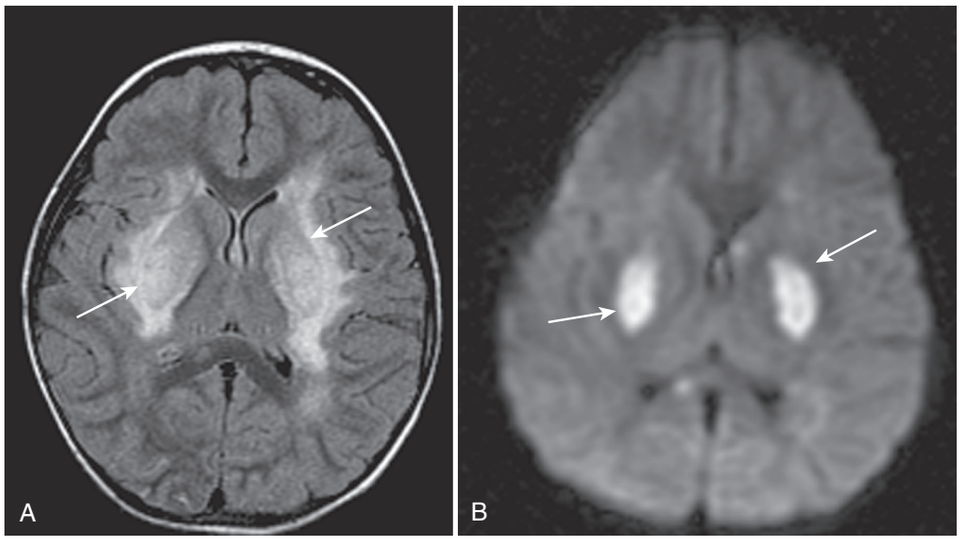

Figure 8-40. Viral encephalitis with bilateral subinsular/basal ganglia involvement (*arrows*) on MRI. **A,** Axial FLAIR image. **B**, Diffusion-weighted image shows reduced diffusion.

Herpes Simplex Virus Type 1

HSV-1 is probably the most common cause of sporadic encephalitis in childhood and is usually associated with orofacial herpes. CNS disease most often results from reactivation of a latent infection involving the gasserian ganglion and trigeminal nerve branches. The necrotic or hemorrhagic meningoencephalitis involves one or both temporal lobes, often spreads to the subfrontal region and insula, but spares the basal ganglia. Imaging findings may be negative early or there may be CT hypodensity, T2 hyperintensity, leptomeningeal or cortical enhancement, and petechial hemorrhage. Reduced or restricted diffusion may also be seen. Other types of encephalitis may involve the cerebral cortex or basal ganglia (e.g., EBV, *Mycoplasma*, Japanese; Fig. 8-40), the brainstem, or the cerebellum (Fig. 8-41).

Acute Disseminated Encephalomyelitis

ADEM is a postinfectious or parainfectious inflammatory condition of the brain or spinal cord that primarily involves white matter (i.e., demyelination). It probably represents an immunologic response to a viral infection. Seizures, lethargy, or neurologic deficit often arise several days following a viral infection or immunization (e.g., measles, mumps, chickenpox, rubella, or pertussis). Complete recovery is common, and corticosteroid therapy may help. Occasionally there may be residual or recurrent disease. In such cases, it may difficult to distinguish ADEM from vasculitis or multiple sclerosis, particularly if there is optic pathway involvement. Multifocal or diffuse CT hypodensity or T2/FLAIR hyperintensity is seen in the cerebral white matter, brainstem, or cerebellum (Fig. 8-42; see Fig. 8-41). Basal ganglia and thalamic involvement may also be present. Enhancement with a contrast agent is variable, but may be very prominent. ADEM must be distinguished from other infectious and postinfectious leukoencephalopathies (as mentioned previously) as well as from metabolic disorders (e.g., leukodystrophies), toxic reactions (e.g., methotrexate, cyclosporin), and reversible conditions (e.g., hypertensive, posterior reversible leukoencephalopathy).

Cerebellitis

Cerebellitis is very common in childhood, may be viral or postviral (e.g., ADEM), and must be distinguished from neoplasm (see Fig. 8-41). Persistent ataxia is a common presentation. CT findings may be negative or unilateral or bilateral hypodensities

may be seen. MRI findings are more often abnormal, with T2/FLAIR hyperintensities. Enhancement with contrast agents is variable. With severe swelling there may be upward or downward herniation and/or hydrocephalus.

Rasmussen Encephalitis

Rasmussen encephalitis is a chronic focal encephalitis that may be viral, postviral, or autoimmune in origin. Intractable focal seizures (epilepsy partialis continua) are characteristic. Imaging shows early edema followed by progressive regional or hemispheric atrophy (including crossed cerebellar diaschisis). Hemispherectomy may be necessary for seizure control.

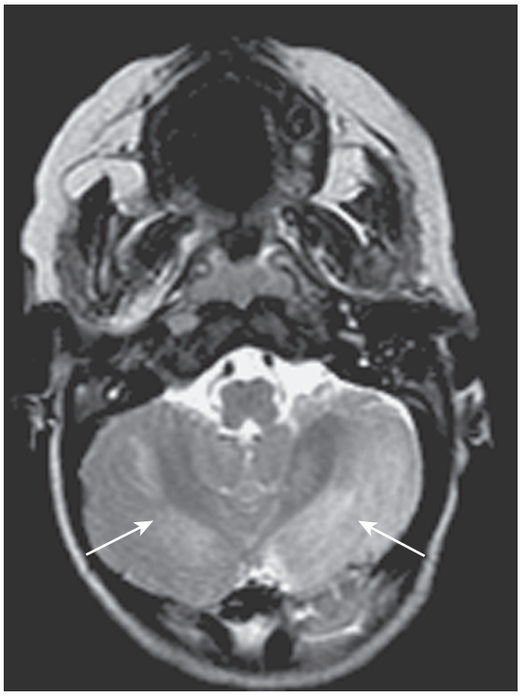

FIGURE 8-41. Cerebellitis with diffuse bilateral areas of high intensity (*arrows*) on axial T2-weighted MR image.

Progressive Multifocal Leukoencephalopathy and Subacute Sclerosing Panencephalitis

PML is an opportunistic papovaviral leukoencephalitis occurring primarily in cell-mediated immunocompromised states (e.g., AIDS, congenital immunodeficiency, immunosuppressive therapy). It is rare in childhood. Regional cerebral demyelination is usually seen and may involve the corpus callosum. Brainstem or cerebellar forms may also be seen. The abnormality is hypodense on CT scans (CT-hypodense) and T2-hyperintense. Mass effect and enhancement are uncommon.

SSPE is probably the result of reactivation of a latent measles infection. Mental status and behavioral changes are often accompanied by seizures and irritability. Imaging shows nonspecific atrophy and patchy white matter hypodensity or T2 hyperintensity without enhancement or mass effect.

Subacute and Chronic Infections

Tuberculosis

Tuberculosis (TB) remains a frequent cause of fatal childhood meningitis worldwide. It results from the miliary spread of *Mycobacterium tuberculosis*. Basilar granulomatous meningitis probably results from rupture of parenchymal tuberculomas (caseating granulomas) into the subarachnoid space (Fig. 8-43). Marked enhancement of the basal leptomeninges is characteristic. Hydrocephalus is usually present. Lenticulostriate/thalamoperforate arterial involvement often results in basal ganglia and thalamic infarction (CT-hypodense, T2-hyperintense, presence or absence of enhancement). Parenchymal tuberculomas appear as enhancing nodular or ring lesions and may occasionally calcify. Other less common, or rare, *Mycoplasma* or mycobacterial CNS infections include *Mycoplasma pneumoniae* meningoencephalitis and leprosy (Hansen disease).

Fungal Infections

Fungal infections of the CNS may result from pathogenic fungi (e.g., *Blastomyces*, *Histoplasma*, *Coccidioides*, *Nocardia*) in immunocompetent patients or from saprophytic fungi (e.g., *Cryptococcus*, *Actinomyces*, *Aspergillus*, *Candida*, *Mucormycosis*) in immunocompromised individuals. CNS fungal infections may produce a granulomatous basal meningitis similar to that seen in TB, including meningeal and cranial nerve enhancement. Enhancing abscesses or granulomas may also be present as well as white matter lesions. Aspergillosis or mucormycosis may cause a vasculitis resulting in infarction or hemorrhage (Fig. 8-44). Sarcoidosis is very rare in childhood and may mimic TB or fungal infection.

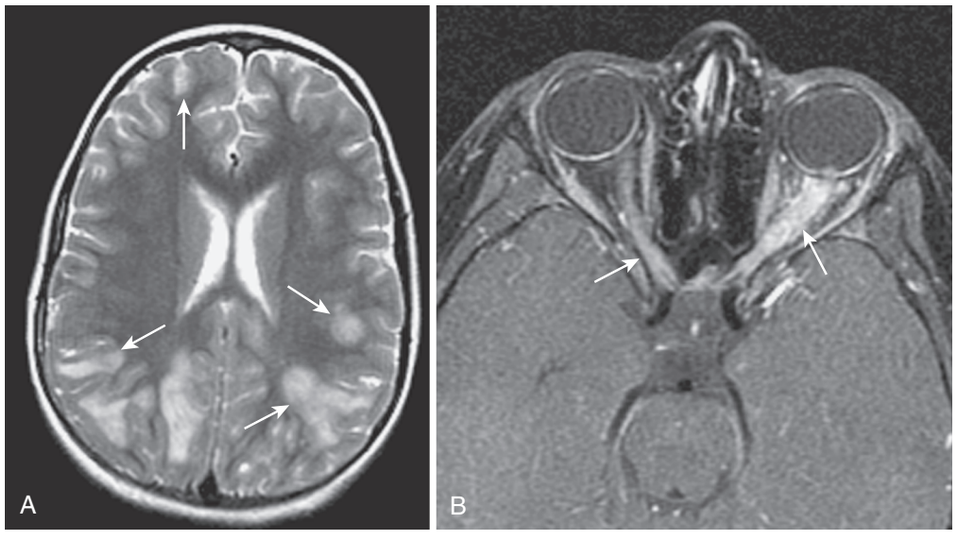

FIGURE 8-42. Acute disseminated encephalomyelitis on MRI. **A,** Multiple white matter lesions (*arrows*) on axial T2-weighted image. **B,** Asymmetric optic nerve enhancement (*arrows*) on gadolinium-enhanced T1-weighted image.

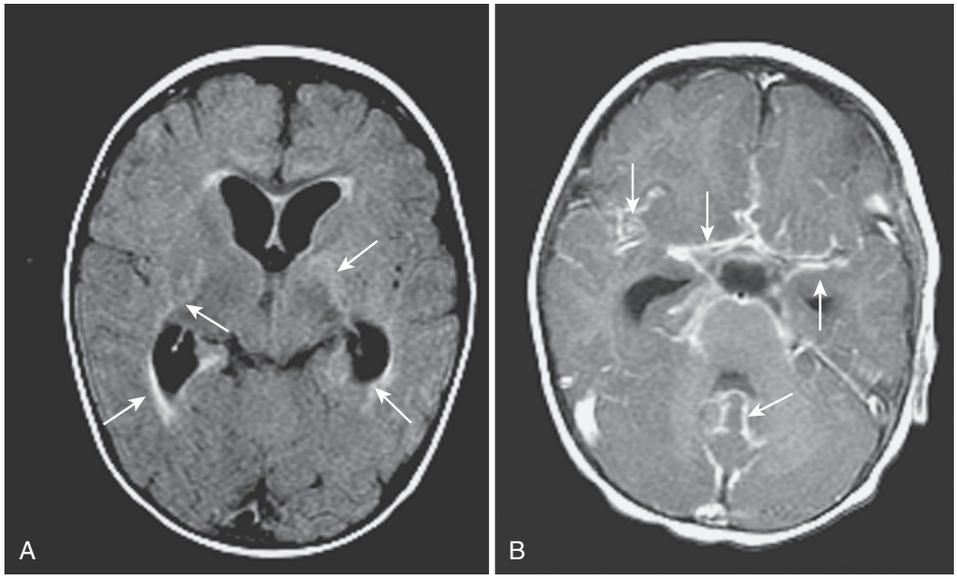

Figure 8-43. Tuberculous meningitis on MRI. **A,** Axial FLAIR image shows basal ganglia infarctions (*short arrows*) and hydrocephalus with periventricular edema (*long arrows*). **B,** Gadolinium-enhanced T1-weighted image shows basilar cistern enhancement (*arrows*).

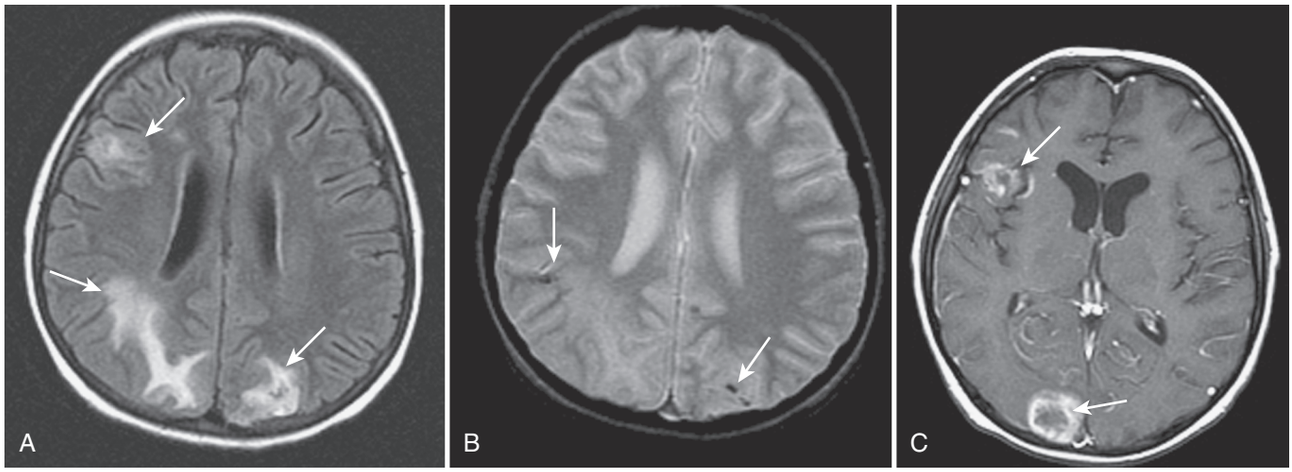

Figure 8-44. Aspergillosis on MRI. **A,** Edema (*arrows*) on axial FLAIR image. **B,** Hemorrhage (*arrows*) on GRE image. **C,** Abscess (*arrows*) on gadolinium-enhanced T1-weighted image.

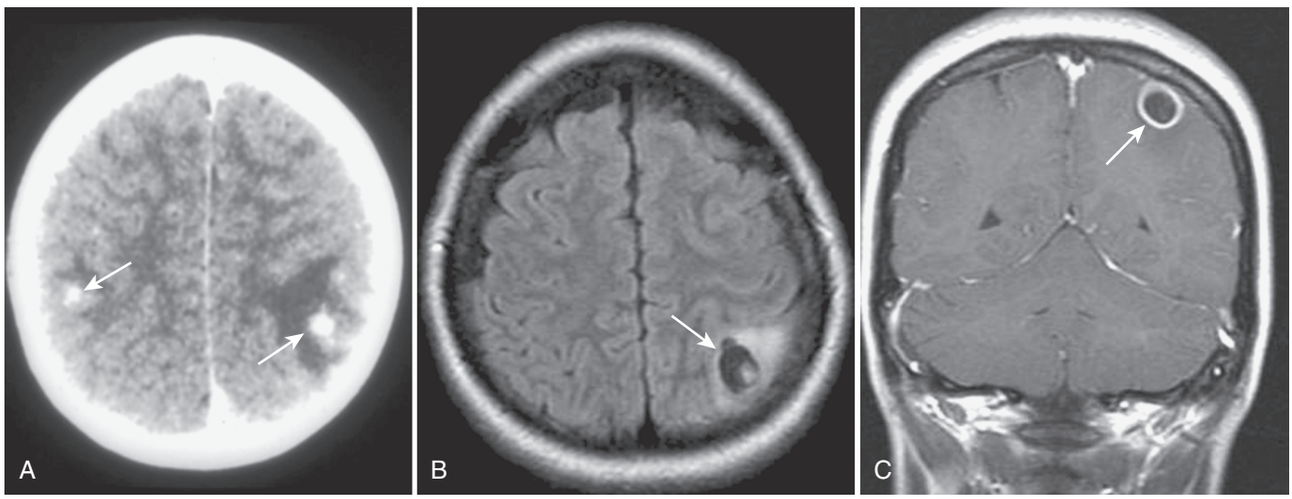

Figure 8-45. Cysticercosis. **A,** Calcification (*arrows*) on CT scan. Axial FLAIR (**B**) and coronal gadolinium-enhanced T1-weighted (**C**) MR images show ring-enhancing cyst with larva (*arrows*) and edema.

Parasitic Infections

Toxoplasmosis (discussed earlier) and cysticercosis are the most common parasitic infections of the CNS. Cysticercosis results from ingestion of material contaminated with pork tapeworm eggs. Seizures are common, and hydrocephalus and vasculitis may also occur. Patterns of involvement include parenchymal, leptomeningeal, intraventricular, and racemose. Parenchymal lesions are the most common form and usually involve gray matter–white matter junctions (Fig. 8-45). The lesions containing live cysticerci are cystic and contain the nodular scolex. The dying, or dead, larval lesions are often associated with edema and peripheral enhancement. The nonviable lesions frequently calcify over a long period. Leptomeningeal cysticercosis is often an enhancing basal granulomatous meningitis that may produce vasculitis with infarction. Intraventricular cysts may be identified from the nodular density or intensity of the contained scolex and may result in hydrocephalus. Racemose cysts lack larvae and most commonly occur in the basal cisterns and sylvian fissures.

Spirochete Infections

Spirochete infections of the CNS other than syphilis (discussed earlier) include Lyme disease and leptospirosis. The tick-transmitted Lyme disease (due to *Borrelia burgdorferi*) usually involves the CNS in the second stage. There may be predominant white matter involvement (CT hypodensity; T2 hyperintensity; presence or absence of ring enhancement) of the cerebrum and cerebellum along with brainstem, basal ganglia, or thalamic lesions. The findings may mimic those in ADEM. CNS disease rarely occurs in the second phase of leptospirosis (i.e., meningoencephalitis).

Vascular Sequelae of Infection

The vascular sequelae of systemic or CNS infection include vasculitis with arterial or venous thrombosis and ischemic or hemorrhagic infarction, mycotic aneurysm with hemorrhage, and hemorrhage related to associated coagulopathy. Vasculitis involving small arteries (arteritis) or small veins (phlebitis) is a common sequela of some meningitides (e.g., TB, fungal, or severe bacterial infections) and encephalitides (e.g., rubella, herpes). Basal ganglia and thalamic infarction is seen with basal meningitis (see Figs. 8-38 and 8-43). Hemorrhagic cortical or subcortical infarction occurs with cortical venous thromboses associated with meningitis or encephalitis (see Fig. 8-38). Smaller vessel occlusions associated with encephalitis (e.g., HSV, aspergillosis) may produce petechial hemorrhagic infarctions (see Figs. 8-35 and 8-44).

Involvement of medium-sized and larger vessels with thrombosis may be associated with CNS or systemic infections or the postinfectious immune-mediated encephalitides; this may include internal carotid or vertebrobasilar arterial or branch arterial occlusions with major arterial territorial infarctions, as has been reported following varicella zoster infection (chickenpox). Superficial or deep dural venous sinus thrombosis may be associated with CNS or systemic infections, particularly when complicated by fluid/electrolyte imbalance (e.g., dehydration). The result may be cortical and subcortical hemorrhagic infarction, deeper periventricular infarction, or intraventricular hemorrhage.

Mycotic aneurysms may be associated with bacterial or fungal infections. The aneurysms are usually fusiform and may be multiple. Risk factors include bacterial endocarditis, heart disease, intravenous drug use, and immunosuppression. Rupture with hemorrhage is often the presenting event.

NEUROVASCULAR DISEASES

Neurovascular disease includes abnormalities of hemodynamics (e.g., hypoxia-ischemia), hematology (e.g., coagulopathy), and vasculature (e.g., angiopathies, malformations), which characteristically manifest as acute neurologic events. Occasionally, the acute deficits may be episodic (e.g., migraine, seizures). A recently discovered but fixed deficit (e.g., hemiplegia) may be the first indication of a remote prenatal or perinatal neurovascular injury. Imaging assists in the clinical evaluation and differentiation of hypoxia-ischemia, hemorrhage, and occlusive vascular disease (Boxes 8-1 and 8-2; Tables 8-3 and 8-4).

Hypoxic-Ischemic Brain Injury

Brain injury may result from decreased oxygenation (e.g., airway obstruction, respiratory failure) or decreased blood flow (i.e., circulatory failure). Hypoxic-ischemic (HI) injury in the fetus is most often related to abnormal hemodynamics (i.e., hypoperfusion). Postnatal HI injury may be hypoxic, ischemic, or combined. HI injury is an important cause of neurodevelopmental decline (e.g., cerebral palsy). HI encephalopathy due to prenatal, peripartum, or postnatal insults may cause seizures, developmental delay, movement disorders, or spasticity. Dysautoregulation, reperfusion, hypercarbia, and acidosis, along with chemical mediators and inflammatory responses, also contribute to the clinical and imaging findings.

The pattern of HI injury depends on the severity and duration of the insult, or insults (e.g., profound, partial prolonged, combined) as well as the timing of the insult (e.g., gestational age [GA]). The maturational state of the brain and its vulnerability vary with GA. Areas of high metabolic activity (i.e., cellular turnover, active myelination) and regions with high concentrations of excitatory neurotransmitters are especially vulnerable. US during the acute phase may show nonspecific hyperechogenicity (Fig. 8-46A). Decreased resistive indices on Doppler US may be more suggestive of HI injury. In the acute phase, CT often shows nonspecific hypodensity and decreased gray matter–white matter differentiation (Fig. 8-46B). Such nonspecific findings may be seen with HI injury, infection, or metabolic disorders. Early-onset encephalopathy (<24 hours after birth) may suggest HI injury, whereas later onset may indicate infection (e.g., GBS, HSV-2)

Box 8-1. **Imaging Patterns of Diffuse or Global Hypoxic-Ischemic Encephalopathy (HIE)***

HEMORRHAGE
Germinal matrix—intraventricular hemorrhage
Choroid plexus—intraventricular hemorrhage
Subarachnoid hemorrhage
Hemorrhagic infarctions

PARTIAL PROLONGED HIE
Preterm: Periventricular leukomalacia
Term/post-term: Cortical/subcortical injury (border-zone, watershed, parasagittal)
Intermediate: combined or transitional pattern
Ulegyria
Cystic encephalomalacia

PROFOUND HIE
Thalamic and basal ganglia injury
Brainstem injury
Hippocampal injury
Cerebral white matter injury
Paracentral injury
Global injury (prolonged profound)

COMBINED PROFOUND AND PARTIAL PROLONGED HIE
Total asphyxia

*Depends on gestational age, chronological age, and duration and severity of the insult.

or metabolic disorders (e.g., hypoglycemia, hyperbilirubinemia, inborn errors of metabolism). In the acute and subacute phases, MRI often shows a more definitive morphologic HI injury pattern (T1 hyperintensity, T2 hypointensity), including restricted diffusion and lactate elevation on MRS, and provides timing and outcome parameters. The long-term result of HI injury is a static encephalopathy (e.g., cerebral palsy). MRI best demonstrates injury in the chronic phase, including atrophy, periventricular leukomalacia, cystic encephalomalacia, and gliosis or mineralization in a characteristic distribution (see later).

Profound HI injury reflects a state of anoxia or circulatory arrest. The injury is shown best by MRI (Fig. 8-47). Although there may be some variation from preterm to term, profound HI primarily involves the basal ganglia (i.e., posterior putamina), thalami (i.e., ventrolateral), posterior limbs of the internal capsule, corona radiata, perirolandic cerebrum, and, occasionally, the cerebellar vermis, midbrain, and hippocampi. The profound HI injury pattern is to be distinguished from other causes of basal ganglia injury, including infection (e.g., neonatal meningitis with basal ganglia infarctions) and metabolic disorders (e.g., kernicterus, aminoacidopathy, organic acidopathy, sulfite oxidase deficiency).

Partial prolonged HI injury reflects a state of hypoxia or hypoperfusion in which there is relative shunting of blood flow from the cerebrum to the vital centers of the basal ganglia and brainstem. The result is cerebral injury along the major arterial border zone or "watershed" regions. In the preterm (e.g., 24-36 weeks' GA) fetus or neonate, the injury may be "multifocal" and predominantly involve the periventricular white matter (e.g., periventricular leukomalacia [PVL]), or there may more "diffuse" white matter injury. US displays early PVL as parietal or frontal periventricular hyperechogenicity. Similar findings, however, may be seen with infection, ischemia (e.g., maternal cocaine use), or metabolic disorders. Evolution to the cystic form of PVL occurs 2 to 6 weeks later (Fig. 8-48A). Hemorrhage may also occur. In chronic PVL, imaging often shows decreased white matter volume, lateral ventricular irregularity with variable enlargement, periventricular CT hypodensity or T2/FLAIR hyperintensity, and thinning of the corpus callosum (Fig. 8-48B). It may mimic colpocephaly. Partial prolonged HI injury in the term, full-term, or post-term fetus (or newborn) (e.g., 37-44 weeks' GA) primarily results in cortical and subcortical cerebral injury along the parasagittal border zones (Fig. 8-49). The base of each gyrus is particularly vulnerable to hypoperfusion. This is reflected in the chronic phase by the characteristic ulegyria pattern ("mushroom-shaped" gyri).

Combined profound and partial prolonged HI injury patterns may be encountered, including components that differ in timing. Very severe partial prolonged, or combined, HI insults may result in cystic encephalomalacia (Fig. 8-50). Injury patterns in the preterm or term child that may mimic HI injury (e.g., PVL or leukoencephalopathy pattern) include infection (e.g., chorioamnionitis, CMV), congenital heart disease, venous thrombosis, hypoglycemia, and other metabolic disorders (e.g., maple syrup urine disease, nonketotic hyperglycinemia, neonatal leukodystrophy).

In older children, HI insults may produce generalized cerebral edema with diffuse CT hypodensity and decreased gray matter–white matter differentiation. Hypodensity of the basal ganglia may be the earliest sign. Differential perfusion renders the brainstem, cerebellum, and tentorium hyperdense ("white cerebellum" sign—see Fig. 8-33A). Capillary and venous congestion renders the cerebral white matter hyperdense relative to the gray matter ("reversal sign"; see Fig. 8-33B) and is a poor prognostic sign. With primarily hypoxic/anoxic insults in infants and young children (e.g., near-drowning), the only imaging abnormality may be restricted diffusion of the cerebral white matter in the subacute phase. Similar findings may be seen with prolonged seizures. Atrophy frequently follows severe HI injury. There may be mineralization, gliosis, or cystic encephalomalacia.

***Box 8-2.* Occlusive Neurovascular Disease in Childhood**

- Idiopathic
- Cardiac disease:
  - Congenital
  - Acquired
- Vascular maldevelopment:
  - Atresia
  - Hypoplasia
- Traumatic:
  - Dissection
  - Vascular distortion
  - Air or fat emboli
- Vasculopathy:
  - Moyamoya disease
  - Fibromuscular dysplasia
  - Marfan syndrome
  - Takayasu arteritis
  - Kawasaki disease
  - Vasculitis
  - Polyarteritis nodosa
  - Systemic lupus erythematosus
- Vasospasm:
  - Migraine
  - Ergot poisoning
  - Subarachnoid hemorrhage
- Drugs:
  - Cocaine
  - Amphetamines
  - L-asparaginase
  - Oral contraceptives
- Hypercoagulopathy:
  - Protein S deficiency
  - Protein C deficiency
  - Antithrombin III deficiency
  - Factor V (Leiden) and prothrombin mutations
  - Antiphospholipid antibody (lupus, anticardiolipin)
  - Heparin cofactor II deficiency
  - Dehydration
  - Nephrotic syndrome
  - Oncologic disease
  - Hemolytic-uremic syndrome
- Hemoglobinopathy:
  - Sickle cell disease
- Infection:
  - Meningoencephalitis
  - Varicella
- Metabolic disease:
  - Homocystinuria
  - Dyslipoproteinemia
  - Fabry disease
  - Mitochondrial cytopathies
  - MTHFR deficiency
  - Familial lipid disorders
- Other:
  - Radiation
  - Emboli from involuting fetal vasculature
  - Placental vascular anastomoses (twin gestation)
  - Co-twin fetal death
  - Fetofetal transfusion

Intracranial Hemorrhage

Intracranial hemorrhage may result from prematurity, trauma, HI injury, a coagulopathy (e.g., thrombocytopenia, disseminated intravascular coagulation, ECMO), or vaso-occlusive disease (e.g., venous thrombosis). Hemorrhage may occasionally be

associated with infection (e.g., HSV-2). Vascular malformations and aneurysms producing intracranial hemorrhage are rare in the neonate and young infant and usually are not encountered until later childhood (see later).

Postischemic reperfusion is a proposed cause for the germinal matrix hemorrhage (GMH), intraventricular hemorrhage (IVH), and the resultant posthemorrhagic hydrocephalus associated with prematurity (<34 weeks' GA). GMH-IVH has been divided into four categories. Grade I is subependymal hemorrhage confined to the germinal matrix (caudothalamic groove). Grade II denotes intraventricular extension without ventricular dilatation. Grade III is subependymal and intraventricular hemorrhage with hydrocephalus. Grade IV refers to additional hemorrhagic periventricular infarction resulting from subependymal venous thrombosis (Fig. 8-51). Poor neurodevelopmental outcome in preterm brain injury generally correlates with the higher grades of GMH-IVH, parenchymal injury (e.g., PVL), and ventriculomegaly (e.g., PVL, posthemorrhagic hydrocephalus).

TABLE 8-4. Central Nervous System Vascular Anomalies of Childhood

Low-flow anomalies	Capillary malformations (telangiectasias) Capillary-venous malformations (e.g., Sturge-Weber) Venous malformations (developmental venous anomaly) Cavernous malformations
High-flow anomalies	Arteriovenous fistulae (dural, pial, intraparenchymal) Arteriovenous malformations (AVMs) Vein of Galen malformations (choroidal, mural, AVM subtypes) Hemangiomas (rare, multisystem hemangioendotheliomas)
Aneurysms	Traumatic (e.g., neonatal peritentorial) Mycotic (endocarditis, sepsis, human immunodeficiency virus) Familial Hypertension Collagen disorders Autosomal dominant polycystic kidney disease Neurofibromatosis Fibromuscular dysplasia Tuberous sclerosis Coarctation of the aorta Klippel-Trenaunay-Weber AVMs (Osler-Weber-Rendu) Radiation Moyamoya disease Metastatic atrial myxoma Craniopharyngioma post-surgery

GMH at term is unusual. Parenchymal hemorrhage in the term infant is most often subpial, in the choroid plexus, subependymal, or thalamic. Such hemorrhage may result from trauma (e.g., subpial), hypoxia-ischemia (e.g., in the choroid plexus, thalamic), coagulopathy, or venous thrombosis (e.g., subpial, subependymal, thalamic). There may be accompanying subarachnoid, subdural, or intraventricular hemorrhage. Hydrocephalus may be a sequela.

Occlusive Vascular Disease

These are single (focal) or multiple (multifocal) infarctions that result from arterial or venous occlusion. The arterial or venous distribution of the lesion(s) may help distinguish occlusive vascular injury from HI injury. Arterial occlusion may result from thrombosis, embolism, or stenosis. This often leads to ischemic infarction. Venous occlusion is usually the result of thrombosis and often produces hemorrhagic infarction.

Arterial Occlusive Disease

Encephalopathy including seizures may indicate acute cerebral infarction (i.e., "stroke") in the newborn. Prenatal stroke, however, may not manifest until later infancy, with early hand preference (i.e., contralateral "congenital hemiplegia") or focal seizures. Acute infarction in an older child, as in an adult, usually manifests as an acute neurologic deficit. Focal cortical ischemic lesions most often involve the middle cerebral artery territory and, less often, the posterior or anterior cerebral artery territory (Fig. 8-52). Multifocal territorial involvement may occasionally be seen, particularly with embolic infarction. The causes of arterial infarction in childhood are diverse (Box 8-2). In addition to heart disease, arteriopathies such as dissection as well as sickle cell, Kawasaki, and moyamoya diseases may result in pediatric stroke. Coagulopathies (e.g., antithrombin III, factor V, antiphospholipid antibody), drug use (e.g., cocaine), and metabolic disorders (e.g., mitochondrial encephalomyopathy with lactic acidosis, and stroke-like episodes [MELAS] syndrome, homocysteinuria) may also be responsible. Meningoencephalitis (e.g., pneumococcal, tuberculosis, varicella) may be complicated by stroke.

Characteristic imaging findings for acute arterial infarction include a wedge-shaped lesion involving the cortex with gyral swelling. Gyriform enhancement may be present in the subacute phase, and there may be petechial or frank hemorrhage (e.g., reperfusion). In the chronic phase there may be focal, or multifocal, atrophy with variable gliosis, porencephaly, or cystic encephalomalacia. MRI offers greater sensitivity for the early detection of infarction than US or CT, but conventional MRI findings may be negative in the early hours after the insult. PWI and DWI now offer earlier demonstration of ischemic lesions. MRA or CTA may show the site of vascular occlusion, especially

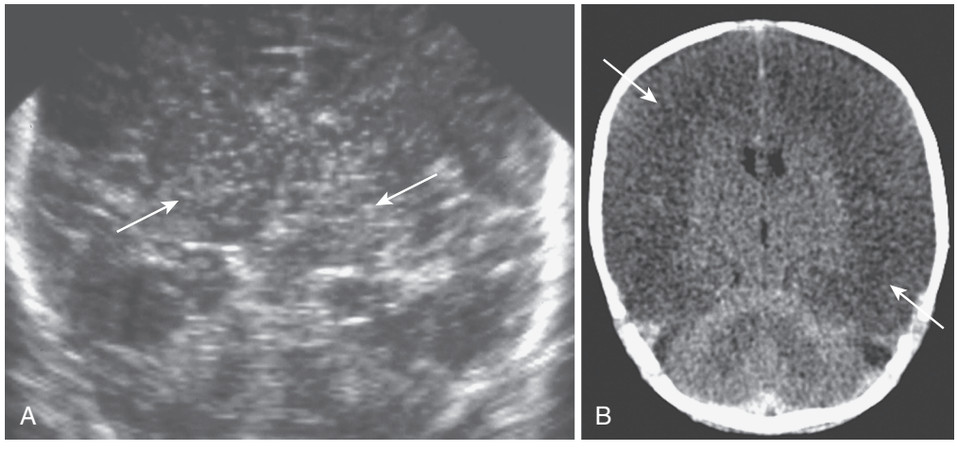

FIGURE 8-46. Acute hypoxia-ischemia with edema. **A,** US scan in a term newborn shows increased echoes of the basal ganglia and thalami (*arrows*). **B,** CT scan in another term newborn shows bilateral cerebral low densities (*arrows*) with decreased gray matter–white matter differentiation.

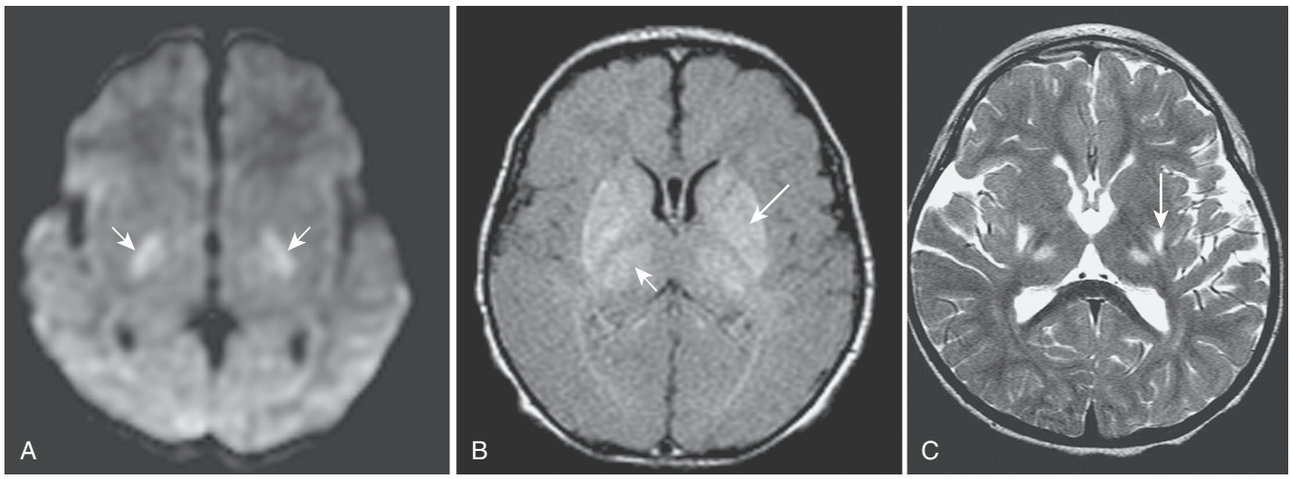

FIGURE 8-47. Profound hypoxia-ischemia on MRI. Acute phase with bilateral putaminal (*long arrow*) and thalamic (*short arrows*) necrosis on axial diffusion-weighted (**A**) and T1-weighted (**B**) images. **C,** Chronic phase with matching gliosis on axial T2-weighted image.

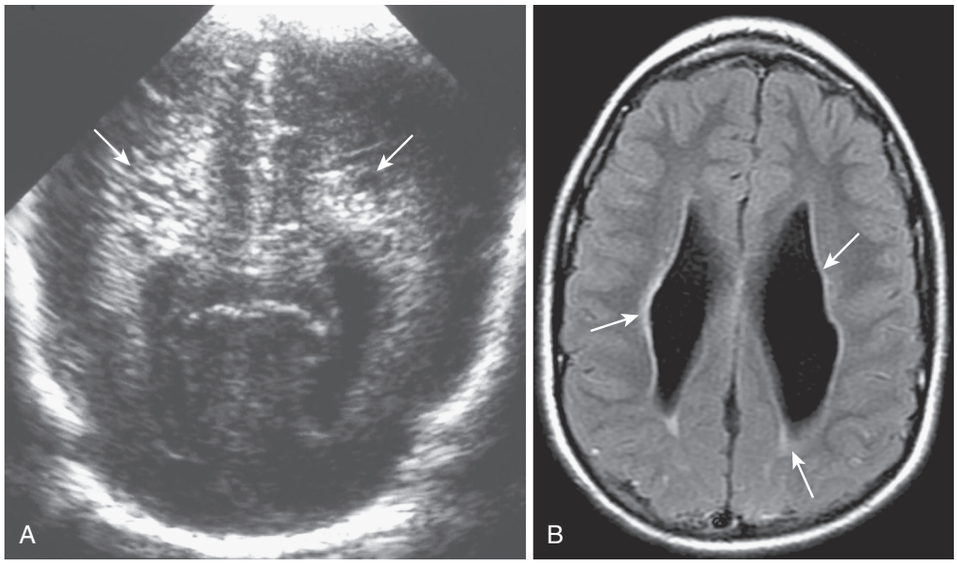

FIGURE 8-48. Periventricular leukomalacia. **A,** US scan of subacute phase with cysts (*arrows*). **B,** Axial FLAIR MR image of chronic phase with irregular ventriculomegaly and periventricular gliosis (*arrows*).

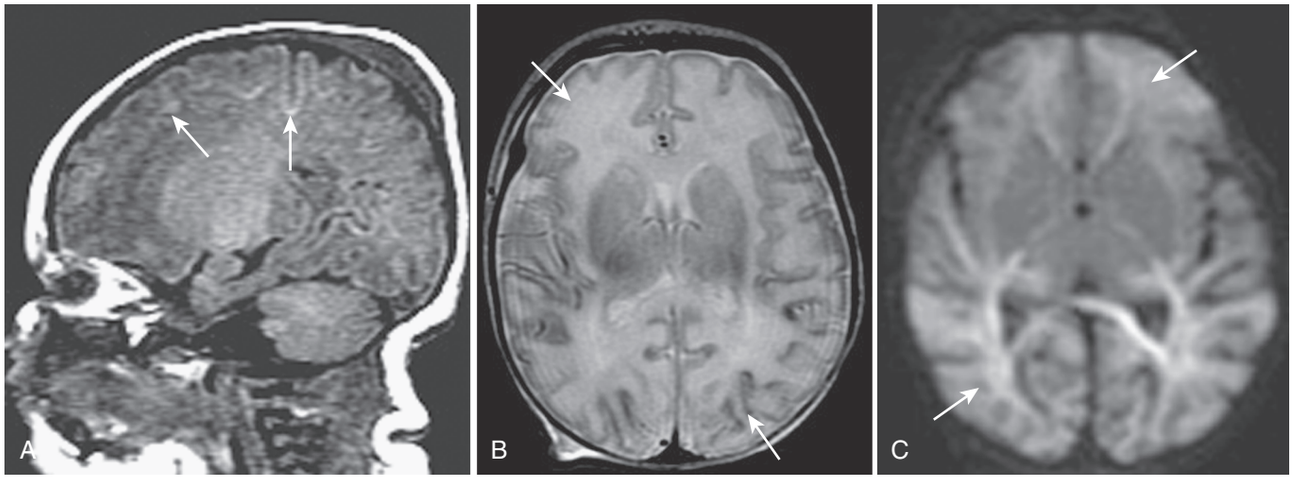

FIGURE 8-49. Partial prolonged hypoxia-ischemia on MRI. Acute phase with watershed injury (*arrows*) on sagittal T1-weighted (**A**), axial T2-weighted (**B**), and axial diffusion-weighted (**C**) images.

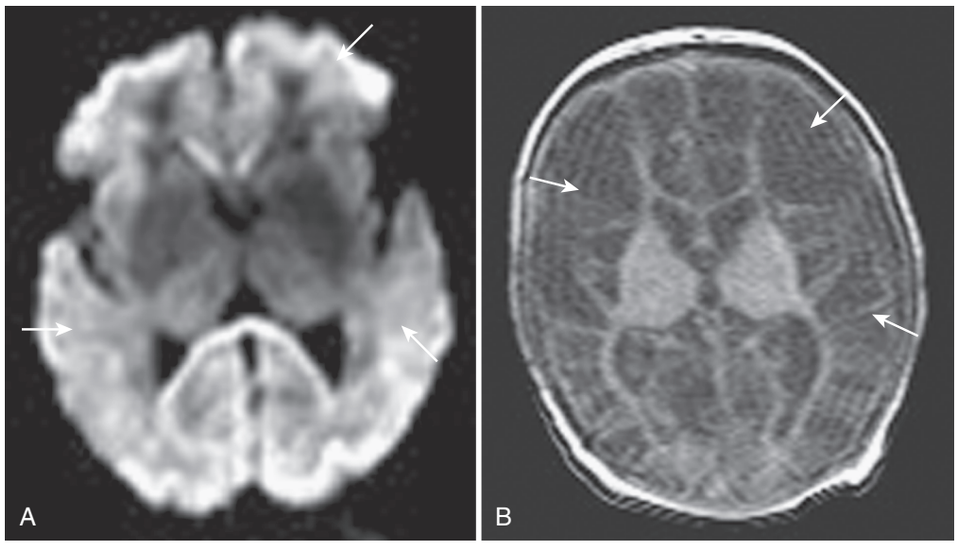

FIGURE 8-50. Cystic encephalomalacia on MRI. **A,** Axial diffusion-weighted image of acute phase showing edema (*arrows*). **B,** Axial T1-weighted image of chronic phase showing cysts (*arrows*).

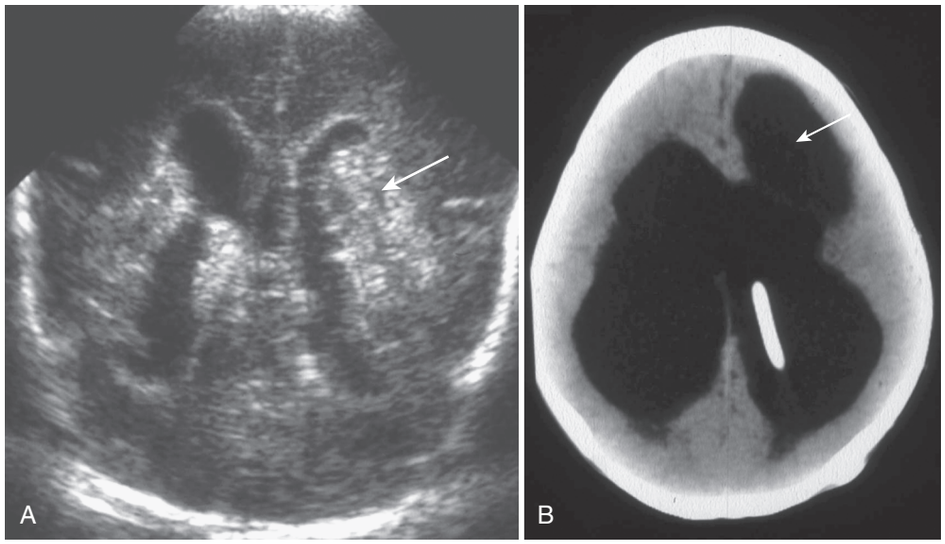

FIGURE 8-51. **A,** Grade IV intraventricular hemorrhage with hemorrhagic infarction (*arrows*) on coronal US scan. **B,** Post-hemorrhagic hydrocephalus with porencephaly (*arrows*) on axial CT scan with shunt catheter.

in large or medium-sized vessels. Smaller vessel lesions (e.g., vasculitis) often require catheter angiography for delineation.

Moyamoya disease is the prototype for pediatric stroke. It is characterized by progressive stenosis and occlusion of the internal carotid artery bifurcation along with the development of prominent basal, leptomeningeal, and transdural arterial collaterals. This disease is usually idiopathic but it may occur in association with neurofibromatosis, radiation therapy, sickle cell disease, or Down syndrome. In the childhood form, the disease is usually bilateral and the collateral vessels are prominent (Fig. 8-53). Ischemia occurs much more frequently than hemorrhage. There may be progressive developmental delay and focal neurologic deficits. Direct or indirect surgical transcranial revascularization between the superficial temporal artery and middle cerebral artery is the treatment of choice. Infarction or gliosis may be shown by CT or MRI and often occurs along the border zones. The basal collateral vessels may appear as flow voids or as enhancement on MRI. Vascular slow-flow areas of high intensity may be seen on FLAIR images. PMRI, perfusion SPECT, or xenon CT may be used for preoperative and postoperative hemodynamic evaluation. Catheter angiography is the procedure of choice for confirmation and preoperative planning.

Venous Occlusive Disease

Venous thrombosis is a common cause of infarction in childhood, including the perinatal period. There may be involvement of the dural venous sinuses or of the cortical, subependymal, or medullary veins. Etiologies include congenital heart disease, dehydration, infection, hypercoagulable states, toxins, chemotherapy (e.g., L-asparaginase) and oral contraceptives. Seizure or neurologic deficits are common, and hemorrhagic infarction is characteristic. Subarachnoid or subdural hemorrhage may also be seen, especially in infants, and the imaging findings may mimic those of NAI. Doppler US, contrast-enhanced CT, CTA, MRI with MRV and gadolinium enhancement, or catheter angiography may be needed to directly demonstrate dural venous sinus thrombosis

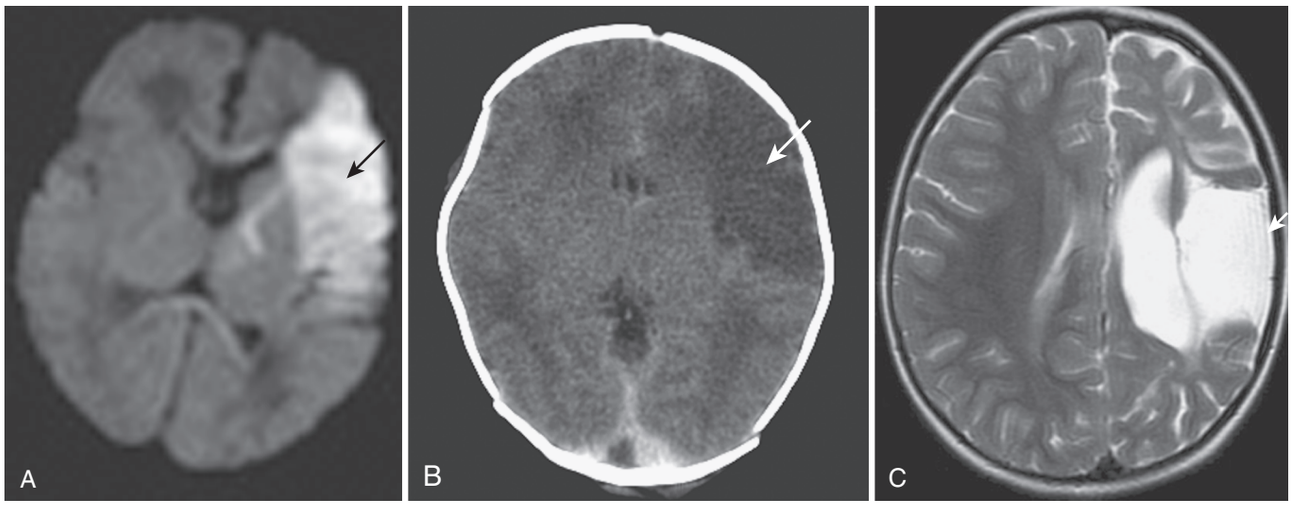

Figure 8-52. Middle cerebral arterial infarction (*arrows*). **A,** Axial diffusion-weighted MR image shows acute phase with edema. **B,** CT scan shows subacute phase. **C,** Axial T2-weighted MR image shows chronic phase with hemiatrophy.

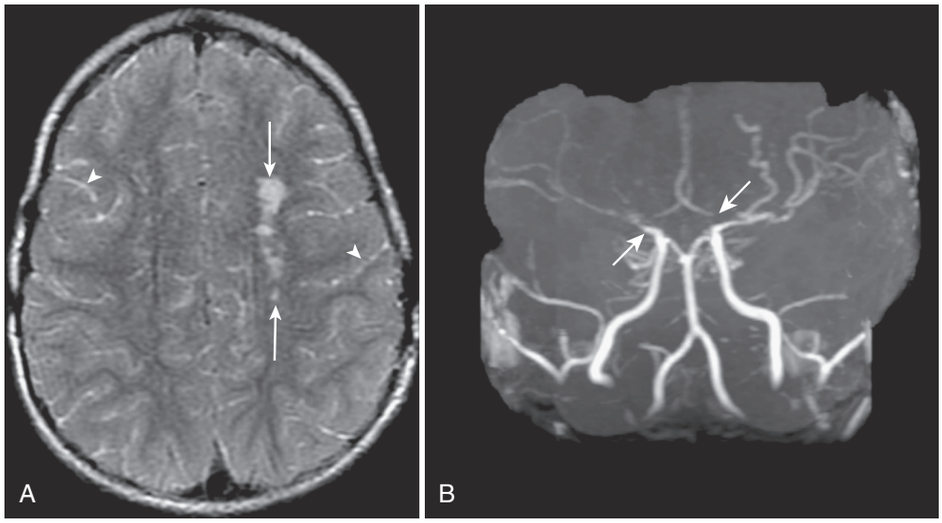

Figure 8-53. Moyamoya disease on MRI. **A,** Axial FLAIR image shows left anterior border-zone infarction (*arrows*) and vascular slow flow (*arrowheads*). B, Frontal MR angiogram shows bilateral arterial stenosis of the internal carotid bifurcation (*arrows*).

(Fig. 8-54). Cortical, subependymal, or medullary venous occlusion may not be directly demonstrated by these techniques, although hemorrhages or thromboses may be present in those distributions. The thrombosis may appear hyperdense on CT, of high intensity on T1-weighted MR images, of low intensity on T2-weighted images, or hypointense on GRE images and may mimic hemorrhage (Fig. 8-54). Intravenous enhancement about the thrombus may be seen on CT as an "empty delta" sign. Depending on the clinical context, treatment may be directed only to the specific cause (e.g., infection) or may also include anticoagulation or thrombolysis.

Vascular Anomalies

Clinically important vascular anomalies of the CNS in childhood include vascular malformations and aneurysms. Vascular malformations are categorized as AVM and arteriovenous fistula (AVF), cavernous malformations, developmental venous anomalies, and capillary telangiectasias. Aneurysms are rare in childhood and of diverse etiology.

AVMs are high-flow malformations in which there are abnormal connections between arteries and veins (no intervening capillaries). The lesions consist of enlarged arterial feeders, a vascular nidus, and draining veins. AVFs are high-flow malformations with one or more direct arteriovenous connections without a nidus. Common presentations include headache, seizure, and neurologic deficit and are often due to hemorrhage. Associated high-flow vasculopathy may produce aneurysms or venous stasis, increasing the risk of hemorrhage. Ischemic injury may result from the associated steal phenomenon. CT may detect high-density hemorrhage, blood pool, or calcification (Fig. 8-55). Contrast-enhanced CT or CTA may show the AVM. MRI using MRA, MRV, and gadolinium enhancement best shows the AVM, its hemorrhagic or ischemic components, and its anatomic relationships. Catheter angiography is required to precisely define the vascular components of the AVM. Treatment options include surgery, endovascular interventional procedures, conformal radiotherapy, or a combination.

The vein of Galen malformations (VGMs) are the prototypical AVM/AVF of infancy. VGMs are classified as choroidal, mural, and AVM types. The choroidal VGM manifests in the neonate as high-output congestive heart failure. Multiple deep AVFs connect with the persistent median prosencephalic vein, which drains into a persistent falcine sinus in the absence of the vein of Galen

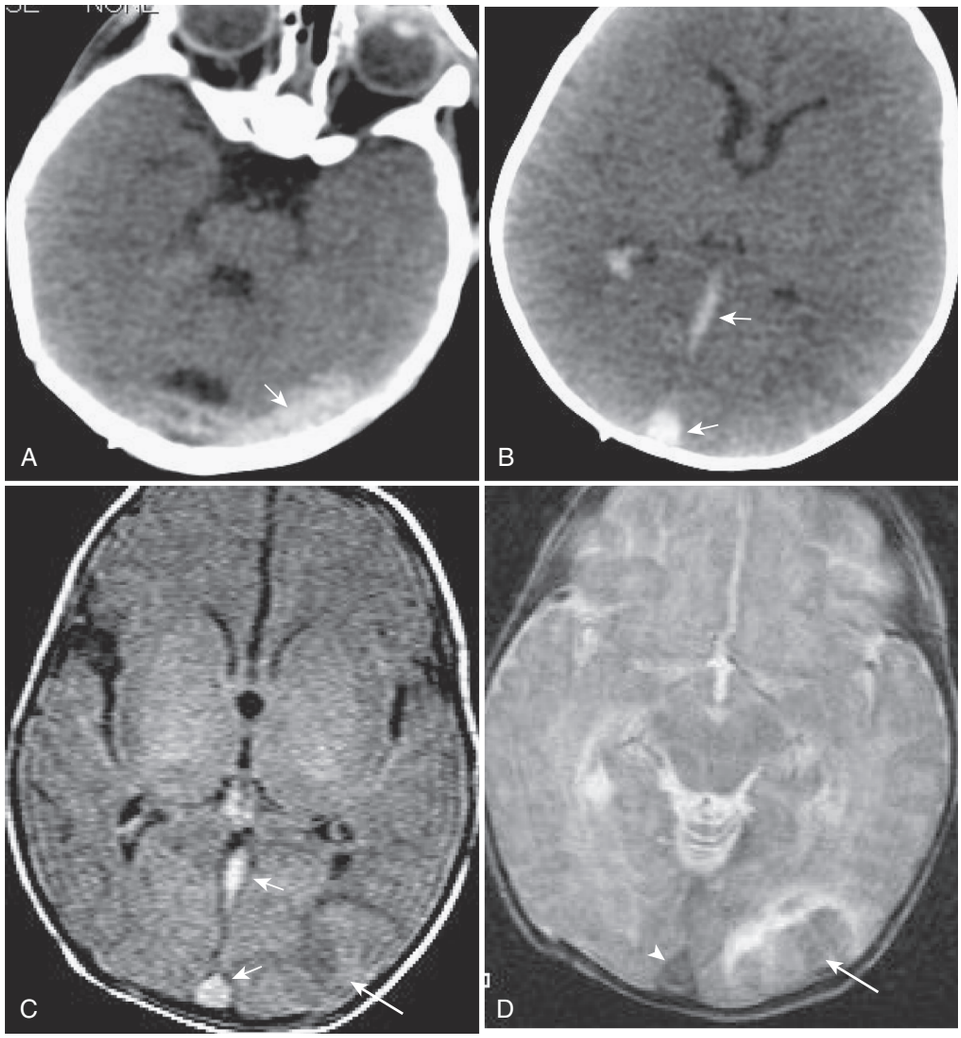

FIGURE 8-54. Venous thromboses (**A** to **C**, *short arrows*; **D**, *arrowhead*) with hemorrhages and infarctions (*long arrows*) on axial CT scans (**A** and **B**) as well as axial T1-weighted (**C**) and GRE (**D**) MR images in an infant with hypercoagulable state (mimicking nonaccidental injury).

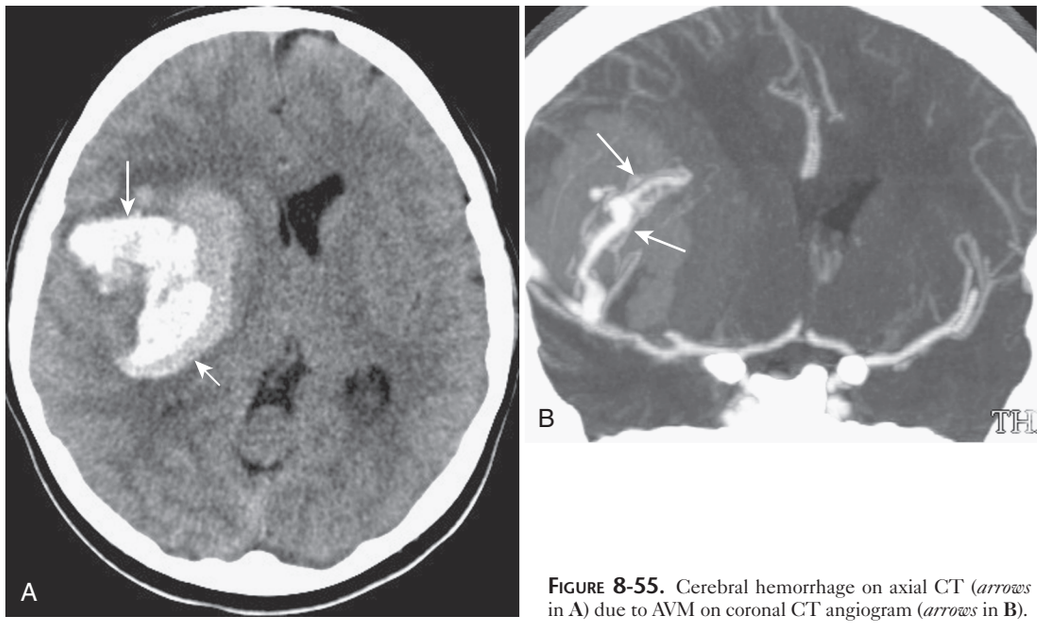

FIGURE 8-55. Cerebral hemorrhage on axial CT (*arrows* in **A**) due to AVM on coronal CT angiogram (*arrows* in **B**).

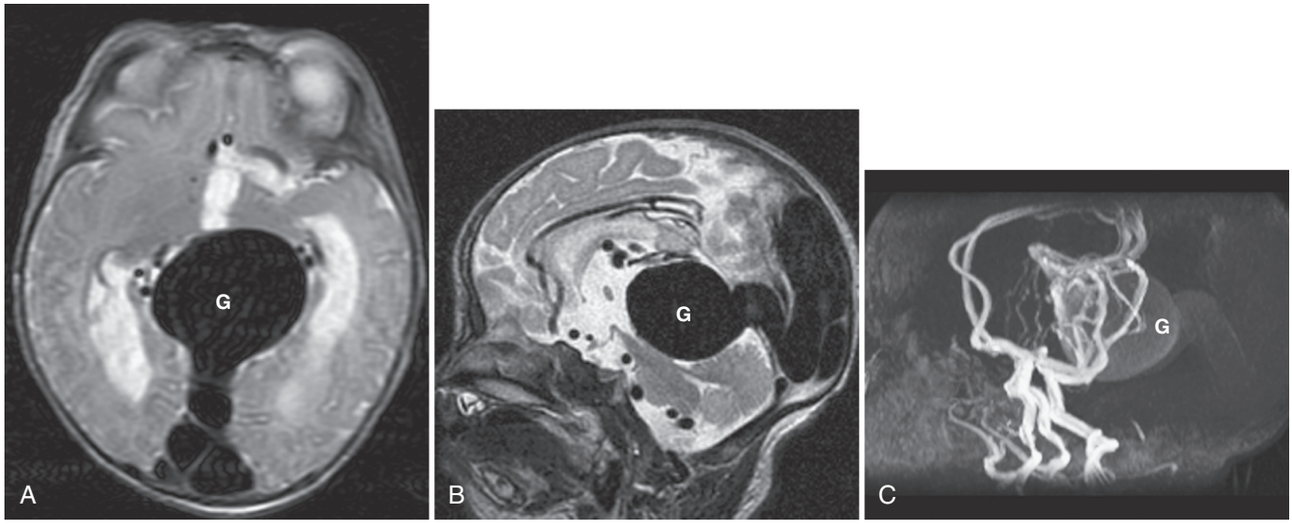

FIGURE 8-56. Vein of Galen (G) arteriovenous fistula (choroidal type) on axial (**A**) and sagittal T2-weighted (**B**) MR images as well as a lateral MR angiogram (**C**).

and straight sinus (Fig. 8-56). The mural VGM manifests later in infancy as hydrocephalus or seizures. One or more AVFs may be present within the wall of the median prosencephalic vein. Often there is outflow venous stenosis, which limits the AV shunting. The third type of VGM is composed of a deep AVM with venous drainage into a dilated vein of Galen. It often manifests as hemorrhage in older children and adults. US with Doppler imaging may provide the diagnosis in the fetus or neonate. CT, contrast-enhanced CT, and CTA may demonstrate the lesion, but MRI and catheter angiography are the best procedures for fully delineating the VGM and its complications, and for planning treatment and follow-up. Depending on the type and presentation, the options for therapy are similar to those described previously.

Cavernous malformations (CMs), also known as cavernomas or cavernous angiomas, are low-flow vascular malformations composed of endothelium-lined spaces without the components of AVM or AVF. They are probably the most common vascular malformation of childhood. Similar lesions may occur following radiotherapy for CNS neoplasia. CMs may be asymptomatic or may manifest as hemorrhage, headache, or seizure. They may be single or multiple, and familial. Occasionally, a CM is associated with a developmental venous anomaly. Nonenhanced CT scans may show a hyperdense lesion with occasional calcification. On MRI, a T1- or T2-hyperintense focus with a T2-hypointense rim is often present (Fig. 8-57). Blood products of varying ages may be evident. These lesions are occult to CTA, MRA, and catheter angiography.

Developmental venous anomalies (DVAs), also called venous angiomas, are low-flow malformations in which one or more anomalous veins drain normal or dysplastic brain. No AVM or AVF components are present. Common sites are the frontal lobes and cerebellum. DVA may be associated with cortical dysplasias or migrational abnormalities. They are typically asymptomatic and incidental findings. DVA may rarely be associated with seizures or

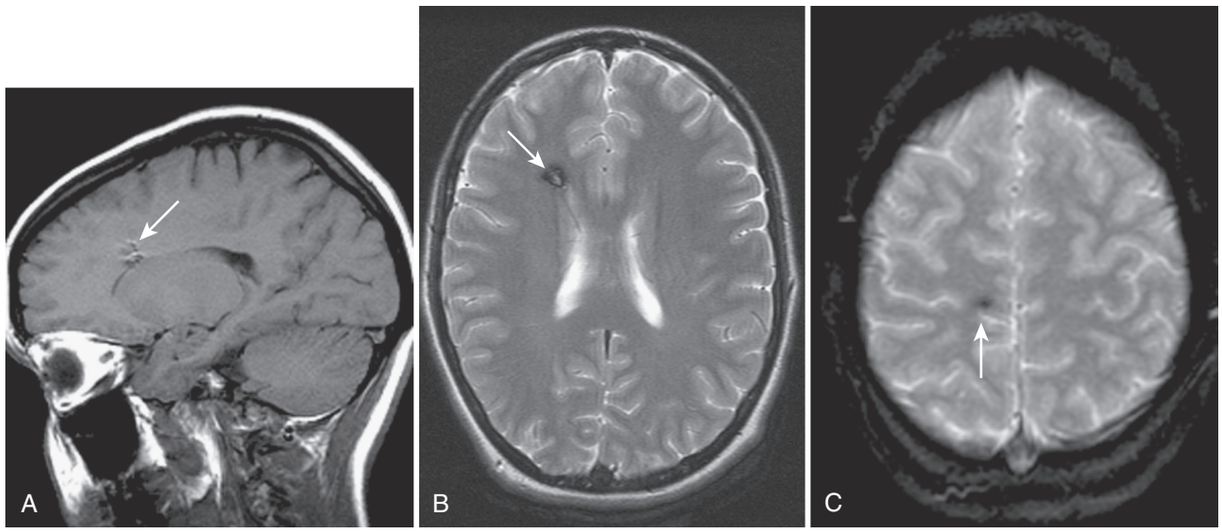

FIGURE 8-57. Familial multiple cavernous malformations (*arrow*) on sagittal T1-weighted (**A**), axial T2-weighted (**B**), and axial GRE (**C**) MR images.

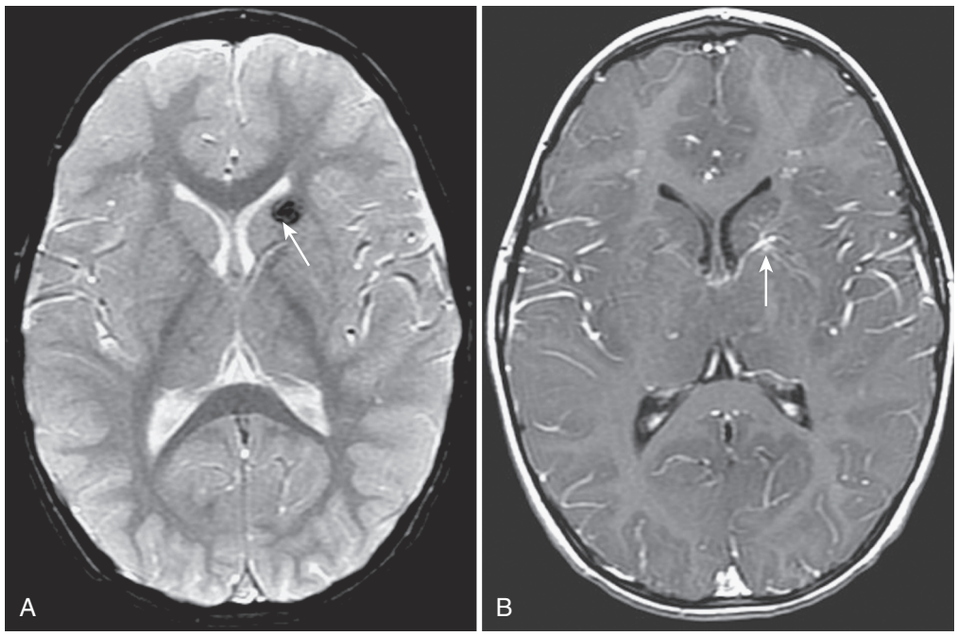

FIGURE 8-58. Cavernous malformation on axial GRE image (*arrow* in **A**) associated with developmental venous anomaly on axial gadolinium-enhanced T1 MR image (*arrow* in **B**).

hemorrhage, particularly when there is a concomitant cavernous malformation (Fig. 8-58). DVA is often demonstrated by imaging as a collection of dilated medullary veins that converge into a single vein that drains into the superficial or deep venous system. These lesions are frequently evident on CT only after contrast enhancement. MRI may show them as vascular flow voids or as gadolinium vascular enhancement. They are also demonstrated by catheter angiography.

Capillary telangiectasias are slow-flow capillary malformations. The lesions usually occur in the pons and are rarely symptomatic in children. They may be detected only on CT or MRI with contrast enhancement or if there is rare hemorrhage. They are usually occult to angiography.

Aneurysms are rare in childhood. They tend to be large (> 1 cm diameter), occur more often in males, and have a higher incidence within the vertebrobasilar system and at the internal carotid artery bifurcation. Aneurysms outside the circle of Willis are common and are usually mycotic or traumatic in origin. Increased risk of aneurysm is associated with certain conditions, such as coarctation of the aorta, polycystic kidney disease, neurofibromatosis, and a positive family history. The clinical presentation is often related to rupture with hemorrhage (e.g., headache) or is due to mass effect (e.g., third cranial palsy). Unenhanced CT often detects subarachnoid or intracerebral hemorrhage and may detect the aneurysm as a focal blood-pool of high density. On MRI, an aneurysm may appear as a focal flow void or as a focal hemorrhage or thrombosis. Catheter angiography is necessary for delineating site and morphology as well as for detecting additional aneurysms. CTA is also useful for surgical planning. MRA or CTA may be useful for aneurysm screening of at-risk patients. Treatment options include surgery and endovascular interventional techniques.

CRANIAL AND INTRACRANIAL TUMORS OF CHILDHOOD

Classification

Tumors of the nervous system constitute the largest group of solid neoplasms in childhood. Neuroepithelial tumors contain cell types derived from the embryonic neuroepithelial tube (e.g., gliomas). Tumors of nonneuroepithelial tissues include those of neural crest or peripheral nervous system origin (e.g., neuroblastoma) as well as those of other cell types (e.g., germinoma and craniopharyngioma). Tumors are generally classified pathologically according to cell type and level of malignancy (World Health Organization [WHO] classification) (Box 8-3). Location and resectability, however, are often more important prognostic factors. Although primary CNS tumors may spread within the subarachnoid space (e.g., medulloblastoma), metastases beyond the CNS are uncommon. From a clinical and imaging perspective, CNS tumors may be categorized according to the major region of involvement, for example, in the posterior fossa, about the third ventricle, in the cerebral hemisphere, and parameningeal.

Although US or CT may detect neoplastic processes manifesting as large masses, MRI is preferred for complete evaluation, including treatment planning and the follow-up of tumor response and treatment effects. Important treatment effects after radiotherapy and chemotherapy include mineralization, ischemic vasculopathy, hemorrhagic vasculopathy, leukoencephalopathy, and second tumors. Functional imaging, including MRS, PMRI, SPECT, and PET, may be needed to distinguish treatment effects from tumor progression.

Posterior Fossa Tumors

Posterior fossa tumors occur more often in childhood than in adulthood. They often manifest as hydrocephalus, cerebellar signs (ataxia), brainstem signs (cranial nerve palsies), or meningeal signs (head tilt). Common lesions include embryonal tumors (i.e., medulloblastoma), cerebellar astrocytoma, brainstem glioma, and ependymoma. Less frequent tumor types are dermoid-epidermoid, teratoma, ganglioglioma, gangliocytoma of Lhermitte-Duclos, choroid plexus papilloma or carcinoma, sarcoma, acoustic neuroma, meningioma, and hemangioblastoma. Nonneoplastic lesions included in the differential diagnosis of posterior fossa "masses" are the Dandy-Walker-Blake spectrum of retrocerebellar cysts, arachnoid cyst, cavernous malformation, abscess, and hemorrhage. Skull base or petrous temporal parameningeal tumors that may invade the posterior fossa include sarcomas, histiocytosis, neuroblastoma, primitive neuroepithelial tumor (PNET), carcinoma, metastases, paraganglioma, and chordoma.

Box 8-3.* Neuropathologic Classification of Central Nervous System Tumors

I. Neuroepithelial tumors
  A. Astrocytic (e.g., astrocytoma, anaplastic, pilocytic, glioblastoma, subependymal Giant Cell Tumor)
  B. Oligodendroglial (e.g., oligodendroglioma, anaplastic)
  C. Ependymal (e.g., ependymoma, anaplastic)
  D. Mixed gliomas (e.g., oligoastrocytoma)
  E. Choroid plexus (e.g., papilloma, carcinoma)
  F. Uncertain origin (e.g., gliomatosis cerebri)
  G. Neuronal/mixed neuronal-glial (e.g., ganglioglioma, dysembryoplastic neuroepithelial tumor, neurocytoma)
  H. Pineal (e.g., pineoblastoma, pineocytoma)
  I. Embryonal (e.g., primitive neuroepithelial tumor, medulloblastoma, atypical teratoid rhabdoid tumor)
II. Cranial and spinal nerve tumors
  A. Schwannoma
  B. Neurofibroma
  C. Malignant peripheral nerve sheath tumor
III. Meningeal tumors
  A. Meningothelial (e.g., meningioma)
  B. Mesenchymal, nonmeningothelial (e.g., sarcoma, rhabdoid)
  C. Primary melanocytic (e.g., melanosis)
  D. Uncertain histogenesis (e.g., hemangioblastoma)
IV. Lymphomas and hemopoietic neoplasms
V. Germ cell tumors
  A. Germinoma
  B. Embryonal carcinoma
  C. Yolk sac tumor
  D. Choriocarcinoma
  E. Teratoma
  F. Mixed
VI. Cysts and other tumor-like lesions (e.g., Rathke cyst, dermoid-epidermoid, colloid cyst, neuroglial cyst, hamartoma, heterotopia)
VII. Tumors of the sellar region
  A. Pituitary adenoma
  B. Pituitary carcinoma
  C. Craniopharyngioma
VIII. Local extensions from regional tumors (e.g., parameningeal neoplasms)
IX. Metastatic tumors (e.g., seeding)
X. Unclassified tumors

*Modified from Louis D, Ohgaki H, Wiestler O, et al: The 2007 WHO classification of tumours of the central nervous system. Acta Neuropathol 2007;114:97-109.

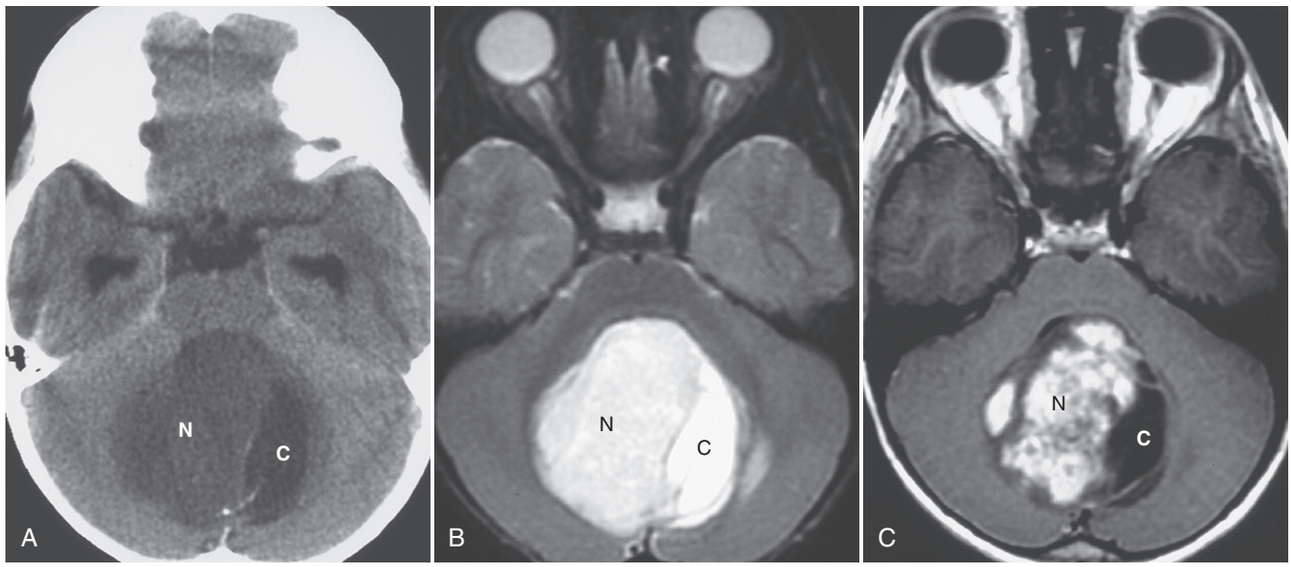

Figure 8-59. Cerebellar astrocytoma with nodular (N) and cystic (C) components on axial CT scan (**A**) as well as axial T2-weighted (**B**) and gadolinium-enhanced T1-weighted (**C**) MR images.

Cerebellar Astrocytoma

Cerebellar astrocytoma is one of the most common posterior fossa neoplasms of childhood. The pilocytic subtype far outnumbers the fibrillary and anaplastic forms. These tumors tend to be slow-growing, circumscribed, and differentiated. They have a good prognosis and usually require only surgical excision. Cerebellar astrocytomas usually arise within the vermis, hemisphere, or both (e.g., paramedian). They may be microcystic or macrocystic and may contain solid or laminar tumor. Associated displacement of the fourth ventricle or aqueduct results in hydrocephalus. On CT, the cystic portion is usually low density and the solid tumor is isodense (Fig. 8-59). Iodine enhancement of the solid component is common. Infrequently the tumor appears more heterogeneous with variable enhancement. Unlike medulloblastoma or ependymoma, cerebellar astrocytomas rarely demonstrate tumor hyperdensity, hemorrhage, or calcification. On MRI, the macrocystic component usually displays intensity patterns characteristic of proteinaceous fluid (see Fig. 8-59). The microcystic component is commonly of low intensity on T1-weighted MRI and isointense to hyperintense on FLAIR and T2-weighted images. The nodular or laminar solid component is commonly isointense on T1-weighted images and isointense to hyperintense on T2-weighted images. Gadolinium enhancement of cerebellar astrocytoma on MRI is quite variable and similar to that described for iodine enhancement on CT.

Medulloblastoma

Medulloblastoma is a PNET in the embryonal category and, in many reported series, the most common posterior fossa tumor of childhood. A number of subtypes exist. *Atypical teratoid rhabdoid tumor* (ATRT), formerly mistaken for medulloblastoma, may be of choroid plexus origin, has the worst prognosis of tumors in the embryonal category, and may arise in the posterior fossa or cerebrum. For all the embryonal tumors, there is a tendency for seeding, although systemic metastasis is rare.

Medulloblastoma usually arises in the midline from the cerebellar vermis and grows into the fourth ventricle. It is often infiltrative, adheres to adjacent structures, and may directly involve the brainstem. It is the most common childhood tumor producing intracranial and intraspinal seeding, which may be present initially. Occasionally the tumor contains areas of necrosis, cysts, hemorrhage, or calcification, appearing similar to ependymoma (Fig. 8-60). In older children, medulloblastoma may arise from the cerebellar hemisphere (e.g., desmoplastic or nodular subtype). This hypercellular tumor is usually isodense to hyperdense on CT and T2-hypointense on MRI (see Fig. 8-60). Marked enhancement is characteristic. A mass with a more heterogenous intensity and enhancement appearance in an infant or very young child should also prompt consideration of ATRT, ependymoma, and choroid plexus carcinoma. Seeding is best demonstrated on gadolinium-enhanced T1-weighted MRI as laminar or nodular enhancing lesions along pial or ependymal surfaces of the brain or spinal cord (see Fig. 8-60). Treatment of medulloblastoma requires a combination of surgery, chemotherapy, and craniospinal radiotherapy.

Ependymal Tumors

Ependymal tumors show considerable histologic diversity. Most ependymomas grow in or adjacent to the ventricular system, although extraventricular (e.g., cortical) lesions also occur. The tumors may be circumscribed and contain calcification, thrombosis or hemorrhage, necrosis, vascular proliferation, or other elements. Anaplastic forms also exist.

Ependymoblastoma is a variant of PNET. Ependymomas often arise within or about the fourth ventricle and produce hydrocephalus. Such a tumor may be small, midline, and confined to the fourth ventricle. Often, however, the tumor is large and eccentric, obliterating posterior fossa landmarks. Commonly

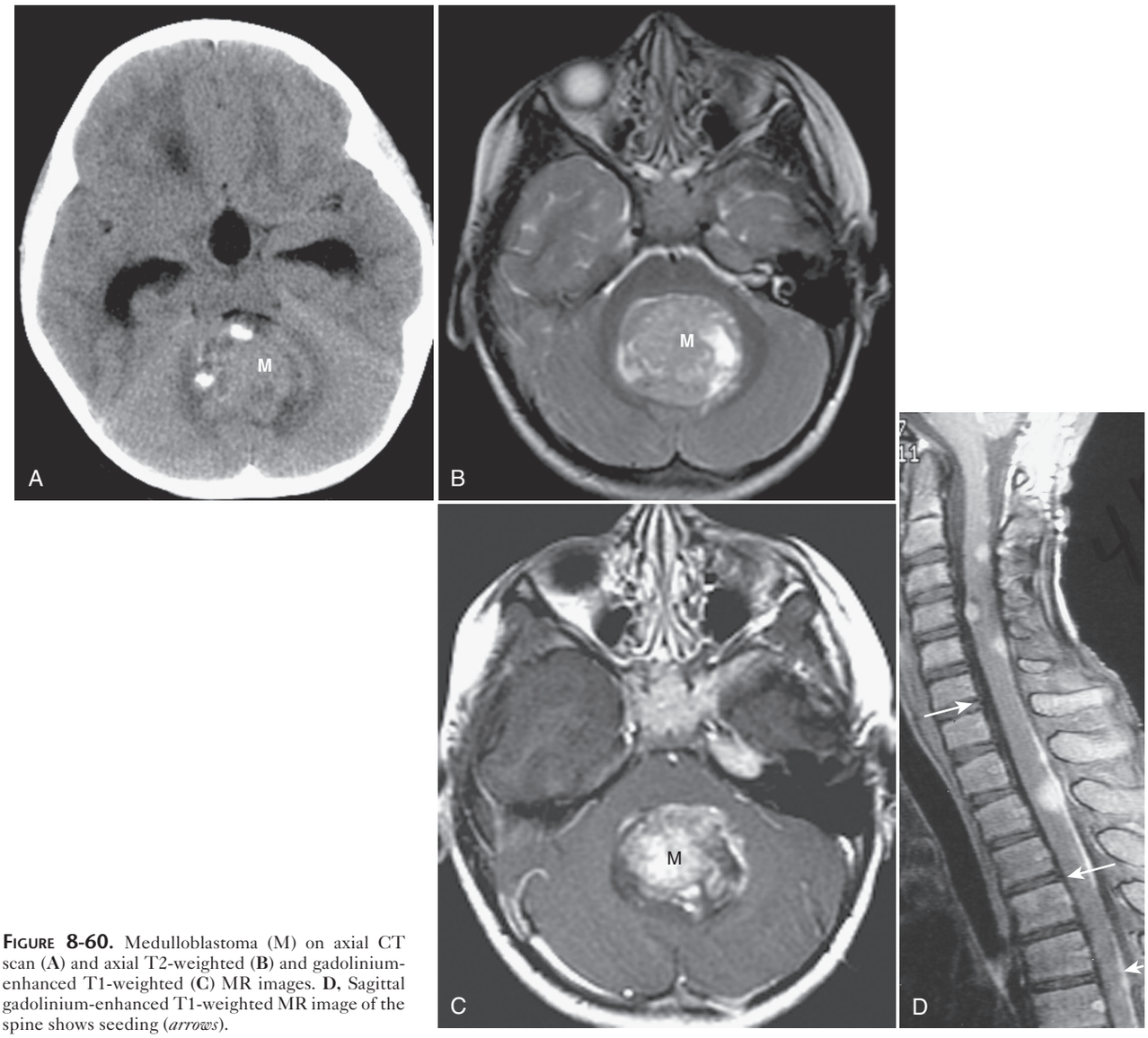

FIGURE 8-60. Medulloblastoma (M) on axial CT scan (**A**) and axial T2-weighted (**B**) and gadolinium-enhanced T1-weighted (**C**) MR images. **D,** Sagittal gadolinium-enhanced T1-weighted MR image of the spine shows seeding (*arrows*).

there is extension through the outlet foramina into the cisterna magna, the cisterns about the brainstem, and the foramen magnum and upper cervical canal about the spinal cord. Involvement of the cerebellum, brainstem, and vertebrobasilar arterial and cranial nerve structures is common. Seeding may rarely occur, especially with anaplastic ependymoma. Associated hemorrhage and hemosiderosis is rare in childhood. Density, intensity, and enhancement heterogeneity is characteristic of ependymomas and represents a mix of tumor, cysts, necrosis, edema, calcification, or hemorrhage (Fig. 8-61). ATRT, nontypical medulloblastoma, and choroid plexus carcinoma are in the differential diagnosis.

Brainstem Tumors

Brainstem tumors are most often gliomas of varying histologic types and grades of malignancy, including pilocytic or anaplastic astrocytoma, glioblastoma, mixed gliomas, and neuronal tumors (e.g., ganglioglioma). Anatomic subtypes include diffuse, focal, cystic, and cervicomedullary. Brainstem gliomas commonly arise in the pons, often diffusely infiltrate into the medulla and midbrain, require chemotherapy and radiotherapy, and have a very poor prognosis (Fig. 8-62). Symptomatic hydrocephalus is unusual early. There may be symmetric expansion with obliteration of the cisterns and fourth ventricle or asymmetric growth with exophytic extension and encasement of the basilar artery or adjacent cranial nerves. Cystic or necrotic changes may be seen with glioblastoma. Focal or cystic tectal, midbrain, thalamic, and cervicomedullary tumors are often lower grade and have a better prognosis. They may require only surgery or conformal radiotherapy. Tectal tumors occur as low-grade gliomas, hamartomas, or gliosis, and may be detected only on MRI (Fig. 8-63). They produce aqueductal stenosis and manifest as hydrocephalus. Cervicomedullary tumors may manifest as recurring emesis and are often only shown on MRI (Fig. 8-64). On imaging, brainstem tumors are often CT-isodense or hypodense, T1-isointense/hypointense, and T2/FLAIR-isointense to hyperintense. Enhancement is variable (e.g., diffuse, nodular, or ring). MRI helps distinguish these tumors from infarction, encephalitis, demyelination, and vascular malformation (e.g., cavernous malformation).

Other Tumors

Choroid plexus papilloma or carcinoma occasionally arises within the fourth ventricle or the angle (also see "Cerebral Tumors"). Mixed gliomas, neuronal, or mixed neuronal-glial tumors may also arise in the posterior fossa, including the dysplastic gangliocytoma (Lhermitte-Duclos). Tumors of cranial and spinal nerves occurring in childhood include schwannoma (neurilemmoma or neurinoma), neurofibroma, and malignant peripheral nerve sheath tumors. Solitary schwannomas (e.g., eighth nerve vestibular schwannoma or acoustic neuroma) are generally sporadic, whereas multiple schwannomas are characteristic of neurofibromatosis 2 (NF-2). Plexiform neurofibromas occur in NF-1. A number of malformative tumors occasionally arise in the posterior fossa, including dermoid/epidermoid, arachnoid cyst, and hamartomas. Epidermoids are of epidermal origin and usually arise in the cisterns about the angles. They are nonenhancing masses with CSF-like density or intensity that are hyperintense on FLAIR MRI and DWI. The latter feature assists in distinguishing them from arachnoid cysts. Dermoids contain epidermal and dermal elements and tend to arise midline in relation to the cerebellar vermis, brainstem, fourth ventricle, or cisterna magna. They exhibit fatlike densities and intensities as well as calcification. Hemangioblastoma rarely occurs in childhood in the absence of von Hippel–Lindau syndrome (see "Neurocutaneous Syndromes"). Lymphomas and hematopoietic neoplasms may also arise in the posterior fossa (see "Parameningeal Tumors"). Germ cell tumors, except teratoma, are extremely rare in the posterior fossa (see "Tumors About the Third Ventricle").

Tumors About the Third Ventricle

Tumors about the third ventricle may be subdivided as to suprasellar/anterior third ventricular tumors, pineal region/posterior third ventricular tumors, intraventricular tumors, and paraventricular tumors. Clinical manifestations often reflect hydrocephalus, neuroendocrine disorder (growth failure, hypopituitarism, precocious puberty, amenorrhea, galactorrhea, diabetes insipidus, diencephalic syndrome, syndrome of inappropriate antidiuretic hormone secretion), and optic pathway or other cranial nerve involvement. In childhood, common neoplasms in this region are optic and hypothalamic glioma, craniopharyngioma, and germ cell tumors. Less common tumors include pituitary adenoma, dermoid/epidermoid, choristoma, histiocytosis, pineal cell tumors (pinealoma, pineoblastoma), third ventricular glioma, ganglioglioma, ependymoma, meningioma, choroid plexus papilloma, paraganglioma, schwannoma, or neoplastic seeding. Nonneoplastic tumors include arachnoid cyst, sphenoidal encephalocele, colloid cyst, Rathke cyst, hamartoma (glial, neuronal, or mesenchymal, e.g., lipoma), ectopic posterior pituitary, aneurysm, galenic varix, cavernous angioma, granuloma, arachnoiditis, infundibulitis, hypophysitis, and sarcoidosis. Extracranial (parameningeal) processes of bone or sinus origin that may invade the midline brain structures include neuroblastoma, PNET, histiocytosis, esthesioneuroblastoma, sarcomas, chordoma, angiofibroma, carcinoma, mucocele, granulomatous processes (aspergillosis, etc.), and metastatic disease.

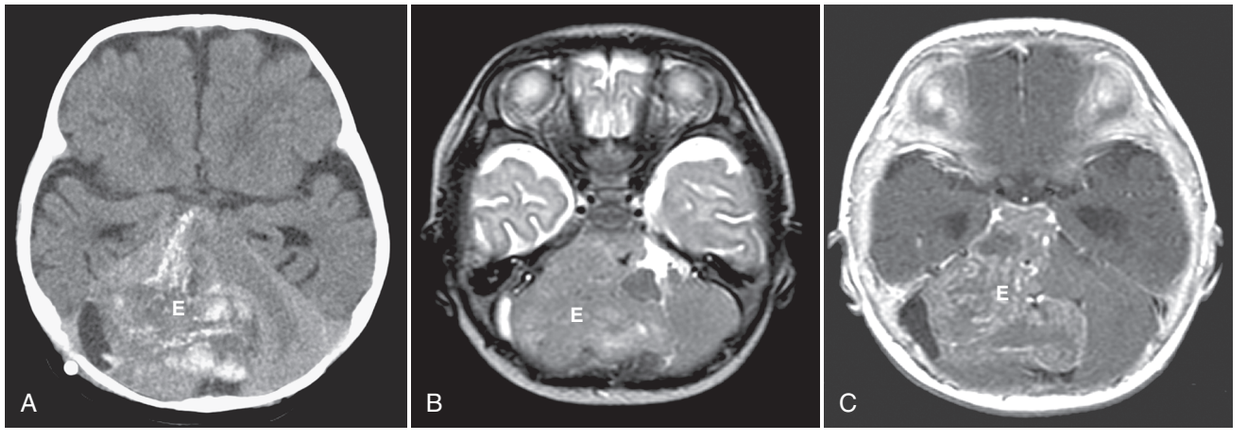

Figure 8-61. Ependymoma (E) with calcification on axial CT scan (**A**). Nonuniform intensity and enhancement on axial T2-weighted (**B**) and axial gadolinium-enhanced T1-weighted (**C**) MR images, respectively.

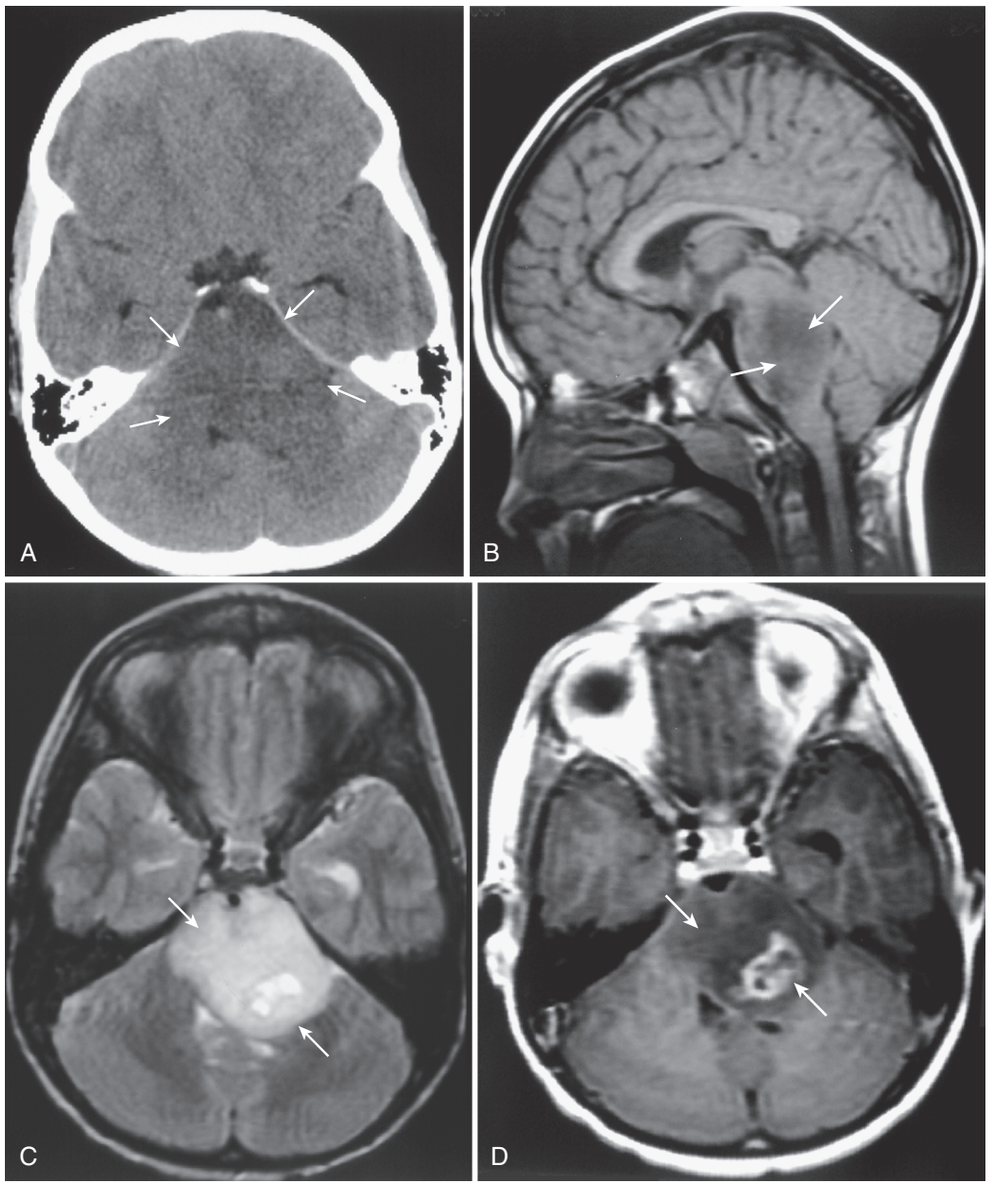

FIGURE 8-62. Pontine/diffuse brainstem glioma (*arrows*) on axial CT (**A**) as well as on sagittal T1-weighted (**B**), axial T2-weighted (**C**), and axial gadolinium-enhanced T1-weighted (**D**) MR images.

Gliomas

Gliomas constitute the largest group of neoplasms arising about the third ventricle. They may arise from the optic pathways, hypothalamus, thalamus, midbrain, foramen of Monro, or wall of the third ventricle. The optic pathway and hypothalamus are the most common sites of origin. The pilocytic astrocytoma characteristically occurs during childhood, often with slow infiltrative growth, and is more commonly solid than cystic in this region. Other astrocytic subtypes and mixed subtypes commonly occur in this region also. Ependymal, oligodendroglial, and choroid plexus tumors are somewhat unusual in this region.

Astrocytomas

Astrocytoma of the optic pathway (i.e., optic glioma) is the most common perisellar tumor of childhood and is frequently associated with NF-1. Exclusively intraorbital lesions include hamartomas, nerve sheath hypertrophy/hyperplasia, and low-grade astrocytomas. Tumors arising from the chiasm and optic tracts may range from hamartomas or low-grade astrocytomas to anaplastic astrocytomas. Multilevel visual pathway involvement also occurs. Glial neoplasms arising primarily within the hypothalamus also range from low-grade to anaplastic astrocytomas. When only a large suprasellar astrocytoma is demonstrated, it may be impossible to distinguish chiasmatic from hypothalamic origin. Diencephalic syndrome is classically associated with large astrocytomas in this region. Imaging of an optic glioma may show optic nerve, chiasm, or tract expansion with anterior or posterior extension (including lateral geniculate bodies and optic radiations). Hypothalamic gliomas are centered behind the chiasm. Astrocytomas are isodense or hypodense on CT, isointense to hypointense on T1-weighted MRI, and isointense to hyperintense on T2-weighted MRI (Fig. 8-65). Enhancement is common and may be homogeneous or irregular. Calcification, cyst, hemorrhage, or tumor hyperdensity is unusual in contrast

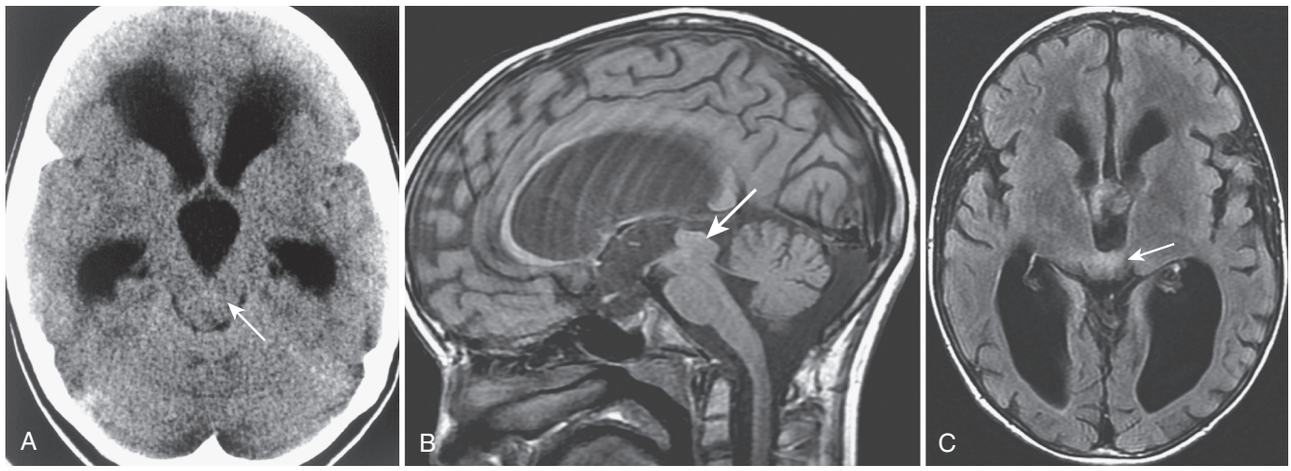

FIGURE 8-63. Tectal glioma (*arrow*) with hydrocephalus on axial CT scan (**A**) and on sagittal T1-weighted (**B**) and axial FLAIR (**C**) MR images.

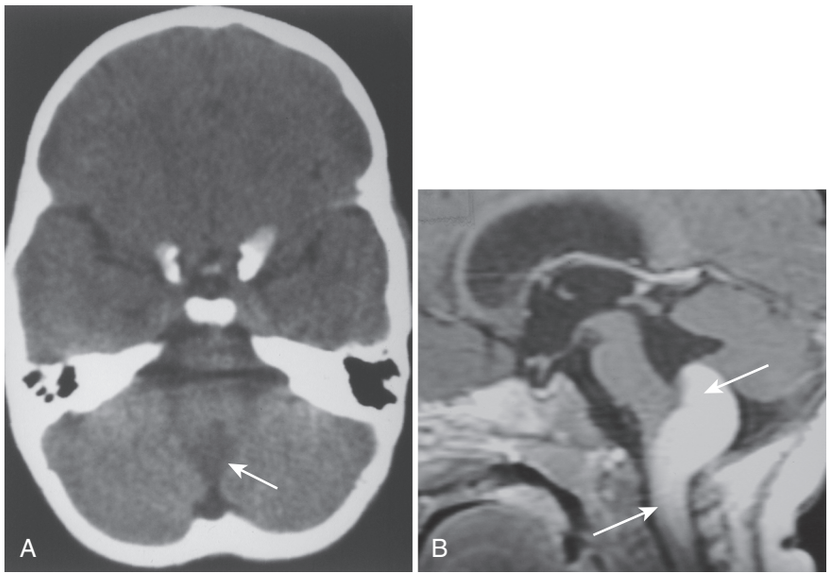

FIGURE 8-64. Cervicomedullary astrocytoma (*arrows*) on axial CT scan (**A**) and gadolinium-enhanced sagittal T1-weighted MR image (**B**).

to craniopharyngioma (calcification, cyst) or germinoma (tumor hyperdensity, hemorrhage). A nonenhancing mass along the tuber cinereum, when associated with precocious puberty, suggests a hamartoma. Differentiation from glioma is necessary especially if there are gelastic seizures. Circumscribed tumors about the third ventricle include the tectal glioma and the giant cell tumor of tuberous sclerosis. The former often manifests as hydrocephalus due to aqueductal stenosis (see "Posterior Fossa Tumors"). The subependymal giant cell tumor of tuberous sclerosis is usually situated near the foramen of Monro and produces asymmetric obstructive hydrocephalus (see "Neurocutaneous Syndromes"). In other cases, the glioma may be infiltrative and poorly marginated with anatomic distortion and extension across the midline (e.g., thalamic astrocytoma). On imaging, the density, intensity, and enhancement characteristics are variable and similar to those of glial tumors arising at other sites (as described earlier). Neuronal and mixed neuronal-glial tumors may also occur about the third ventricle (see "Cerebral Tumors").

Germ Cell Tumors

Germ cell tumors are composed of elements derived from the primitive germ layers. They most commonly arise along the midline in the hypothalamic region, pineal region, or both. Off-midline tumors occasionally occur, especially in Asian populations. This classification includes germinoma, embryonal carcinoma, endodermal sinus tumor, choriocarcinoma, and teratoma. Mixed germ cell tumors also occur. These are considered malignant tumors, except for mature teratomas, and have a tendency for CSF seeding. The "pure" germinoma is highly responsive to combined chemotherapy and radiotherapy, unlike the other "nongerminomatous" tumors. Elevated CSF and serum markers (e.g., alpha-fetoprotein, human chorionic gonadotrophin) are more often associated with the latter group. Imaging of "pure" germinomas demonstrates a midline or paramedian mass that typically is CT-isodense to hyperdense, is T1- and T2-isointense to hypointense with surrounding hyperintensity, and markedly enhances (Figs. 8-66 and 8-67). It is often associated with abnormal pineal calcification, occasionally

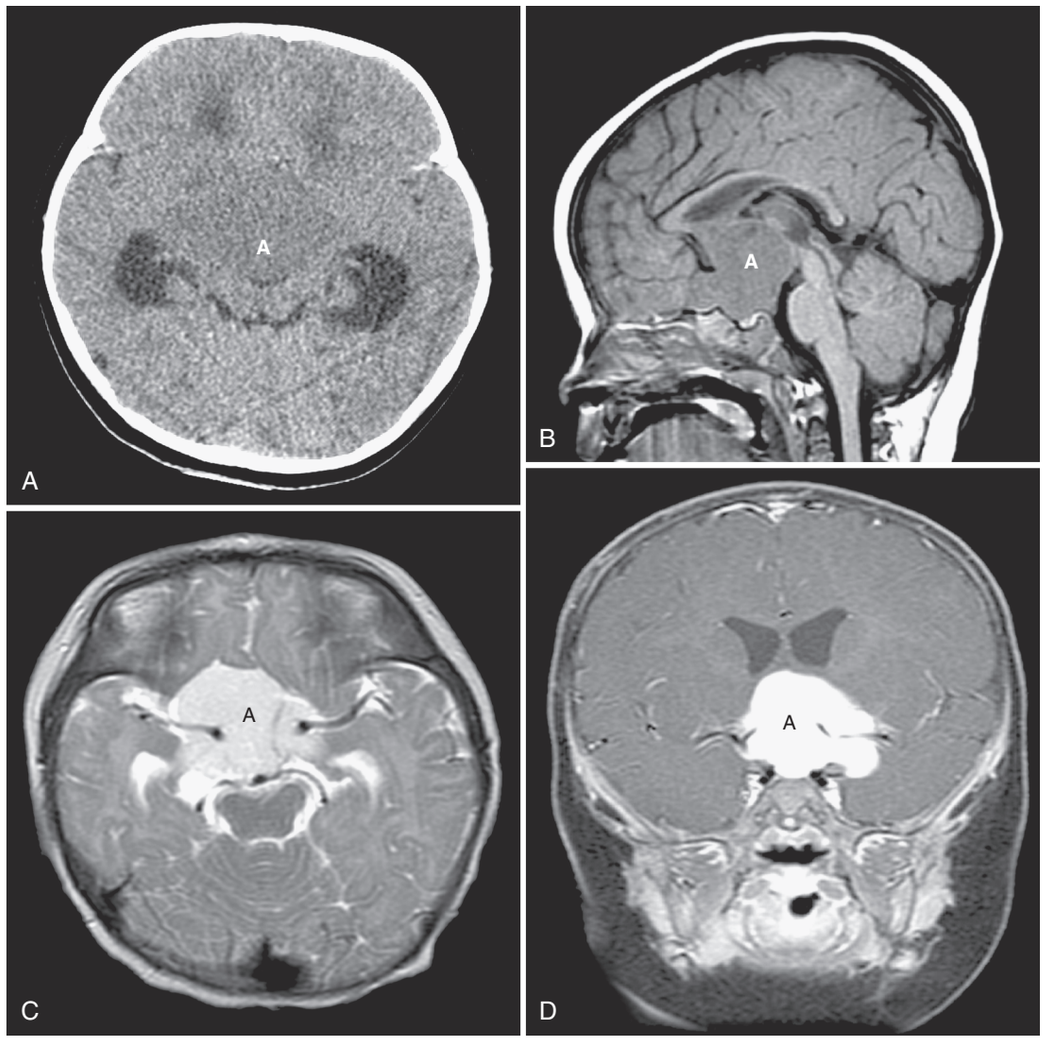

FIGURE 8-65. Optic-hypothalamic astrocytoma (A) on axial CT scan (**A**) and on sagittal T1-weighted (**B**), axial T2-weighted (**C**), and coronal gadolinium-enhanced T1-weighted (**D**) MR images.

hemorrhagic, but rarely cystic. Hypothalamic germinomas often manifest as central diabetes insipidus as indicated by absence of the normal posterior pituitary bright spot (see Figs. 8-1G and 8-66). Langerhans cell histiocytosis may have a similar presentation and imaging findings. Embryonal carcinoma, yolk sac tumor, choriocarcinoma, and teratoma often exhibit more heterogenous density, intensity, and enhancement characteristics. Teratomas are usually composed of a mixture of differentiated tissues representing derivatives of the three embryonic germ layers. They are often circumscribed and cystic masses that may contain calcification, bone, cartilage, teeth, or adipose tissue. Teratomas are divided into mature (e.g., adult tissue elements) and immature (e.g., embryonic elements) types. Mature teratomas are slow growing and benign. Immature teratomas are predominantly neuroepithelial and may be benign or malignant in behavior. Teratomas containing other germ cell tumor, carcinoma, or sarcoma elements (i.e., teratocarcinomas) are malignant. Imaging of a teratoma usually demonstrates a lobulated or cystic mass with heterogenous CT densities and MRI intensities containing fat, calcium, ossification, or cartilage (Fig. 8-68). Contrast enhancement may be more prominent in the malignant forms.

Pineal Parenchymal Tumors

Pineal parenchymal tumors include pineoblastoma, pineocytoma, and mixed/transitional pineal tumors. Pineoblastomas occur primarily in childhood. They are embryonal tumors similar to PNETs, and are considered highly malignant neoplasms with a propensity to disseminate in the CSF pathways. Imaging often shows a large lobulated pineal region mass with extensive calcification. The tumor is often CT-isodense to hyperdense, T1-isointense to hypointense, and T2-isointense to hypointense. Marked enhancement and hydrocephalus are common. Pineocytomas are generally circumscribed and may be calcified.

Malformative Tumors

The common malformative tumors occurring about the third ventricle include craniopharyngioma, Rathke cyst, colloid cyst, pineal cyst, arachnoid cyst, lipoma, hamartoma, and dermoid/epidermoid.

The *craniopharyngioma* (CPG) is a benign but aggressive squamous epithelial neoplasm arising in the suprasellar or intrasellar region. It is probably of Rathke pouch origin and most commonly occurs in childhood. CPGs are usually cystic and calcified but often have a solid component. They tend to deform, encase, or adhere

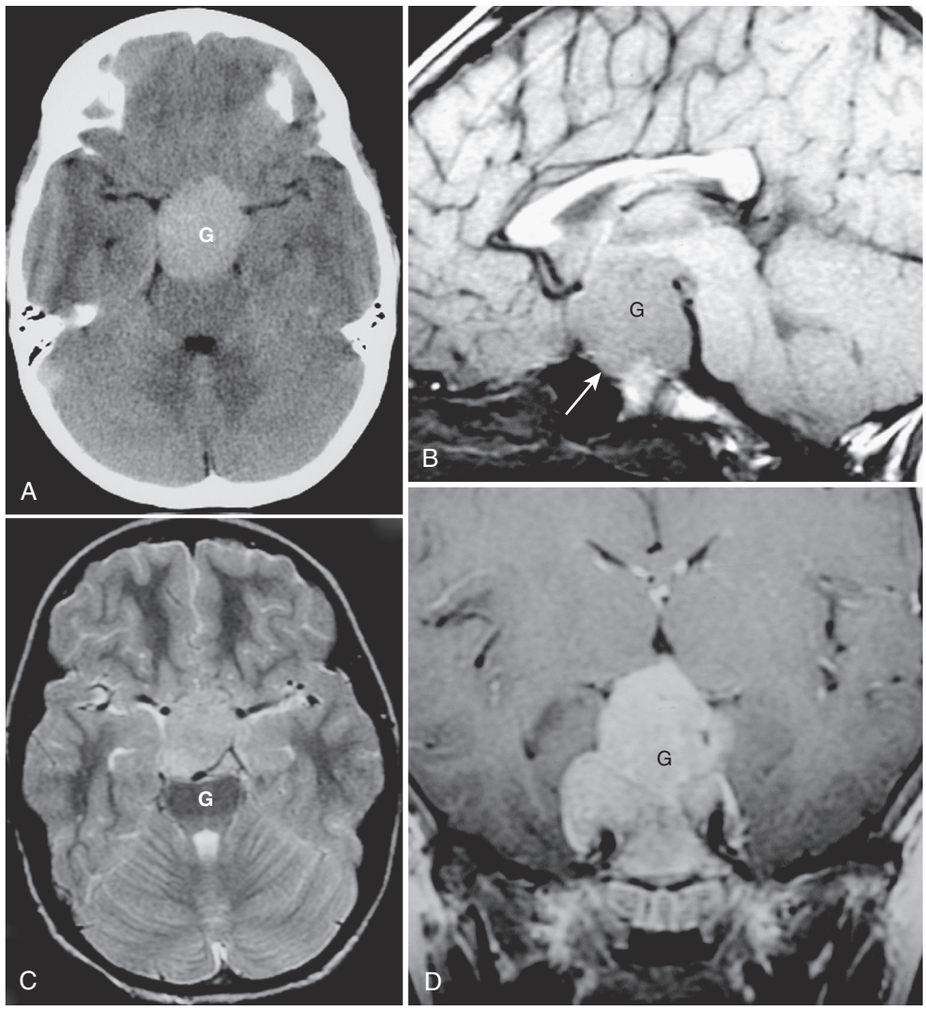

FIGURE 8-66. Hypothalamic germinoma (G) with absence of the posterior pituitary bright spot (*arrow* in **B**) on axial CT scan (**A**) as well as sagittal T1-weighted (**B**), axial T2-weighted (**C**), and coronal gadolinium-enhanced T1-weighted (**D**) MR images.

to adjacent structures and are associated with a gliotic reaction. The solid component of a CPG is CT-isodense or hypodense, T1-isointense to hypointense, and T2-isointense to hyperintense. Enhancement of the solid tumor or cyst wall is common. The calcified, ossified, or keratinized components of CPG are CT-hyperdense and of variable intensity on MRI. On CT, the cyst may be primarily hypodense (e.g., cholesterol or serous), or isodense to hyperdense (e.g., protein, hemorrhage, keratin, or calcium). On MRI, the cyst is characteristically of high intensity on all sequences, particularly on T1-weighted images (Fig. 8-69). Hypointensity may indicate keratin, calcium, or iron. The differential diagnosis may include the rare cystic or calcified glioma or teratoma. *Rathke cyst*, an epithelial cyst also of Rathke pouch origin, may be similar in appearance to CPG; however, calcification and nodular enhancement are unusual.

The *colloid cyst* is probably of neuroepithelial origin and occurs more often in adulthood. It has a fibrous wall and proteinaceous content. It arises in the wall or roof of the third ventricle at the foramina of Monro and often produces hydrocephalus. Occasionally there is hemorrhage. The colloid cyst is usually hyperdense and nonenhancing (rarely isodense or hypodense) on CT. It may be of low or high intensity on T1- and T2-weighted images.

Other neuroepithelial cysts (e.g., glioependymal) may arise in a variety of locations, including the choroid plexus and the pineal gland. They may be detected only with MRI and usually appear T1-hypointense, FLAIR-hyperintense, and T2-hyperintense. Enhancement of the cyst wall is common, although there may be delayed enhancement within the cyst. The *pineal cyst* may be associated with deformity of the adjacent tectum and aqueduct, but hydrocephalus is rare. *Arachnoid cysts* are arachnoid-lined cysts that contain CSF, usually arise in the subarachnoid spaces, and commonly occur in the suprasellar region or about the quadrigeminal plate region (see Figs. 8-11, 8-16, and 8-17). They are CT-hypodense, conform to CSF intensities on MRI sequences (T1-hypointense, FLAIR-hypointense, T2-hyperintense, DWI-hypointense, ADC-hyperintense), do not enhance, and may have no perceptible wall. These features distinguish arachnoid cysts from neuroepithelial cysts (see earlier) and tumor cysts. Associated hemorrhage or infection, however, may change their appearance.

Lipomas are benign mesenchymal hamartomas consisting of adipose tissue (neutral fat). There may be associated muscle, fibrous, or vascular elements. They most commonly occur along the hypothalamus or stalk, quadrigeminal plate, and corpus callosum (e.g., in callosal hypogenesis). CT shows fatty hypodensity and occasional calcification. MRI demonstrates the tumor's characteristic high intensity on T1-weighted and FLAIR images, isointensity to hypointensity on T2-weighted images, chemical shift artifact, and signal loss on fat suppression sequences (Fig. 8-70A). In the suprasellar region, lipoma is to be distinguished from an ectopic posterior pituitary. Normally, the posterior pituitary is demonstrated on T1-weighted MRI as a posterior intrasellar hyperintensity (probably related to the carrier protein for antidiuretic hormone). The pituitary's presence usually indicates normal

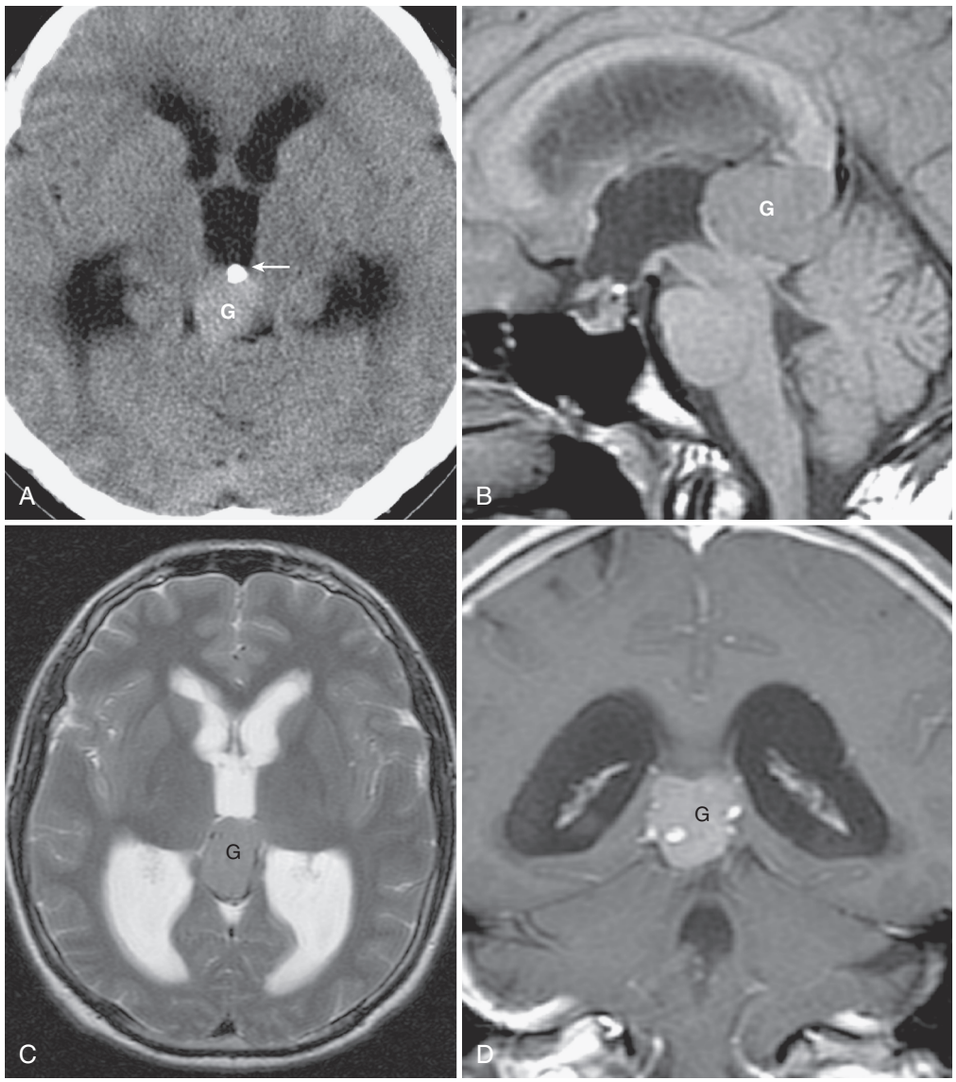

FIGURE 8-67. Pineal germinoma (G) with calcification (*arrow*) and hydrocephalus on axial CT (**A**) as well as sagittal T1-weighted (**B**), axial T2-weighted (**C**), and coronal gadolinium-enhanced T1-weighted (**D**) MR images.

antidiuretic hormone physiology (see Fig. 8-1G); its absence usually correlates with diabetes insipidus and often with hypothalamic or stalk tumor (see Fig. 8-66). Ectopic posterior pituitary is usually associated with "idiopathic" growth hormone deficiency, appears as a hypothalamic or infundibular hyperintensity on T1-weighted MRI, and is associated with absence of the normal intrasellar posterior pituitary bright spot (Fig. 8-70B). Often there is absence, interruption, or attenuation of the stalk. Lipoma and ectopic posterior pituitary are usually centered posterior to the stalk, whereas craniopharyngioma and Rathke cyst are usually more anterior.

Neuroepithelial hamartomas are composed of disorganized neuronal or glial elements. The hypothalamic location (i.e., hamartoma of the tuber cinereum) may be associated with precocious puberty, gelastic seizures, or NF-1. The hamartoma is usually CT-isodense to hypodense, T1-isointense, FLAIR-isointense to hyperintense, and T2-hyperintense (Fig. 8-71). Enhancement is unusual. Other hamartomatous lesions are ectopic masses of neural, glial, or meningeal tissue that develop in juxtacranial or extracranial locations, for example, nasal glioma. *Meningioangiomatosis* is a rare hamartomatous condition consisting of local proliferation of arachnoid cells, vessels, and Schwann cells.

Epidermoid and dermoid tumors tend to be cystic and probably result from inclusion of epithelial elements at the time of neural tube closure. Epidermoid cysts are of ectodermal origin and are lined with keratinizing stratified squamous epithelium. They often contain desquamated cellular debris and cholesterol, the latter as a breakdown product of keratin. Dermoids are also of ectodermal origin. Additional elements are derived from skin appendages, including hair, sebaceous glands, and sweat glands. The breakdown products of these elements produce an oily lipid-like mixture. Occasionally these tumors also contain calcification, bone, cartilage, or, rarely, teeth (i.e., teratoid), thus raising the question of a link with true teratomas. Epidermoids more commonly arise off the midline and conform to CSF densities and intensities. Occasionally there is cyst wall calcification. Their hyperintense appearance on FLAIR MRI and DWI distinguish them from arachnoid cysts. Dermoid cysts arise as midline lesions, contain calcification or formed elements, have lipid densities and intensities, and are often associated with a dermal sinus or bony defect; however, it may be impossible to distinguish among these three entities. Cyst rupture may be associated with aseptic meningitis or arachnoiditis and hydrocephalus. T1-hyperintense lipid particles or lipid-CSF levels may be present.

Pituitary Tumors

The most common intrasellar neoplasms include the pituitary adenoma and the craniopharyngioma (see earlier). Pituitary adenomas are currently divided into hormonally active (about

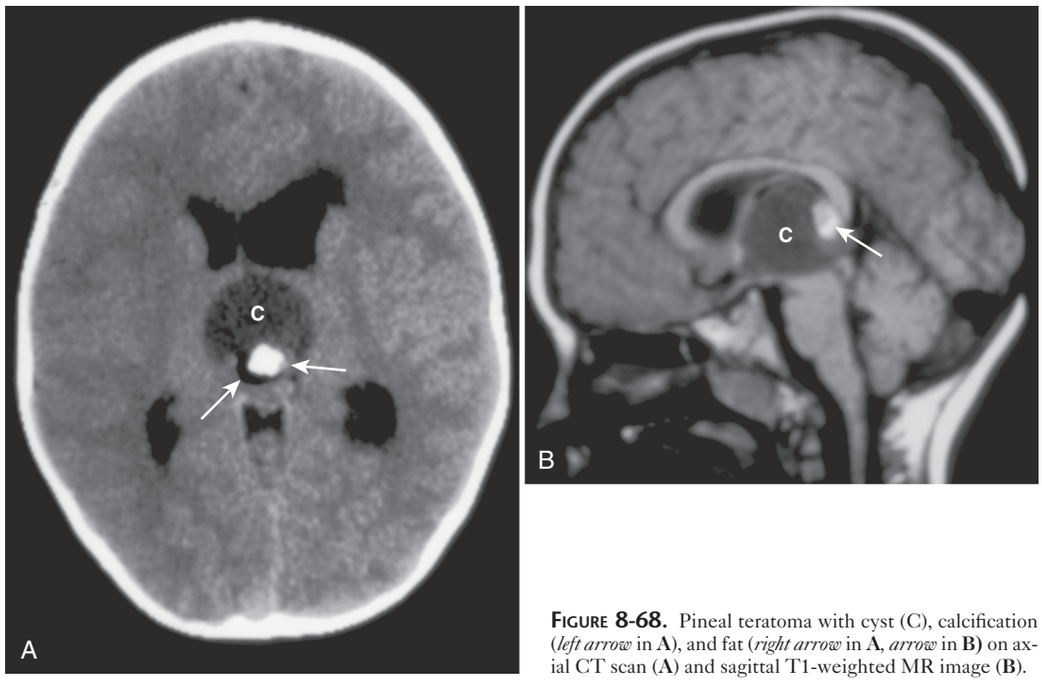

FIGURE 8-68. Pineal teratoma with cyst (C), calcification (*left arrow* in **A**), and fat (*right arrow* in **A**, *arrow* in **B**) on axial CT scan (**A**) and sagittal T1-weighted MR image (**B**).

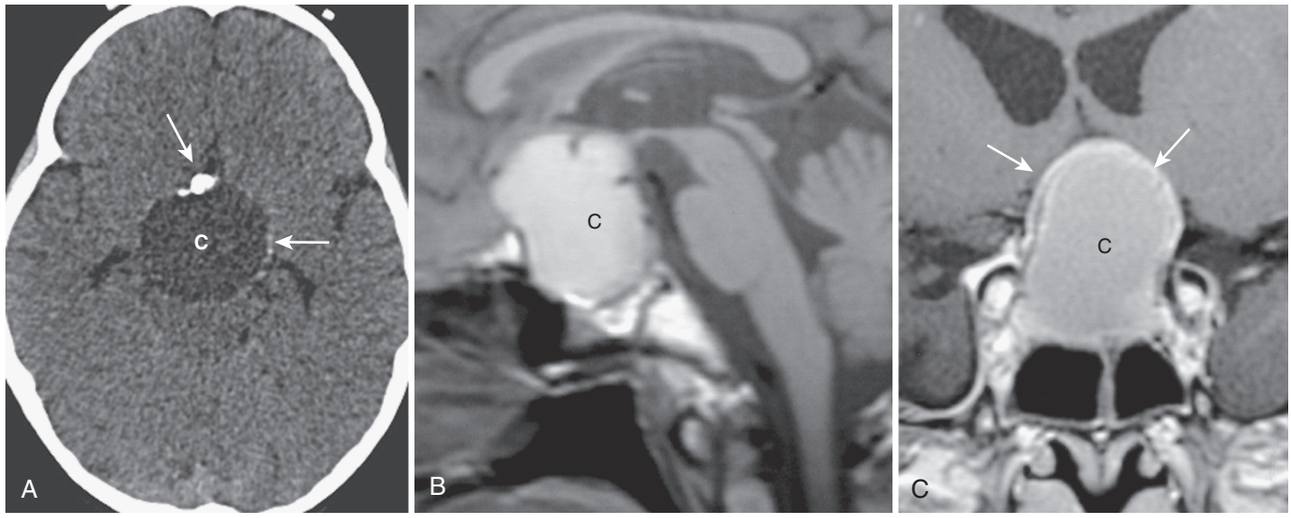

FIGURE 8-69. Craniopharyngioma with cyst (C), calcifications (*arrows* in **A**), and wall enhancement (*arrows* in **C**) on axial CT (**A**) as well as sagittal T1-weighted (**B**) and coronal gadolinium-enhanced T1-weighted (**C**) MR images.

70%) and inactive groups. They are more common in adults than in children. The most common hormonally active tumors secrete prolactin, growth hormone, or a combination. Many of the prolactin-secreting or adrenocorticotropic hormone–secreting tumors are microadenomas (<1 cm diameter). Hemorrhagic, prolactin-secreting macroadenomas characteristically occur in adolescent males. Often there is suprasellar extension of the T1-hyperintense mass, and it may be mistaken for craniopharyngioma or a Rathke cyst (Fig. 8-72).

Meningeal tumors, especially meningioma, may arise in the perisellar region or in the pineal region from the tentorium. However, these tumors are extremely rare in childhood. For meningeal tumors arising about the sella, differential diagnostic considerations include fibrous dysplasia, pituitary adenoma, and aneurysm.

Cerebral Tumors

Cerebral hemispheric tumors may manifest as seizures, hemiparesis, movement disorder, headache, other sensory phenomena, increased pressure, or cognitive disorders. Most intracranial masses or "tumors" of infancy are nonneoplastic and "cystic" (e.g., porencephaly, arachnoid cyst, Dandy-Walker cyst, galenic varix). Neoplasms, although rare in infancy, may be astrocytomas, embryonal tumors (e.g., PNET, ATRT), germ cell tumors (e.g., teratoma), choroid plexus tumors (papilloma, carcinoma), or mesenchymal tumors (e.g., sarcoma). In older children and adolescents, most intracranial tumors are of neuroepithelial origin, including gliomas, neuronal or mixed neuronal and glial tumors (e.g., ganglioglioma, neurocytoma, dysembryoplastic neuroepithelial tumor), and embryonal tumors (e.g., PNET). Nonneoplastic supratentorial masses include arachnoid cysts, abscess or empyema, hamartomas,

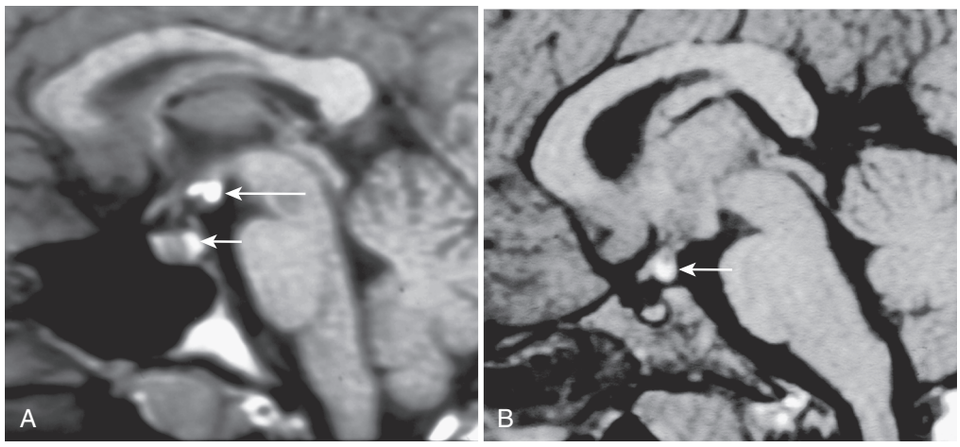

FIGURE 8-70. **A,** Hypothalamic lipoma (*long arrow*) with normal posterior pituitary bright spot (*short arrow*) on sagittal T1-weighted MR image. **B,** Ectopic posterior pituitary (*arrow*) on sagittal T1-weighted MR image.

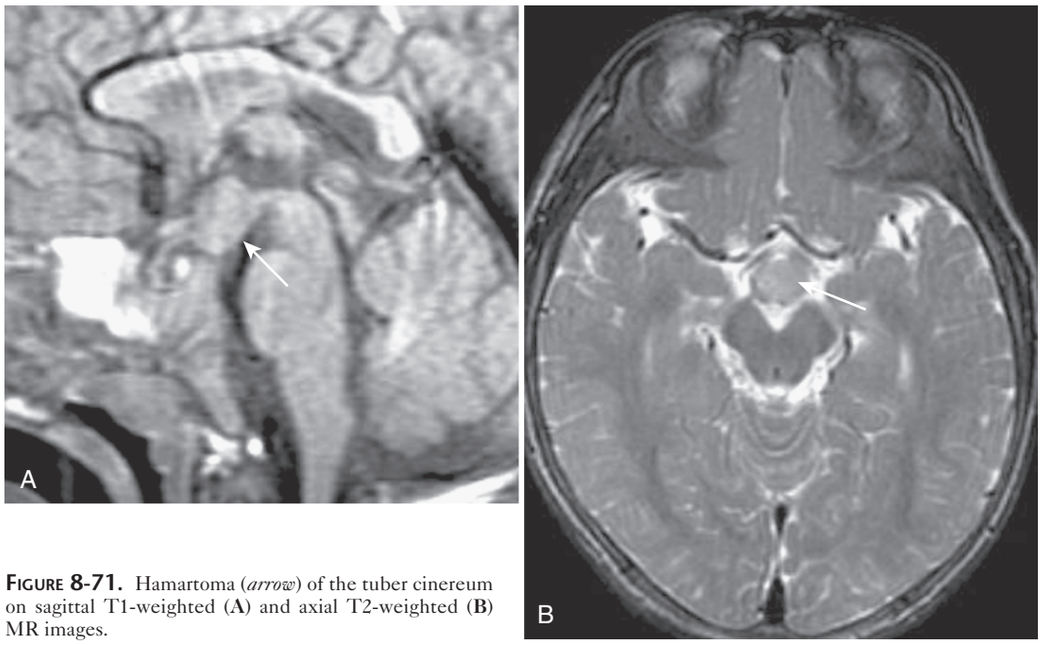

FIGURE 8-71. Hamartoma (*arrow*) of the tuber cinereum on sagittal T1-weighted (**A**) and axial T2-weighted (**B**) MR images.

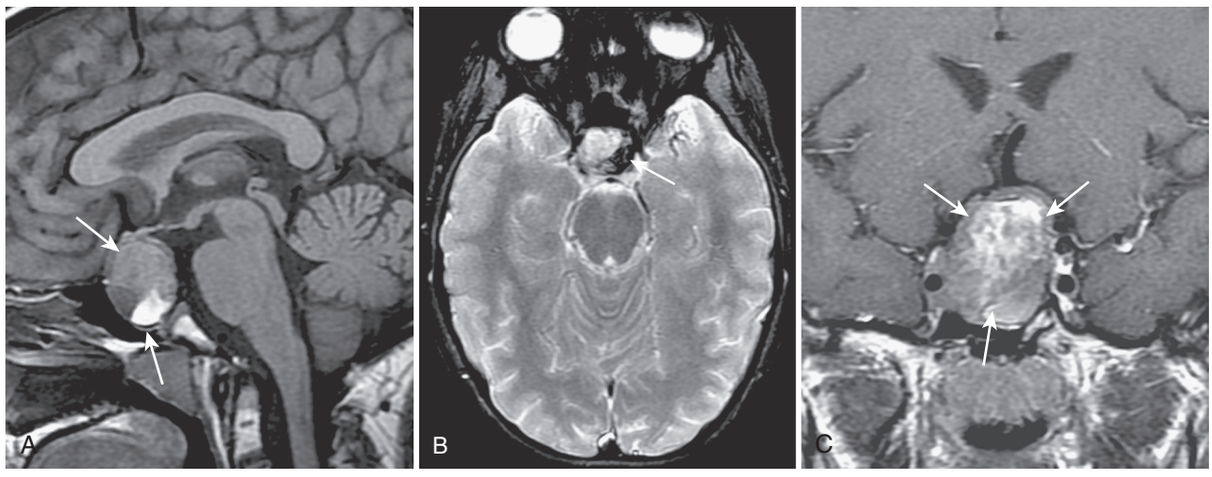

FIGURE 8-72. Hemorrhagic pituitary adenoma (*arrows*) on sagittal T1-weighted (**A**), axial GRE (**B**), and coronal gadolinium-enhanced T1-weighted (**C**) MR images.

vascular malformations (e.g., cavernous malformation), hematoma, and so forth. Extradural, calvarial, or scalp lesions (parameningeal) that may encroach upon the cerebral hemisphere include metastases (e.g., neuroblastoma), osteoma, dermoid-epidermoid, histiocytosis, hemangioma or other vascular anomaly, fibrous dysplasia, sarcomas, lymphoma, leukemia, neurofibroma, fibroma/fibromatosis, and infections.

Astrocytic Tumors

Astrocytic tumors account for the majority of gliomas and primary cerebral tumors in childhood. The tumors may be well-defined and circumscribed (e.g., pilocytic astrocytoma), ill-defined and infiltrating (e.g., fibrillary or anaplastic astrocytoma), or both (e.g., glioblastoma). These neoplasms may be cystic, solid, or calcified. Often, the tumors are CT-isodense to hypodense, T1-isointense to hypointense, and T2-isointense to hyperintense. Enhancement is variable (Fig. 8-73). A well-defined tumor in which the gadolinium enhancement matches the extent of the T2 hyperintensity may suggest a pilocytic astrocytoma. Imaging findings that may occasionally indicate the tendency for higher grades of malignancy include density or intensity heterogeneity, irregular shape and poor margination, mass effect, edema, hemorrhage, and irregularly thick and nodular ring-like or solid enhancement (Fig. 8-74). However, density, intensity, and enhancement characteristics do not consistently correlate with grade of malignancy nor serve as accurate indicators of tumor margins (tumor vs. edema). For astrocytic tumors, as well as most other CNS neoplasia, maximum safe surgical excision or debulking is preferred to biopsy. Radiotherapy, chemotherapy, or both are important in the treatment of higher-grade tumors as well as recurrent or symptomatic lower-grade tumors. Higher-grade tumors often show faster response rates but recur earlier than lower-grade tumors. A transient increase in tumor volume, including mass effect, edema, and enhancement, may occur after radiotherapy, particularly after stereotactic radiosurgery or stereotactic (fractionated) radiotherapy.

Glioblastoma

Glioblastoma (GBM) is generally considered an anaplastic form of astrocytoma. GBM occurs primarily in the cerebrum during adolescence and is the most malignant of the neuroepithelial tumors, in terms of seeding potential and poor survival. A congenital form has also been reported. Variants include the giant cell glioblastoma and the gliosarcoma. The imaging findings are diverse and range

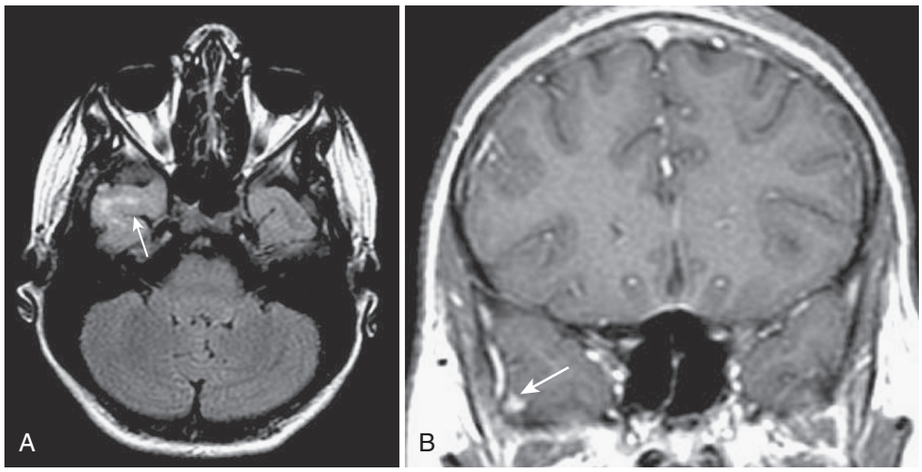

FIGURE 8-73. Temporal lobe epilepsy with astrocytoma (*arrows*) appears as focal hyperintensity on an axial FLAIR MR image (**A**) and as nodular enhancement on a coronal gadolinium-enhanced T1-weighted MR image (**B**).

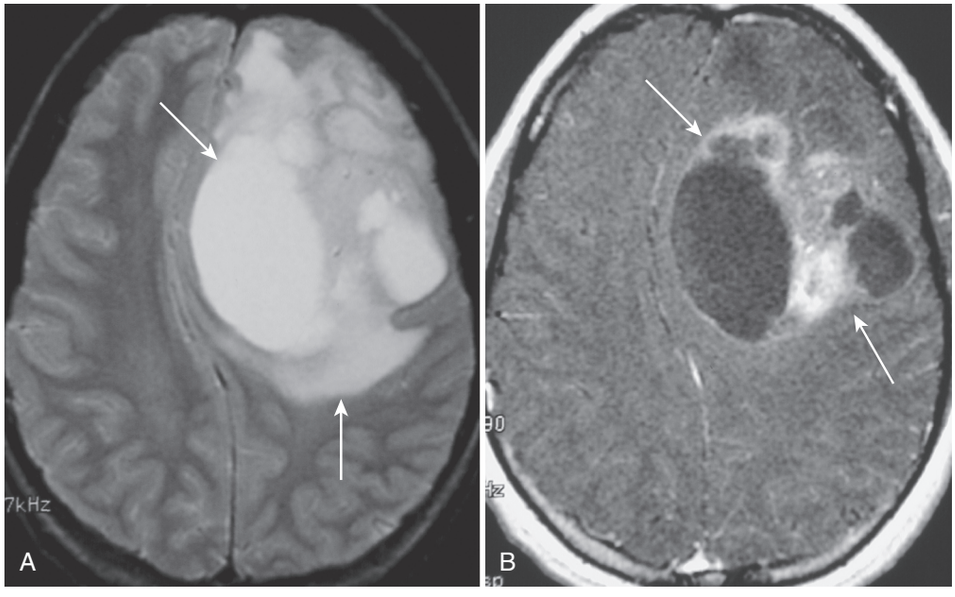

FIGURE 8-74. Frontal anaplastic astrocytoma/glioblastoma (*arrows*) on axial T2-weighted (**A**) and axial gadolinium-enhanced T1-weighted (**B**) MR images.

from a circumscribed mass to a diffuse process. Often GBMs are large, heterogenous, solid or cystic, and usually enhancing tumors with mass effect, edema, or hemorrhage (see Fig. 8-74). Calcification is occasionally present. Irregular nodular ring enhancement with a necrotic center and surrounding vasogenic edema is often characteristic. The giant cell GBM may appear as a cyst with a mural nodule. *Gliomatosis cerebri* refers to the rare entity of diffuse infiltrative glioma that involves either multiple sites or large areas of the CNS, usually the cerebral hemispheres. Pathologically, gliomatosis cerebri resembles diffuse astrocytoma, although foci of GBM may occur. It is distinguished from diffuse leptomeningeal or intraventricular spread of malignant glioma. Imaging usually underestimates the extent of tumor involvement in gliomatosis.

Other Gliomas

Ependymomas of childhood occasionally arise within the cerebrum. Oligodendrogliomas and mixed gliomas occur less often in children than in adults.

Ependymal tumors often project outward from the lateral ventricular ependyma or arise from ependymal cell rests in the cortex (i.e., cortical ependymoma). Imaging may demonstrate a heterogenous or occasionally homogeneous density or intensity mass, often with calcification and cyst formation plus irregular enhancement (Fig. 8-75). Other tumors with a similar appearance that are part of the differential diagnosis of ependymomas include PNET, ATRT, choroid plexus carcinoma, anaplastic gliomas, and GBM. Anaplastic forms may seed.

The well-differentiated or pure *oligodendroglioma* (ODG), a common tumor of adulthood, rarely occurs in childhood. It may contain other glial elements, most often astrocytic (i.e., oligoastrocytoma). Other circumscribed cerebral cortical tumors that occur more commonly in childhood and may be mistaken for ODG include dysembryoplastic neuroepithelial tumor, ganglioglioma, astrocytoma, astroblastoma (cortical ependymoma), and pleomorphic xanthoastrocytoma (PXA). These are often slow growing and circumscribed, may calcify, and may thin the cranial inner table. Rarely is there invasion or spread into the leptomeninges. The imaging appearance is often that of a circumscribed mass of uniform density or intensity that is solid, cystic, or both (Fig. 8-76). Calcification may be the major feature. The tumor itself is often CT-isodense to hypodense with calcific high density, T1-isointense to hypointense, and T2-isointense to hyperintense. Edema is often lacking, and the extent of enhancement is variable. Nonneoplastic lesions which may be revealed by CT as a solitary calcific high density are cavernous angiomas, neuroglial hamartomas (e.g., tuber), and inflammatory lesions (e.g., cysticercosis). A poorly marginated tumor with heterogenous density/intensity characteristics, irregular enhancement, edema, or dissemination may indicate a mixed or anaplastic glioma (e.g., anaplastic ependymoma), or a mixed glioneuronal tumor (e.g., anaplastic ganglioglioma). The *subependymoma*, also rare in childhood, is a special type of mixed glioma composed of astrocytes and ependymal cells arising beneath the ventricular ependyma.

Choroid Plexus Tumors

Tumors of the choroid plexus origin are encountered primarily in early childhood and are usually associated with hydrocephalus. *Papillomas* are generally circumscribed intraventricular tumors usually involving the lateral ventricle and rarely the third or fourth ventricle (Fig. 8-77). Carcinomas are malignant and invasive, often extend beyond the ventricular margins, and are associated with mass effect and edema (Fig. 8-78). These are hypercellular and highly vascular neoplasms that often calcify or hemorrhage. These are usually CT-isodense to hyperdense, T1-isointense to hypointense, and T2-isointense to hyperintense. Marked contrast enhancement is common. ATRT may also be of choroid plexus origin.

Embryonal Tumors

The common embryonal tumors arising within the cerebral hemispheres include the *primitive neuroectodermal tumors* and, less often, the cerebral neuroblastoma or ATRT. Like other embryonal tumors (e.g., medulloblastoma), PNET is a malignant, hypercellular tumor with a tendency for seeding. Imaging commonly shows a large heterogenous mass with calcification or cyst, occasional hemorrhage, but variable edema. It is CT-isodense to hyperdense, T1-isointense to hypointense, and T2-isointense to hypointense with surrounding hyperintense edema (Fig. 8-79). Marked enhancement is common. Other tumors in the differential diagnosis with similar findings include ependymoma (see Fig. 8-75), choroid plexus carcinoma (see Fig. 8-78), and ATRT (Fig. 8-80).

Neuronal Tumors

Common neuronal, or mixed neuronal-glial, tumors of the cerebrum include ganglioglioma, dysembryoplastic neuroepithelial tumor, and neurocytoma.

Gangliogliomas are cortical tumors that are often cystic or calcified and are frequently associated with focal seizures. They are CT-isodense or hyperdense, T1-isointense to hypointense, and T2-isointense to hyperintense, and they commonly enhance (Fig. 8-81). The desmoplastic ganglioglioma characteristically occurs in infancy and is often cystic with nodular enhancement

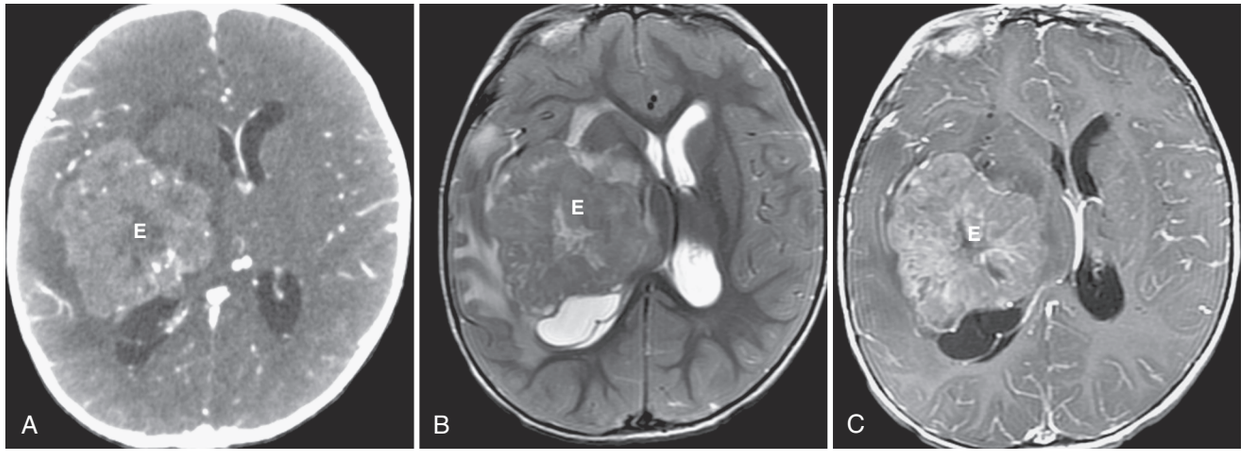

FIGURE 8-75. Cerebral ependymoma (E) on contrast axial CT scan (**A**) and on axial T2-weighted (**B**), and gadolinium-enhanced T1-weighted (**C**) MR images, which demonstrate calcifications, enhancement, and edema.

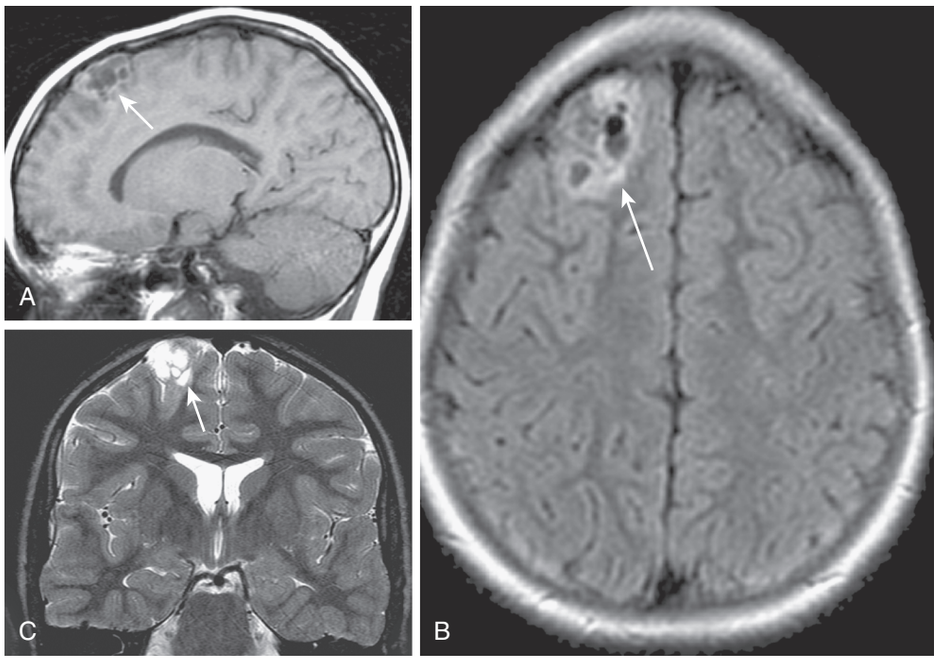

FIGURE 8-76. Frontal cortical ependymoma (*arrow*) on sagittal T1-weighted (**A**), axial FLAIR (**B**), and coronal T2-weighted (**C**) MR images; the features are similar to those of a dysembryoplastic neuroepithelial tumor.

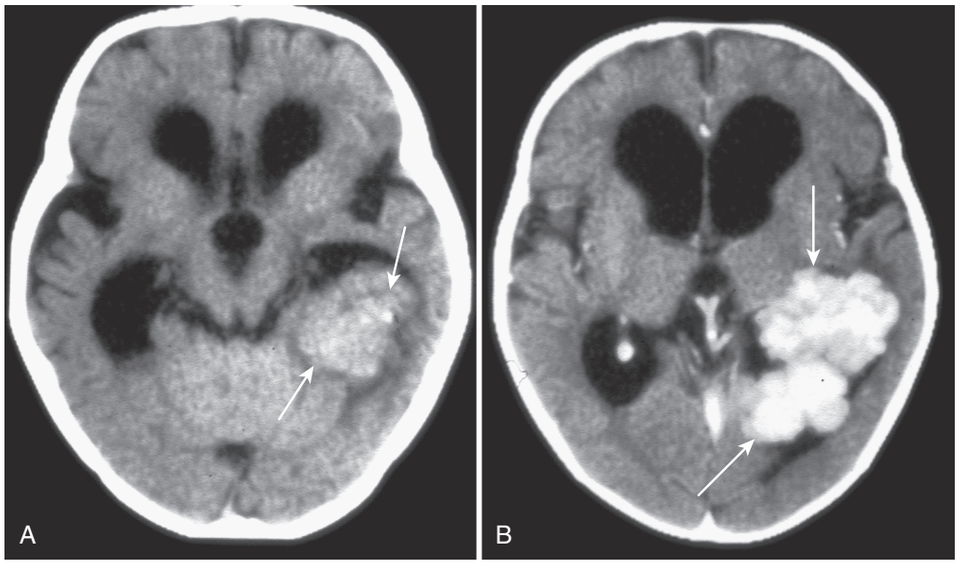

FIGURE 8-77. Choroid plexus papilloma (*arrows*) with hydrocephalus on pre-contrast (**A**) and post-contrast (**B**) CT scans, which demonstrate calcifications and enhancement.

(Fig. 8-82). It may be indistinguishable from the desmoplastic astrocytoma of infancy.

Dysembryoplastic neuroepithelial tumors are typically associated with partial seizures that may be intractable. They are well-defined cortical lesions with little or no edema. Mass effect and cortical effacement are often subtle. Nodularity, or a bubbly appearance, is characteristic, whereas focal contrast enhancement, calcification, or cystic change is less frequent (Fig. 8-83). A hyperintense rim on FLAIR MR imaging may be seen, along with thinning of the adjacent cranium.

The *central neurocytoma* typically occurs about the lateral ventricles, often in the region of the foramen of Monro. Calcification is common. The differential diagnosis may include other circumscribed periventricular tumors, such as giant cell tumor or subependymal giant cell astrocytoma (e.g., tuberous sclerosis), astrocytoma, ependymoma, and choroid plexus papilloma.

Meningeal Tumors

Meningioma occurs uncommonly in childhood. It may be sporadic, associated with NF-2, or radiation-induced. Such tumors tend to be durally based or to arise from the choroid plexus. Imaging often demonstrates a circumscribed extracerebral or intraventricular mass with calcification, marked vascularity, and lytic or blastic (hyperostosis) bony involvement. The tumor tends to be CT-isodense or hyperdense, T1-isointense to hypointense, and T2-isointense to hyperintense or hypointense, and it enhances markedly with a dural tail (Fig. 8-84). Other *nonmeningothelial mesenchymal tumors* arising from the meninges include lesions such as meningeal sarcoma and ATRT. These show a variety of findings, including density, intensity, and enhancement heterogeneity with vascular, calcific, and cystic or necrotic components. *Primary melanocytic lesions* of the meninges include melanosis (e.g., neurocutaneous melanosis),

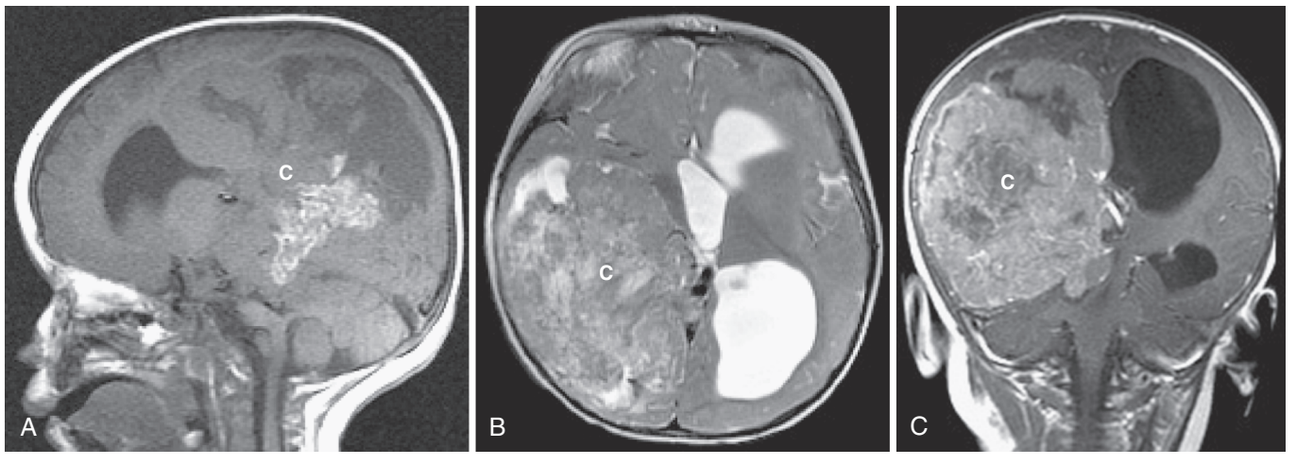

FIGURE 8-78. Choroid plexus carcinoma (C) on sagittal T1-weighted (**A**), axial T2-weighted (**B**), and coronal gadolinium-enhanced T1-weighted (**C**) MR images, which demonstrate calcifications, hemorrhage, and enhancement.

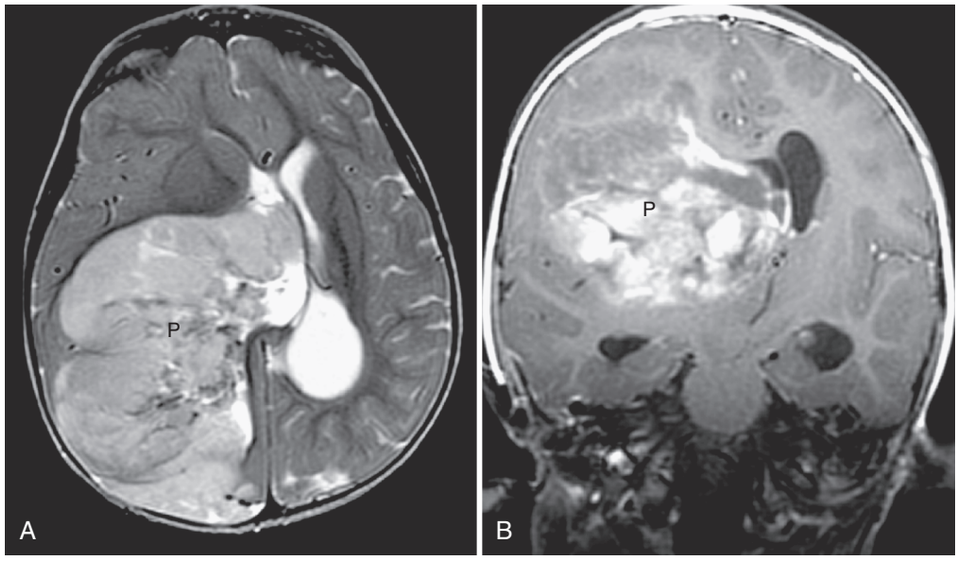

FIGURE 8-79. Cerebral primitive neuroepithelial tumor (P) on axial T2-weighted (**A**) and coronal gadolinium-enhanced T1-weighted (**B**) MR images.

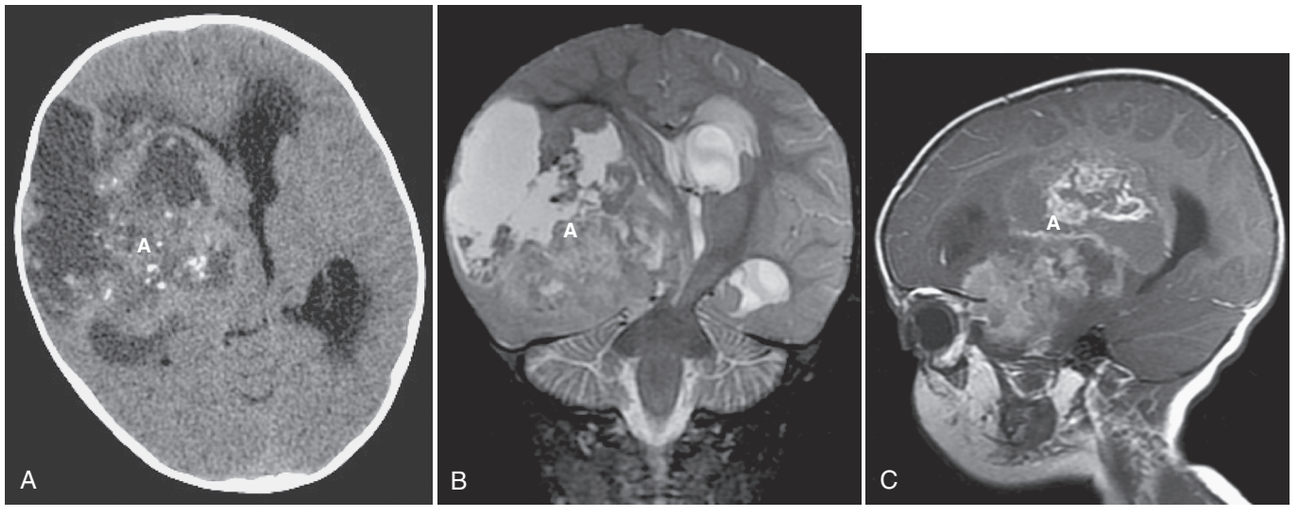

FIGURE 8-80. Cerebral atypical teratoid rhabdoid tumor (A) on axial CT (**A**), coronal T2-weighted (**B**), and sagittal gadolinium-enhanced T1-weighted (**C**) MR images.

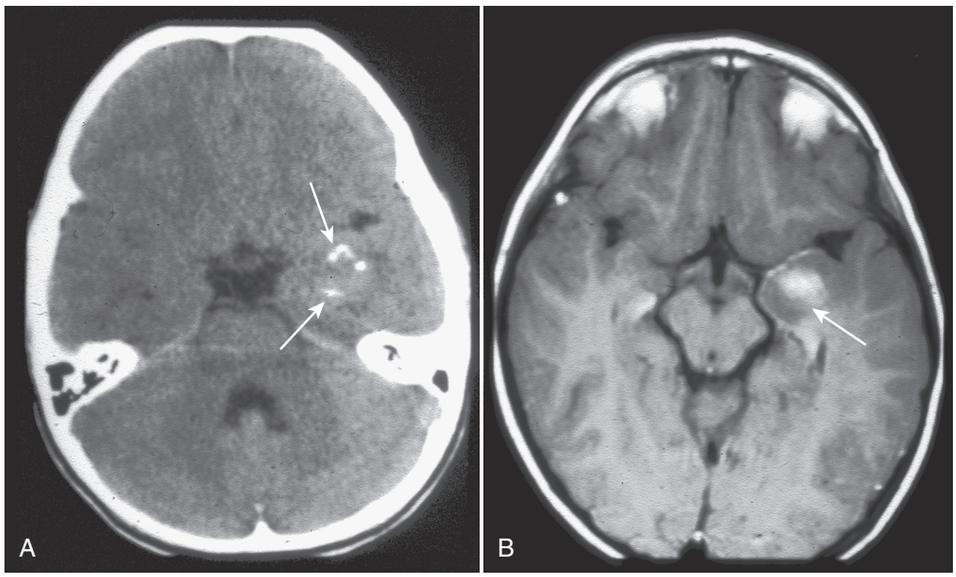

FIGURE 8-81. Temporal ganglioglioma (*arrows*) on axial CT scan (**A**) and axial gadolinium-enhanced T1-weighted MR image (**B**) showing calcification and enhancement.

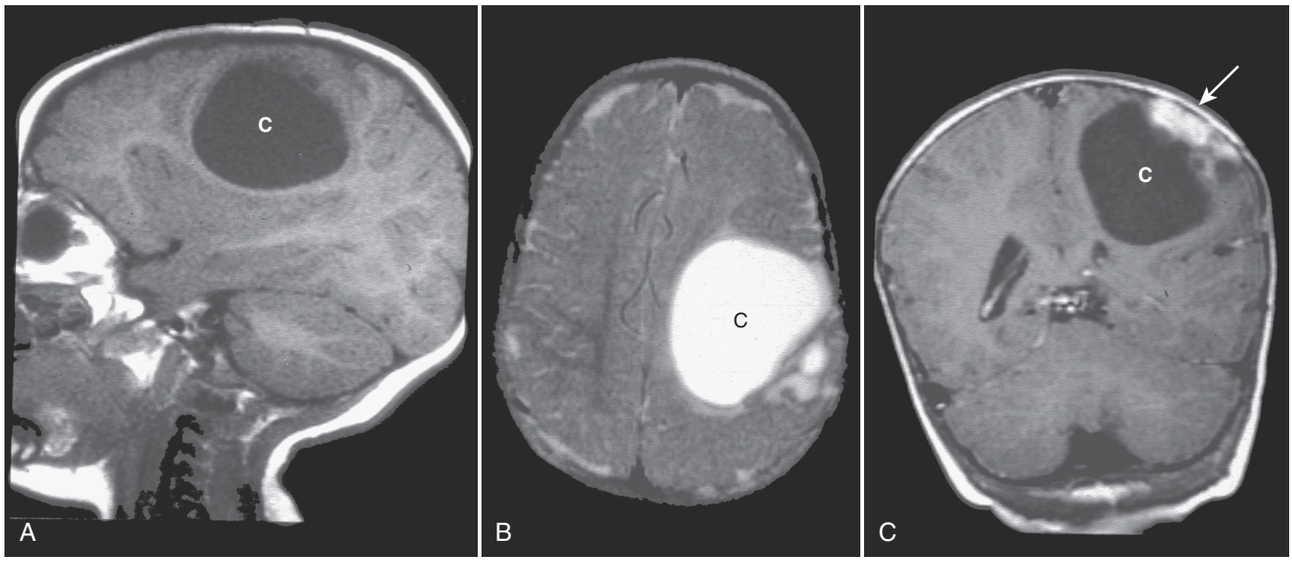

FIGURE 8-82. Desmoplastic ganglioglioma (C) on sagittal T1-weighted (**A**), axial T2-weighted (**B**) MR images. **C,** Coronal gadolinium-enhanced T1-weighted MR image demonstrates nodular enhancement (*arrow*).

melanocytoma, melanoma, and melanomatosis. Melanin-containing tumors are characteristically CT-hyperdense, T1-hyperintense, and T2-hypointense, often with hemorrhage and enhancement.

Other Tumors

Involvement of the CNS secondarily by *lymphoid and other hematologic malignancies* is uncommon in childhood. These may occur in the setting of leukemia (e.g., chloroma), lymphoma, or an underlying congenital or acquired immunodeficiency disorder (e.g., HIV-AIDS, post-transplant lymphoproliferative disorder). The lesions are often CT-isodense to hyperdense, T1-isointense to hypointense, and T2-hypointense with variable enhancement (Fig. 8-85).

Parameningeal and Metastatic Tumors

Parameningeal tumors arise outside (i.e., extradural) but are contiguous with the CNS (see Chapter 10). They may involve the intracranial or intraspinal structures without specific neurologic symptoms or signs. Parameningeal tumors of the head and neck may arise from or involve the scalp, cranial vault, cranial base, sinuses or pharynx, orbits, petrous temporal structures, or soft tissues of the face or neck. Although invasive parameningeal processes are often malignant neoplasms, benign neoplasms (e.g., epidermoid; Fig. 8-86) or nonneoplastic processes (e.g., inflammatory) may occasionally be aggressive. Dysplastic conditions may also be associated with bony defects or soft tissue masses and may mimic neoplasm (e.g., fibrous dysplasia, NF-1). The common invasive parameningeal tumors of childhood are neuroblastoma, rhabdomyosarcoma, histiocytosis (Fig. 8-87), plexiform neurofibroma, and angiofibroma.

The presence and nature of the intracranial involvement are critical to patient management. With advances in craniofacial and skull base surgery, ablation may be possible without sacrifice of function or cosmesis. In cases with intracranial involvement, surgery may serve primarily to establish the diagnosis and the extent of disease. Tumor debulking reduces the local tumor burden for chemotherapy

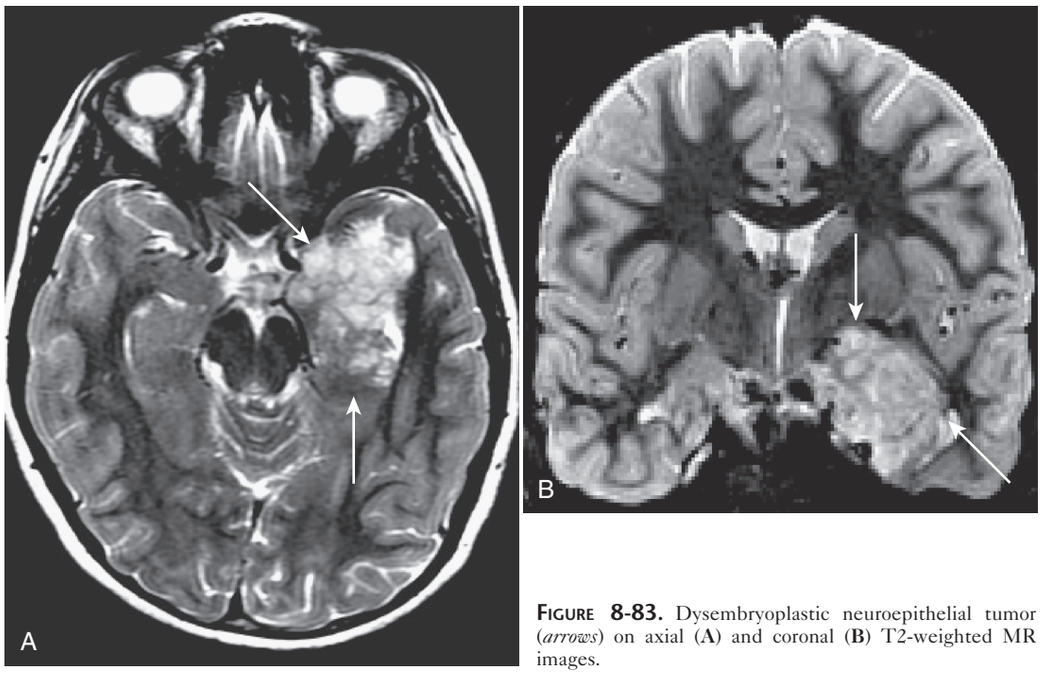

FIGURE 8-83. Dysembryoplastic neuroepithelial tumor (*arrows*) on axial (**A**) and coronal (**B**) T2-weighted MR images.

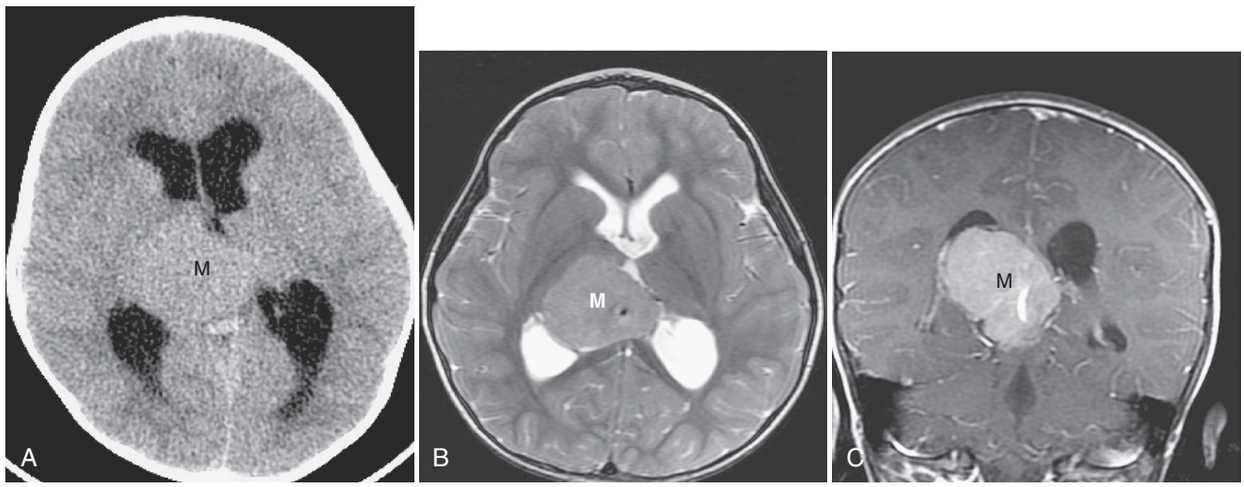

FIGURE 8-84. Meningioma (M) on axial CT scan (**A**) and on axial T2-weighted MR image (**B**). **C,** Enhancement can be seen on a coronal gadolinium-enhanced T1-weighted MR image.

and radiotherapy. Imaging often requires CT for bony involvement and calcification, and MRI for neuroanatomy and vascularity.

In addition to involvement by direct extension, the CNS may be involved by distant metastases (e.g., sarcomas; Fig. 8-88). Some primary CNS neoplasms, especially embryonal tumors, malignant gliomas, and germ cell tumors, show a propensity to disseminate in the subarachnoid space. Most metastatic neoplasms arising from non-CNS primary tumors are of hematogenous origin, although subarachnoid spread may occur, with tumors reaching the CNS originally by direct extension. CT or MRI may demonstrate single or multiple masses, which often enhance with contrast agent.

Tumor Response and Treatment Effects

Common long-term treatment effects after radiotherapy and chemotherapy include mineralization, ischemic vasculopathy (e.g., moyamoya disease), hemorrhagic vasculopathy (e.g., telangiectasia, cavernous malformation), leukoencephalopathy, and second tumors (e.g., meningioma, sarcoma, glioma). These effects may be minimized with the use of more conformal therapies (e.g., stereotactic radiotherapy, stereotactic radiosurgery, proton beam, gamma knife). A transient increase in tumor volume, including mass effect, edema, and enhancement, may occur after radiotherapy, particularly conformal therapy. Functional imaging, including MRS, PMRI, SPECT, or PET, may be needed to distinguish treatment effects (e.g., radionecrosis) from tumor progression (Fig. 8-89).

NEUROCUTANEOUS SYNDROMES

The neurocutaneous syndromes, or phakomatoses, are a group of disorders primarily affecting tissues of ectodermal origin (Box 8-4). This group may also include a number of angiodysplastic syndromes of childhood (see Chapter 10). Neurologic symptoms are a prominent feature of these diseases. The common

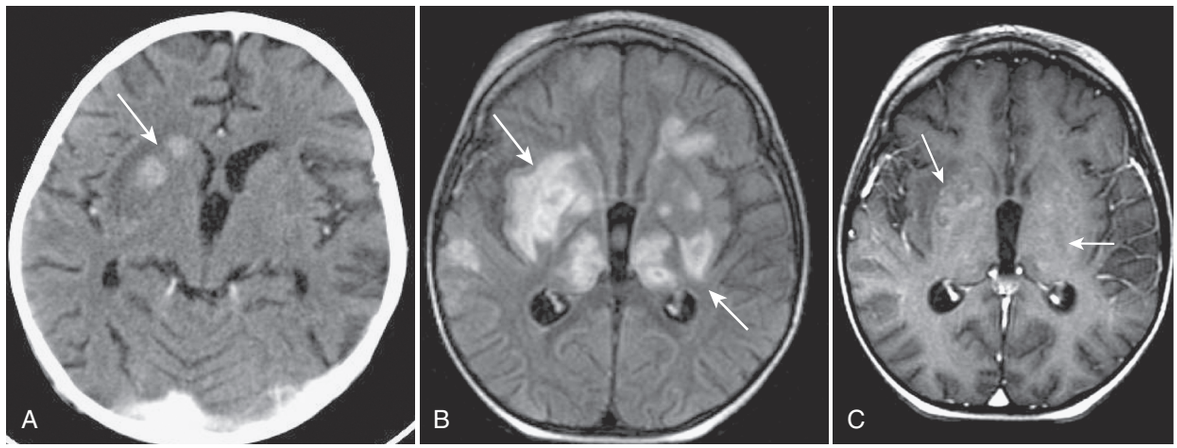

Figure 8-85. Post-transplant lymphoproliferative disorder with lymphoma (*arrows*) on axial CT scan (**A**) and on axial T2-weighted (**B**) and axial gadolinium-enhanced T1-weighted (**C**) MR images.

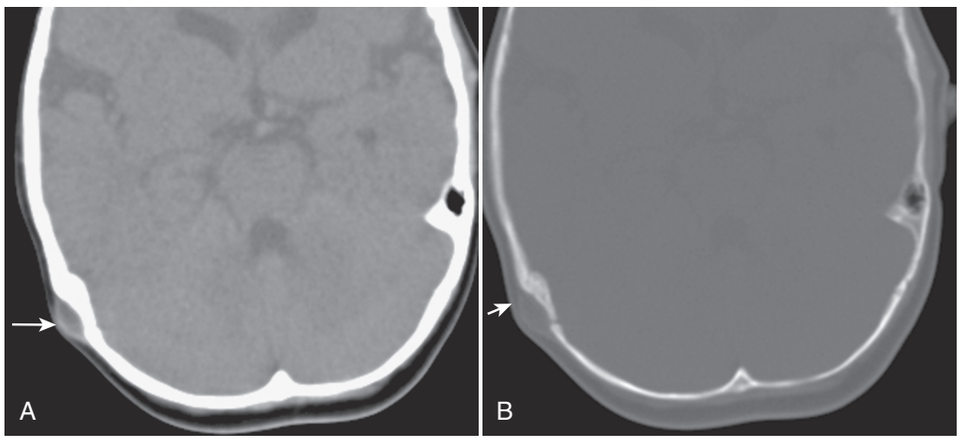

Figure 8-86. Cranial epidermoid (*arrows*) with bony deformity on axial CT scans using soft tissue (**A**) and bone (**B**) algorithms.

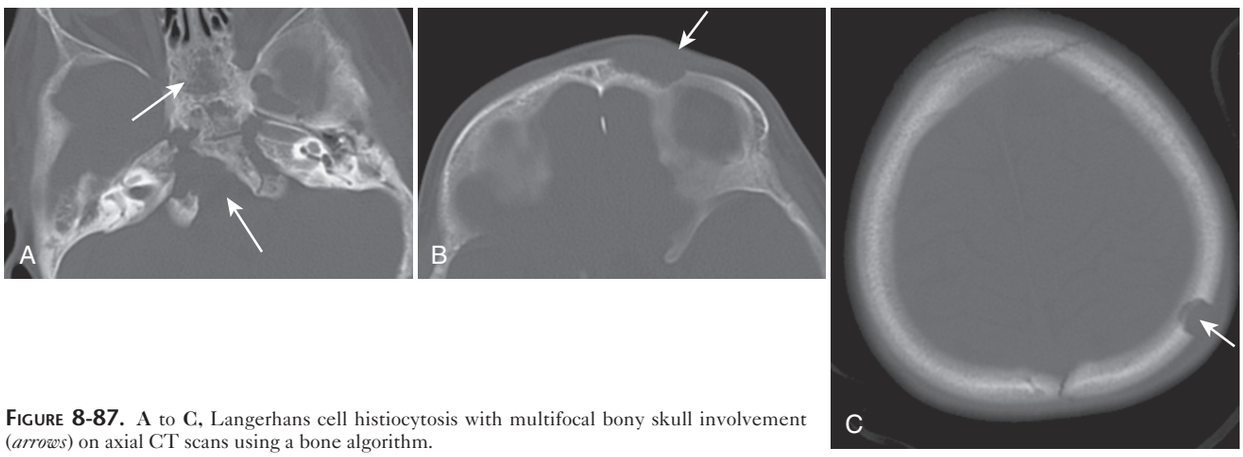

Figure 8-87. **A** to **C**, Langerhans cell histiocytosis with multifocal bony skull involvement (*arrows*) on axial CT scans using a bone algorithm.

neurocutaneous syndromes of childhood include neurofibromatosis 1 (NF-1), tuberous sclerosis, and Sturge-Weber syndrome. Less common are NF-2 and von Hippel–Lindau syndrome. Some of the rarer syndromes listed here are presented in greater detail in other texts.

Neurofibromatosis

Neurofibromatosis is the most common neurocutaneous disorder of childhood. To date, it has been divided into eight subgroups. NF-1 and NF-2 are the most common subtypes (NF-3 has features of both NF-1 and NF-2). NF-1 (von Recklinghausen

disease) is the most common of the phakomatoses. It is inherited as an autosomal dominant disorder (chromosome 17) with variable penetrance and usually manifests in the first decade. Both dysplastic and neoplastic intracranial lesions are found in NF-1. Neurologic symptoms are often nonspecific and include developmental delay, seizures, visual disturbances, and stroke. Neuroimaging has an important role in the evaluation of optic pathway lesions and in the delineation of other neoplastic/dysplastic glial lesions and craniospinal mesodermal dysplasia that typify the disease.

The most common CNS lesions of NF-1 are the "histogenetic foci" or "NF-1 spots" (Fig. 8-90). Within the globus pallidus they are characteristically T1-hyperintense (i.e., heterotopic Schwann cells or melanin?) and do not enhance. They also appear as foci of T2/FLAIR hyperintensity (undermyelination?) in the cerebellum, brainstem, internal capsule, splenium, and thalamus. The latter are usually present before 1 year of age, increase in number and size up to puberty, and then regress (myelination?). These foci show histologic features of hamartomas, atypical glial cells, and vacuolar myelinopathy. Increased size, mass effect, and enhancement may indicate "neoplastic transformation" (e.g., astrocytoma).

The most frequently encountered intracranial neoplasms in NF-1 are optic pathway gliomas (OPGs). These are usually low-grade and frequently pilocytic astrocytomas. The tumors may involve any part of the optic pathways. Tumors confined to the optic nerve are slow-growing and have a favorable prognosis. Lesions involving the chiasm or hypothalamus tend to be more aggressive. OPGs are usually CT-isodense to hypodense,

FIGURE 8-88. Metastatic cerebral osteosarcoma (*long arrow*) on axial contrast-enhanced CT scan, which demonstrates foci of bone (*short arrow*) and enhancement plus edema.

Box 8-4. Neurocutaneous Disorders and Angiodysplastic Syndromes

Neurofibromatosis 1, 2, 3 (and others)
Tuberous sclerosis
Sturge-Weber syndrome
Klippel-Trénaunay-Weber syndrome
PHACES (posterior fossa abnormalities and other structural brain abnormalities, hemangioma(s) of the cervical facial region, arterial cerebrovascular anomalies, cardiac defects, aortic coarctation and other aortic abnormalities, eye anomalies, and sternal defects and/or supraumbilical raphe)/hemangiomatosis
Wyburn-Mason syndrome
Proteus syndrome
Cowden syndrome
von Hippel–Lindau disease
Ataxia-telangiectasia
Hereditary hemorrhagic telangiectasia (Osler-Rendu-Weber syndrome)
Nevoid basal cell carcinoma syndrome (Gorlin syndrome)
Neurocutaneous melanosis
Epidermoid nevus
Linear sebaceous nevus
Hypomelanosis of Ito
Incontinentia pigmenti
Bannayan-Riley-Ruvalcaba syndrome
Encephalocraniocutaneous lipomatosis
Meningoendotheliohemangiomatosis
Facial nevi with anomalous venous return and hydrocephalus
Chédiak-Higashi syndrome
Parry-Romberg syndrome (progressive facial hemiatrophy)

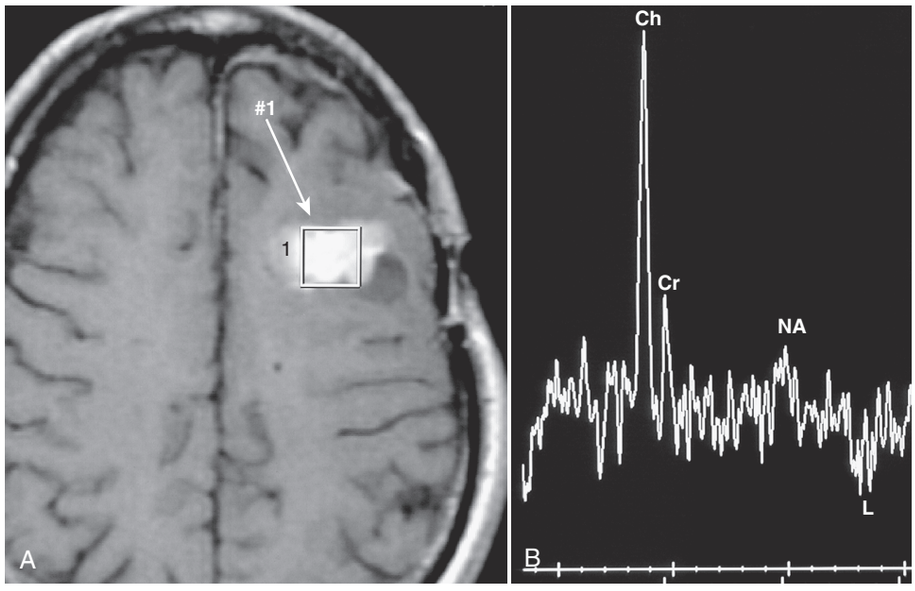

FIGURE 8-89. A, Recurrent anaplastic astrocytoma (*arrow* and *box*) on axial gadolinium-enhanced T1-weighted MR image. **B,** Spectroscopy of the tumor shows very high choline (Ch), low creatine (Cr), and low *N*-acetyl-aspartate (NA) concentrations as well as an inverted lactate doublet (L).

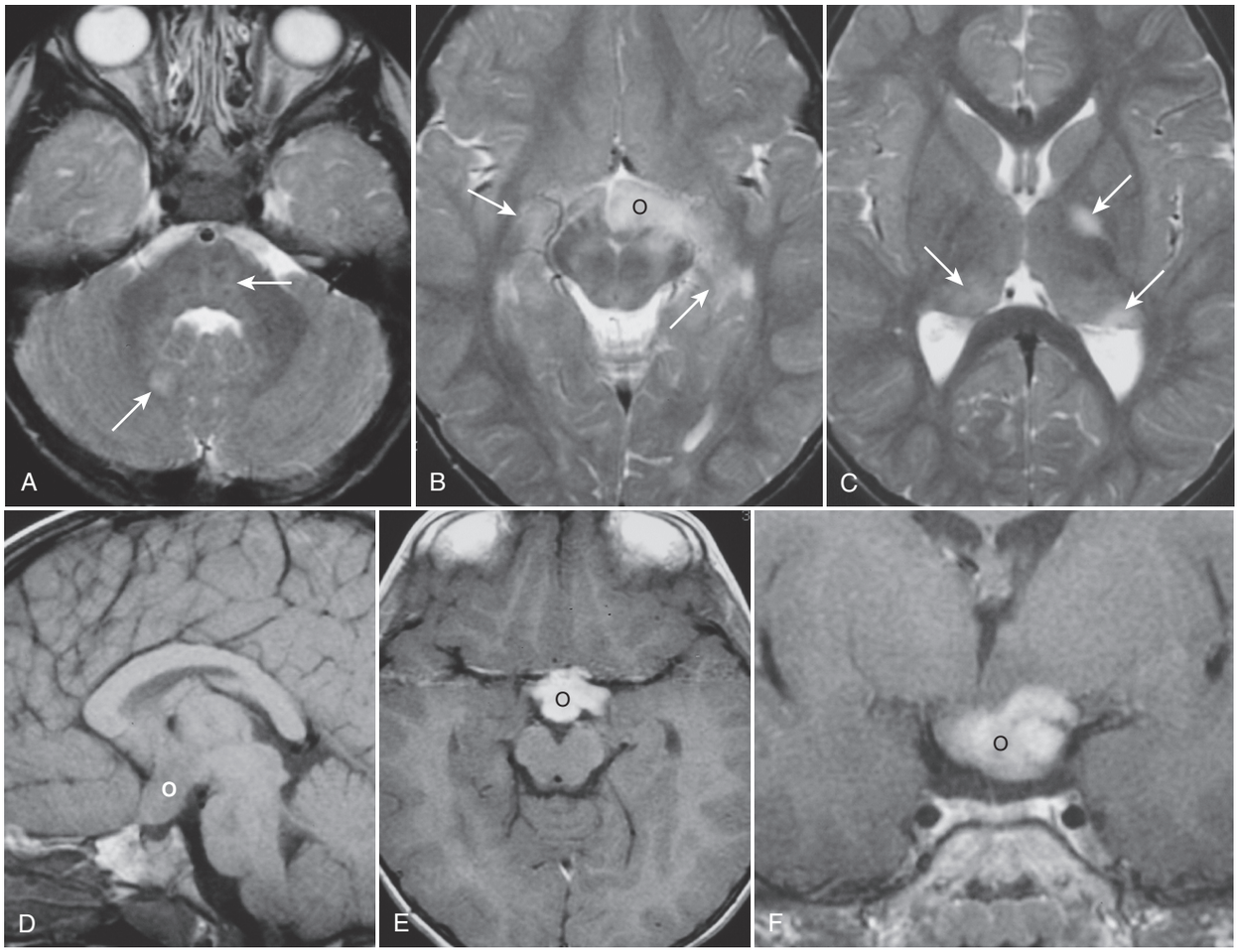

FIGURE 8-90. Neurofibromatosis 1 with "dysplastic foci" (*arrow*) and optic glioma (O) on axial T2-weighted (**A** to **C**) and sagittal T1-weighted (**D**) MR images. Axial (**E**) and coronal (**F**) gadolinium-enhanced T1-weighted MR images show tumor enhancement.

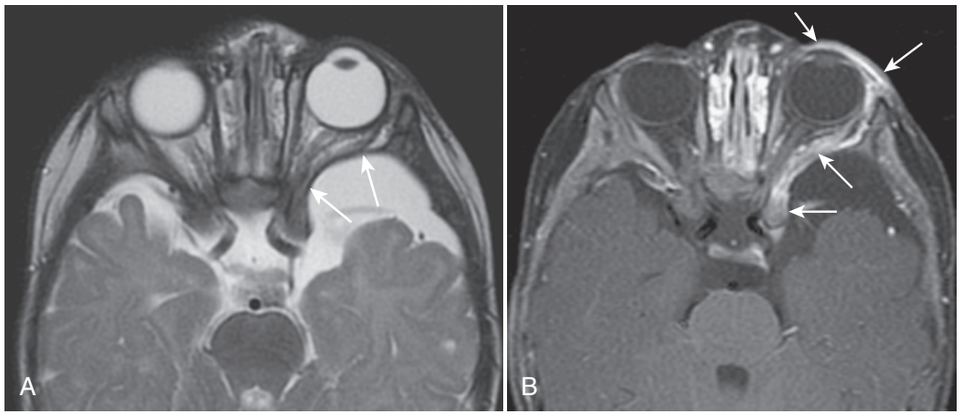

FIGURE 8-91. A, Neurofibromatosis 1 and sphenorbital dysplasia with bony deformity (*arrows*) on axial T2-weighted MR image. **B,** Enhancing orbital plexiform neurofibroma (*arrows*) on axial gadolinium-enhanced T1-weighted MR image.

T1-isointense to hypointense, and T2-isointense to hyperintense (see Fig. 8-90). Enhancement is variable but frequently intense. Cavitation or cyst formation occasionally occurs, but calcification is rare. Astrocytomas may also arise in the tectum, pons, or cerebellum. Hydrocephalus may result from tumoral or nontumoral aqueductal stenosis in NF-1.

Plexiform neurofibromas, the hallmark of NF-1, are tortuous cords of tumor composed of disorganized neurons, Schwann cells, and collagen. They commonly arise in the head and neck region, especially the scalp and orbit (Fig. 8-91). Orbital involvement is often associated with buphthalmos or glaucoma. Paraspinal involvement is also common in NF-1. The lesions are irregular, nonhomogeneous masses that are CT-hypodense, T1-hypointense, and T2-hyperintense, with variable enhancement. The "target sign" is characteristic.

Another characteristic feature of NF-1 is mesodermal dysplasia, including dural ectasia, bony defects, and vascular lesions. Optic nerve sheath ectasia may simulate OPG but is distinguished by its perioptic subarachnoid CSF intensities. Dural ectasia may produce widening of the internal auditory canal and simulate

tumor; the CSF intensity character and the absence of abnormal enhancement differentiate it from tumor (e.g., acoustic neuroma). One of the most common bony defects in NF-1 is sphenoid dysplasia affecting the greater wing. The result may be an alar cephalocele producing pulsatile exophthalmos. This is often associated with intraorbital and periorbital neurofibromas (see Fig. 8-91). A paralamboid skull defect, also characteristic of NF-1, is commonly associated with an overlying neurofibroma.

Mesodermal dysplasia also affects the spine in NF-1 (see Chapter 9). A short-segment kyphoscoliosis with vertebral deformities and scalloping is characteristic. Dural ectasia and meningoceles result in spinal canal and foraminal widening. A paraspinal meningocele is distinguished from a plexiform neurofibroma by its CSF intensities and lack of abnormal enhancement. Neurovascular complications of NF-1 include steno-occlusive disease and aneurysm formation. Cerebral infarction from arterial stenosis may occur in patients with NF-1 after radiotherapy for OPG, or as part of a systemic vascular dysplasia. When severe, the steno-occlusive disease may result in a moyamoya syndrome. Aneurysm formation is less common and occurs later in life.

NF-2 rarely occurs prior to puberty and is inherited as an autosomal dominant trait (chromosome 22). The genetic defect in NF-2 has been localized to chromosome 22. Tumors of the coverings of the brain are characteristic of NF-2 and include acoustic schwannomas and meningiomas. Schwannomas are tumors composed of abnormal Schwann cells surrounding neurons. The most commonly involved cranial nerves (CNs) are CN VIII, CN V, CN IX, and CN X. Bilateral vestibular schwannomas (aka acoustic neuromas) are diagnostic of the disorder. The tumors are typically CT-hypodense, T1-hypointense, markedly T2-hyperintense, markedly enhance, and rarely calcify (Fig. 8-92). Cystic degeneration and hemorrhage occasionally occur. Expansion of the internal auditory canal (IAC) is common with larger CN VIII lesions. Meningiomas manifest at an earlier age in patients with NF-2 than in the general population. The tumors are usually dura-based (e.g., parasagittal, convexity, or perisellar) or intraventricular. Imaging often demonstrates a circumscribed extracerebral or intraventricular mass with calcification, marked vascularity, and lytic or blastic (hyperostosis) bony involvement. The tumor tends to be CT-isodense or hyperdense, T1-isointense to hypointense, T2-isointense to hyperintense or hypointense, and to markedly enhance with a dural tail (see "Cerebral Tumors").

Tuberous Sclerosis

Tuberous sclerosis (Bourneville disease) is a multisystem, autosomal dominant disorder characterized by the clinical triad of mental retardation, seizures, and adenoma sebaceum (angiofibromas). The brain lesions, which are neuroglial hamartomas composed of giant balloon "stem" cells (i.e., tubers), likely result from defective development of the radial glial-neuronal unit. They may arise at any point from subependymal to cortical. Subependymal, subcortical white matter, and cortical tubers are common. Calcification of the subependymal tubers is characteristic although unusual in the first year of life. In the immature brain, these lesions are typically CT-hypodense, T1-hyperintense, and T2-hypointense relative to the unmyelinated white matter (Fig. 8-93). With maturation, the lesions become isodense and isointense in relation to the myelinated white matter and appear as periventricular nodules with little or no enhancement (Fig. 8-94). Subependymal tubers near the foramen of Monro have a tendency to enlarge and develop a preponderance of giant cells (i.e., giant cell tumors or astrocytomas). Hydrocephalus may be the result. These tumors usually enhance on CT or MRI but are rarely invasive (see Fig. 8-94).

Occasionally, cysts or hemorrhage (e.g., aneurysm) may occur in tuberous sclerosis. White matter lesions consist of either hamartomatous clusters or linear bands of unmyelinated axonal fibers radiating outward from the ventricles. Calcification may occur but enhancement is not expected. Cortical tubers are a hallmark of tuberous sclerosis. They consist of giant cells, disordered myelin, and gliosis, and are associated with broad and flat gyri. Their imaging features also vary with age and generally appear T2/FLAIR-hyperintense in the mature brain (see Fig. 8-94). Enhancement of such lesions is unusual and may indicate tumor.

Sturge-Weber Syndrome

Sturge-Weber syndrome, or encephalotrigeminal angiomatosis, is a neurocutaneous disorder characterized by low-flow vascular malformations of the face, globe, and leptomeninges. A "port-wine" facial capillary nevus is almost always present, is usually unilateral, and most often follows the ophthalmic division (V1) of the trigeminal nerve. The pial capillary-venous malformation of this syndrome is likely the result of persistence of primordial sinusoids and dysgenesis or thrombosis of the cortical venous system. It typically involves the parieto-occipital or temporal region. Similar involvement of the choroid may result in buphthalmos. Seizures are common and often manifest as infantile spasms. Mental retardation, hemiparesis, and hemianopia are also frequent. Features of the Sturge-Weber syndrome may also be associated with the Klippel-Trenaunay-Weber syndrome (visceral, truncal, and extremity low-flow vascular malformations).

Enhanced MRI best demonstrates the extent of the pial malformation, which decreases with age (Fig. 8-95). Enlarged

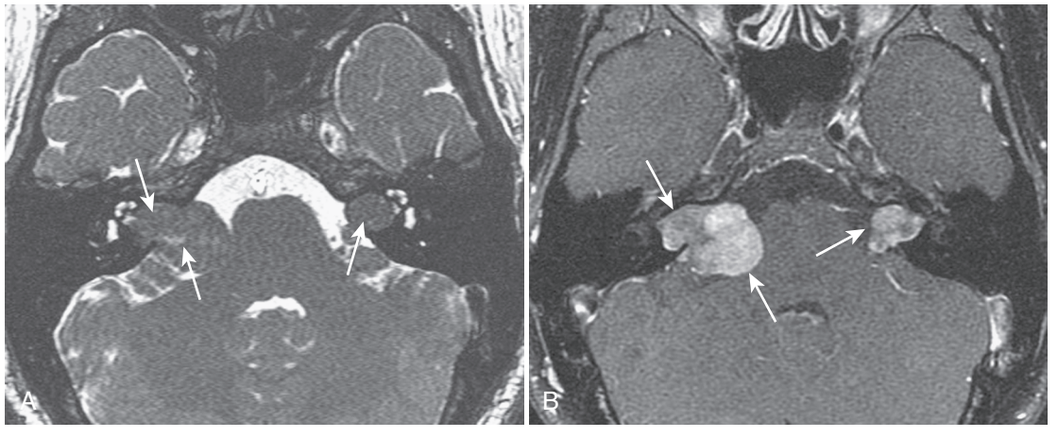

FIGURE 8-92. Neurofibromatosis 2 with bilateral acoustic neuromas (*arrows*) on axial T2-weighted (**A**) and axial gadolinium-enhanced T1-weighted (**B**) MR images.

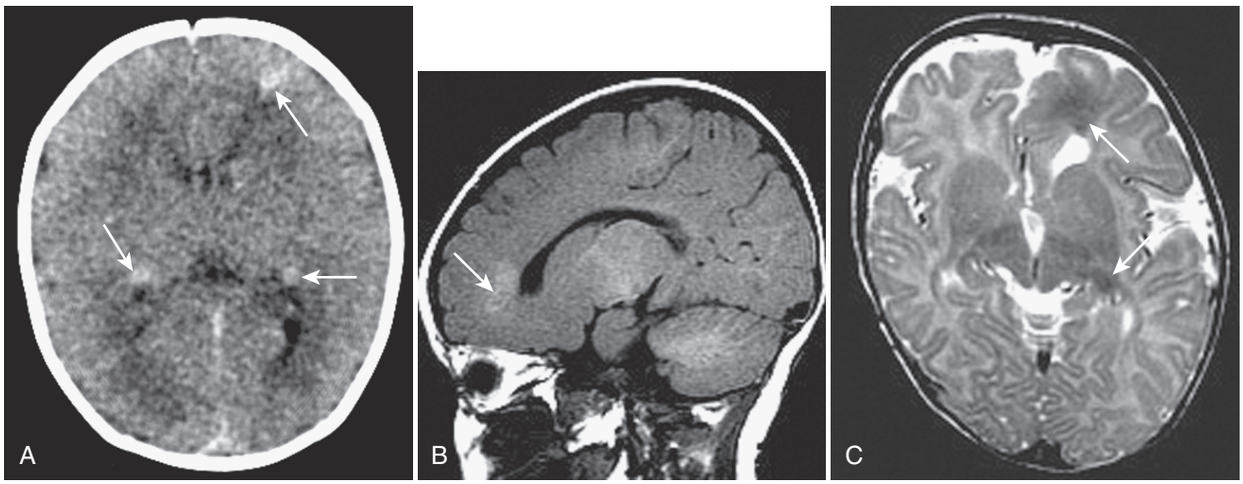

Figure 8-93. Infantile tuberous sclerosis with periventricular and subcortical tubers (*arrows*) on CT scan (**A**) and on sagittal T1-weighted (**B**) and axial T2-weighted (**C**) MR images.

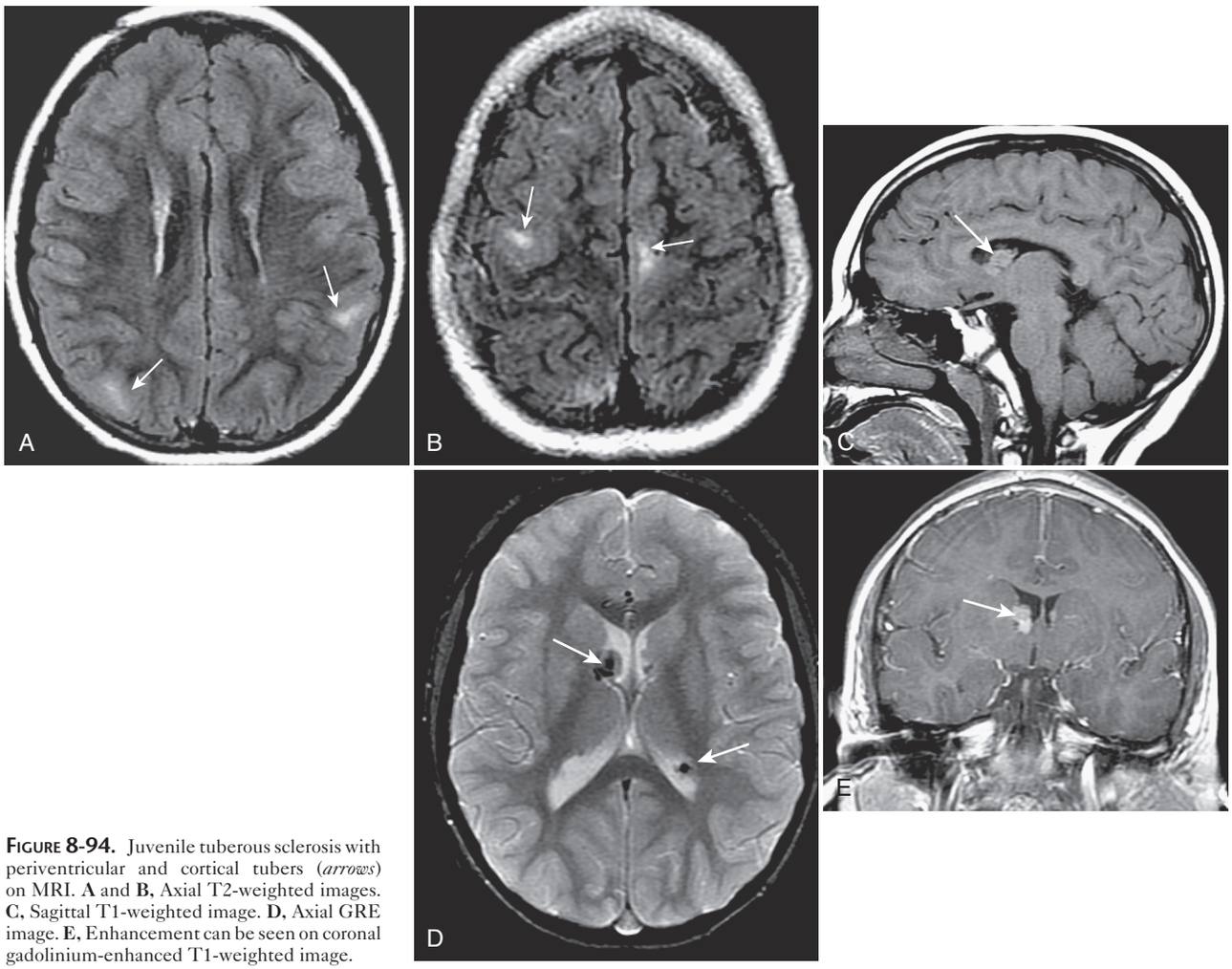

Figure 8-94. Juvenile tuberous sclerosis with periventricular and cortical tubers (*arrows*) on MRI. **A** and **B,** Axial T2-weighted images. **C,** Sagittal T1-weighted image. **D,** Axial GRE image. **E,** Enhancement can be seen on coronal gadolinium-enhanced T1-weighted image.

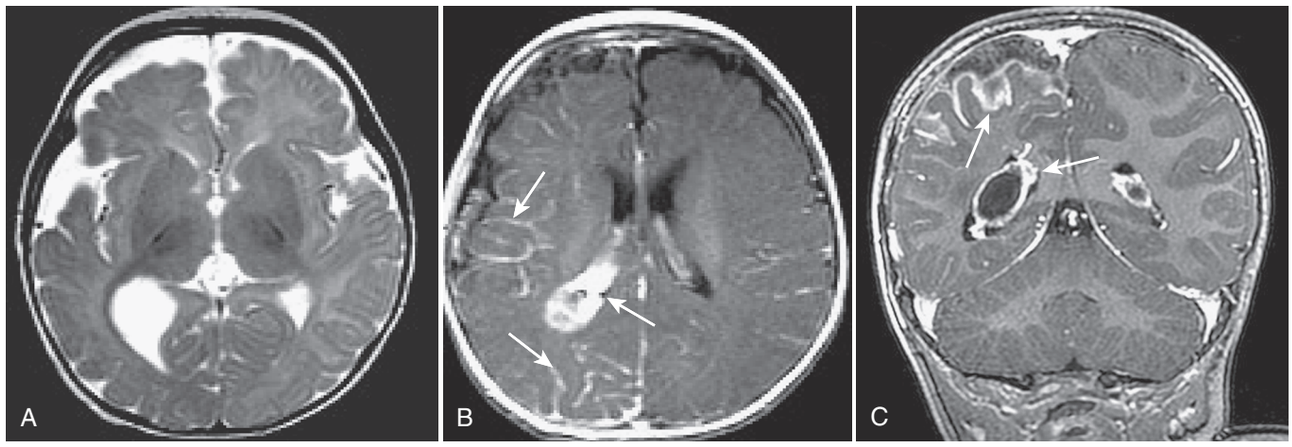

FIGURE 8-95. Sturge-Weber syndrome with atrophy on axial T2-weighted MR image. Vascular malformative enhancement can be seen (*arrows*) on axial (**B**) and coronal (**C**) gadolinium-enhanced T1-weighted MR images.

medullary and subependymal veins result from the diversion of superficial drainage. The choroid plexus is usually hypertrophied on the same side. Subjacent cortical calcification is likely related to venous ischemia, increases with age, and may not be present in infancy. It is best detected by CT. Corresponding cerebral underdevelopment, dysgenesis, hypermyelination, or atrophy is usually evident. The atrophy worsens with age. Angiography best demonstrates the malformation and associated venous abnormalities for the planning of surgery for intractable seizures. Sturge-Weber syndrome is to be distinguished from meningiangiomatosis and Wyburn-Mason syndrome.

von Hippel–Lindau Disease

Von Hippel–Lindau disease is an autosomal dominant disorder (chromosome 3) with incomplete penetrance and multisystem involvement. It is characterized by hemangioblastomas of the retina and CNS, along with renal cell carcinoma, pheochromocytoma, and cysts of the abdominal viscera. The onset of symptoms is unusual in childhood and often related to ocular complications (e.g., hemorrhage, retinal detachment, glaucoma, or cataract). CNS hemangioblastomas are highly vascular lesions that most commonly arise within the cerebellum and spinal cord. Involvement of the brainstem and cerebrum may rarely occur. CT or MRI typically shows an intensely enhancing nodule that is often associated with a cyst and prominent vessels. Occasionally there may be hemorrhage. The spinal cord lesions may be associated with hydrosyringomyelia.

Other Neurocutaneous Diseases

Ataxia-telangiectasia (Louis-Bar syndrome) is an autosomal recessive disorder characterized by capillary telangiectasias of the face and conjunctiva, progressive cerebellar atrophy, immunodeficiencies, and an increased incidence of lymphoma, leukemia, and other malignancies. The ataxia is often evident before the appearance of the telangiectasias. CT or MRI shows progressive cerebellar degeneration with atrophy involving the cerebellar hemispheres and vermis. Embolic infarction may result from associated pulmonary vascular malformations. Cerebral telangiectasias may hemorrhage.

Basal cell nevus syndrome (Gorlin syndrome) is an autosomal dominant syndrome composed of multiple basal cell carcinomas, keratocysts of the maxilla and mandible, mental retardation, seizures, hydrocephalus, dural calcification (e.g., falx), and callosal hypogenesis. There is an increased prevalence of neoplasia, including medulloblastoma, meningioma, craniopharyngioma, ameloblastoma, and astrocytoma.

Neurocutaneous melanosis is a disorder in which large pigmented cutaneous nevi are seen in association with abnormal meningeal, perivascular, and brain melanin deposition. The anterior temporal lobe (e.g., amygdala) and the cerebellum are most often involved. The lesions tend to be CT-isodense to hyperdense, T1-hyperintense, and T2-hypointense. Enlarging and enhancing brain or leptomeningeal lesions suggest malignancy (e.g., melanoma). There may be associated hydrocephalus. Other reported findings include arachnoid cysts, Dandy-Walker spectrum, and hydrosyringomyelia.

Hypomelanosis of Ito is characterized by cutaneous hypopigmentation in association with scoliosis, skull defects, syndactyly, cleft palate, and ocular abnormalities. Seizures and mental retardation are common. Atrophy, porencephaly, white matter changes, and heterotopias have been reported.

METABOLIC, NEURODEGENERATIVE, AND TOXIC DISORDERS

Classification and Differential Diagnoses

The clinical hallmark of metabolic and neurodegenerative disorders is "progressive" neurologic impairment in the absence of a CNS tumor or another readily identifiable process (e.g., infection). These are rare disorders but some are specifically treatable. Many are heredofamilial, so genetic counseling and prenatal screening are important. These disorders are to be distinguished from the "nonprogressive" static encephalopathies (e.g., cerebral palsy) that may be related to maldevelopment, hypoxia-ischemia, infection, or other conditions.

Diagnosis is primarily clinical and involves metabolite testing, genetic testing, or biopsy of CNS or extra-CNS tissues. MRI is superior to CT in evaluating disease extent and anatomic distribution. In the evaluation of developmental delay (e.g., static encephalopathy versus neurodegenerative disease), MRI is the only modality that can provide an accurate assessment of brain maturation based on myelination and cortical development (including the use of MRS and DTI). Occasionally MRI may demonstrate characteristic imaging findings. Proton MRS has the potential to contribute specific metabolic characterization of these disorders. Stereotactic CT or MRI may serve as a guide for biopsy.

Metabolic, degenerative, and toxic disorders may be classified in a number of ways, including metabolic defect and anatomic predilection (Table 8-5). Clinical features are also important. For example, macrocephaly is often characteristic of maple

Table 8-5. Classification of Metabolic, Degenerative, and Toxic Disorders of the Central Nervous System

Metabolic and Degenerative Disorders	
Lysosomal Disorders	
Lipidoses	Fabry, Gaucher, and Niemann-Pick diseases GM_1 gangliosidosis GM_2 gangliosidosis (Tay-Sachs and Sandhoff diseases) Neuronal ceroid lipofuscinosis
Mucopolysaccharidoses (MPS)	Hurler, Scheie, Hurler-Scheie syndrome Hunter syndrome Sanfilippo types A-D Morquio syndromes A and B Maroteaux-Lamy syndrome Sly syndrome
Mucolipidoses	Mannosidosis Fucosidosis Sialidosis
Lysosomal leukodystrophies	Metachromatic leukodystrophy Globoid cell leukodystrophy (Krabbe disease)
Peroxisomal Disorders	Adrenoleukodystrophy complex Neonatal leukodystrophy Zellweger syndrome Infantile Refsum syndrome Rhizomelic chondrodysplasia punctata Hyperpipecolic acidemia Cerebrotendinous xanthomatosis
Other Leukodystrophies	Pelizaeus-Merzbacher disease Canavan disease Alexander disease Cockayne syndrome Leukodystrophy with calcifications
Mitochondrial (Respiratory Oxidative) Disorders	Leigh disease Kearns-Sayre syndrome MELAS (mitochondrial encephalomyopathy with lactic acidosis, and stroke-like episodes) syndrome MERRF (myoclonus epilepsy associated with ragged-red fibers) syndrome Alpers syndrome (poliodystrophy) Menkes disease (trichopoliodystrophy) Marinesco-Sjögren syndrome Infantile bilateral striatal necrosis Leber hereditary optic atrophy l-Carnitine deficiency
Amino Acid Disorders	Phenylketonuria Homocystinuria Nonketotic hyperglycinemia Maple syrup urine disease Glutaric aciduria, type I Glutaric aciduria, type II Methylmalonic and propionic acidurias Urea cycle defects (e.g., ornithine transcarbamylase deficiency) Oculocerebrorenal syndrome Pyridoxine dependency
Carbohydrate and Other Storage Disorders	Galactosemia Glycogen storage diseases (i.e., Pompe disease) Niemann-Pick disease Gaucher disease Farber disease Infantile sialidosis
Liver Metabolic Disorders	Wilson disease (hepatolenticular degeneration) Hallervorden-Spatz disease Hyperbilirubinemia (see "Toxic Encephalopathies") Hepatocerebral syndromes (see "Toxic Encephalopathies")
Diseases of the Cerebellum, Brainstem, and Spinal Cord	Friedreich ataxia Olivopontocerebellar atrophies Ataxia-telangiectasia Carbohydrate-deficient glycoprotein syndrome Infantile neuraxonal dystrophy
Other Metabolic and Neurodegenerative Diseases	Juvenile multiple sclerosis Molybdenum cofactor deficiency 3-Hydroxy-3-methylglutaryl–coenzyme A lyase deficiency Idiopathic leukoencephalopathy

(Continued)

TABLE 8-5. Classification of Metabolic, Degenerative, and Toxic Disorders of the Central Nervous System—cont'd

Diseases of the Basal Ganglia	Sulfur oxidase deficiency Parathyroid disease Tuberous sclerosis Down syndrome Progressive encephalopathy with basal ganglia calcifications and cerebrospinal fluid lymphocytosis Inflammatory, toxic, and anoxic conditions Radiation therapy Renal tubular acidosis and osteoporosis Huntington disease Fahr disease Hallervorden-Spatz disease Cockayne syndrome Wilson disease
Toxic Encephalopathies	
Exogenous Internal Toxicities	Hyperbilirubinemia Hepatocerebral syndromes Hypoglycemia Hypothermia and hyperthermia Paraneoplastic toxins Hemolytic uremic syndrome Uremia Ion imbalance disorders Endocrinopathies Porphyria
Exogenous External Toxicities	Vitamin deficiencies/depletions: Vitamin B_1 Folate Vitamin B_{12} Biotin Vitamin K Vitamin C Vitamin D Toxins: Mercury Methanol Toluene Carbon monoxide Cyanides and sulfides Lead Alcohol Cocaine and heroin Anticonvulsants Drug-induced: Methotrexate Cyclosporine Tacrolimus Carmustine, cytosine arabinoside

syrup urine disease, Canavan disease, Alexander disease, and the lysosomal disorders (e.g., Tay-Sachs disease, the mucopolysaccharidoses, and metachromatic leukodystrophy). Although there is considerable overlap among the disorders, most imaging classifications use predominant anatomic involvement as follows: white matter (subcortical, periventricular), gray matter (cortical, deep), basal ganglia, brainstem, cerebellum, spinal cord, and peripheral nervous system. Specific conditions are presented in greater detail in other texts.

Disorders Primarily Affecting the Cortical Gray Matter

Disorders primarily affecting cortical gray matter include the storage diseases that result from lysosomal enzyme defects (see Table 8-5), such as the lipidoses (e.g., GM1 gangliosidosis, neuronal ceroid lipofuscinosis), the mucopolysaccharidoses, and the mucolipidosis (e.g., mannosidosis). CT and MRI show cortical atrophy (gyral thinning and sulcal/fissural widening), abnormal cortical densities and intensities, and ventriculomegaly (Fig. 8-96). Associated white matter changes reflect secondary axonal degeneration. These disorders are to be differentiated from the more common causes of cortical underdevelopment or atrophy, including the chronic static encephalopathies (e.g., maldevelopment, hypoxia-ischemia, infection, idiopathic), and atrophy related to chronic systemic disease, malnutrition, or certain types of therapy (e.g., steroids, chemotherapy, radiation, anticonvulsants, transplantation).

Disorder Primarily Affecting Deep Gray Matter

Disorders primarily affecting deep gray matter often show abnormally high or low densities and intensities of the basal ganglia or thalami, including mineralization (calcium, iron, etc.) (see Table 8-5). Third or lateral ventriculomegaly (e.g., frontal horns) may be an important finding. Disorders primarily involving the caudate and putamen include mitochondrial (e.g., Leigh syndrome; Fig. 8-97, MELAS syndrome), organic and amino acidopathies (e.g., glutaric aciduria; Fig. 8-98), juvenile Huntington disease, Wilson disease, Fahr disease (Fig. 8-99), and Cockayne syndrome (Fig. 8-100). More common causes, however, include profound hypoxia-ischemia (see Fig. 8-47), toxic exposure (e.g., methane, cyanide), osmolar myelinolysis, striatal necrosis, hypoglycemia, and meningoencephalitis. Disorders primarily involving the

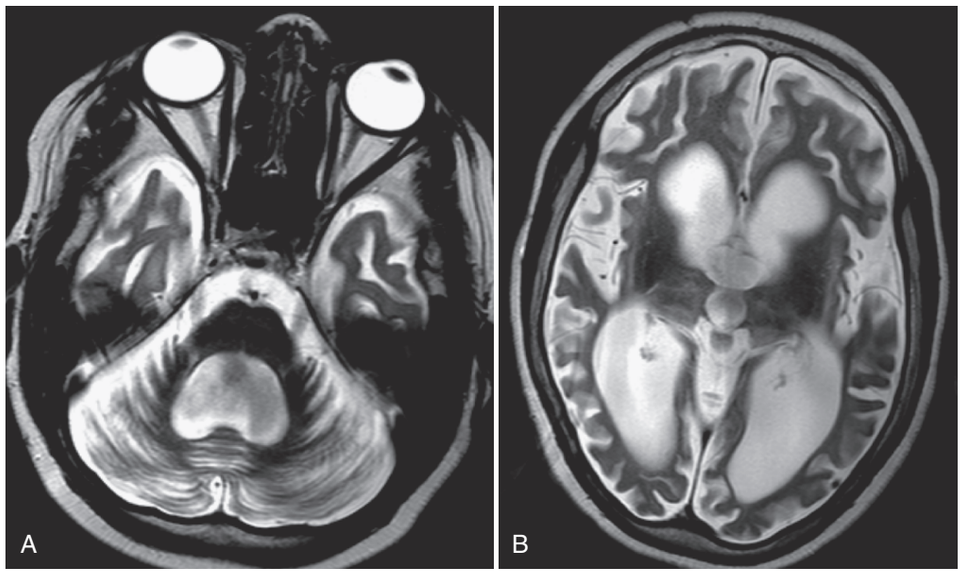

FIGURE 8-96. **A** and **B,** Neuronal ceroid lipofuscinosis with cerebellar and cerebral atrophy on axial T2-weighted MR images.

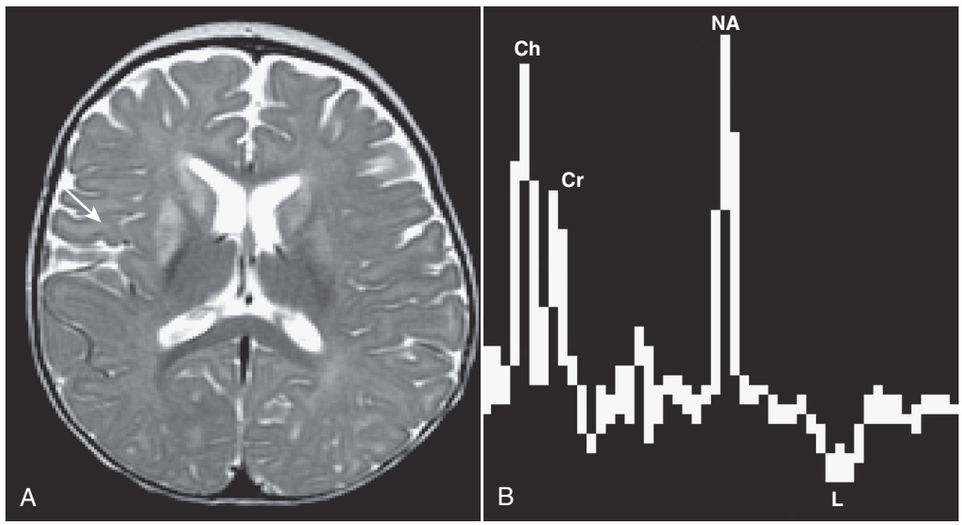

FIGURE 8-97. **A,** Leigh syndrome with bilateral caudate and putaminal high intensities on axial T2-weighted MR image. **B,** A lactate doublet (L) on MR spectroscopy.

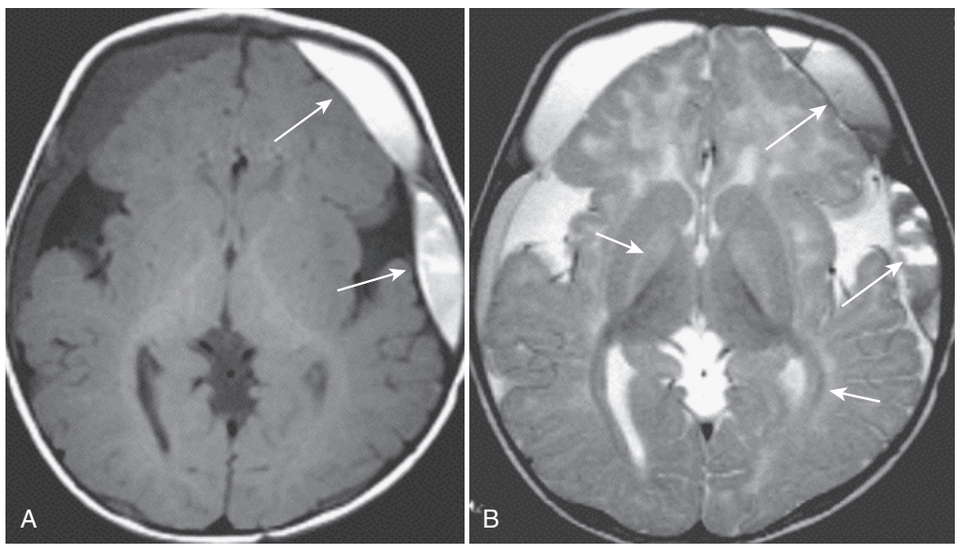

FIGURE 8-98. Glutaric acidopathy (GA1), a mimic of nonaccidental injury, with large sylvian fissures, and subdural hemorrhage (*long arrows*) as well as basal ganglia and white matter abnormalities (*short arrows* on **B**) on axial T1-weighted (**A**) and T2-weighted (**B**) MR images.

globus pallidus include pantothenate kinase–associated neurodegeneration (formerly Hallervorden-Spatz disease; Fig. 8-101) and the aminoacidopathies (e.g., methylmalonic acidopathy). More common causes include hyperbilirubinemia (bilirubin encephalopathy, kernicterus; Fig. 8-102), and toxic exposure (e.g., carbon dioxide). Isolated involvement of the thalami is unusual in metabolic disorders. However, thalamic involvement may be a feature of sulfur oxidase deficiency (Fig. 8-103), Krabbe disease, GM2 gangliosidosis, or the infantile form of Leigh disease (along with extensive brainstem, basal ganglia, and cerebral white matter involvement). Ventrolateral bithalamic lesions are often characteristic of profound perinatal hypoxia-ischemia (see Fig. 8-47).

Disorder Primarily Affecting White Matter

Disorders primarily affecting white matter, of various etiologies, are often referred to as *leukoencephalopathies*. There may be superficial involvement of the cortical/subcortical white matter (e.g., arcuate U fibers), deep involvement of the central white matter (periventricular/capsular/basal ganglia), or both (see Table 8-5). CT and MRI show abnormally low or high densities and intensities. Secondary gray matter involvement with atrophy occurs late. Traditionally, leukoencephalopathies have been divided into dysmyelinating and myelinoclastic disorders. In dysmyelinating disorders (also called leukodystrophies), there is an intrinsic (e.g., inherited, enzyme deficiency) abnormality of myelin formation, breakdown, or turnover. The cerebral involvement is often symmetric and diffuse, and spares the arcuate U fibers. Additional, symmetric cerebellar white matter involvement is common. In this category are the lysosomal disorders (e.g., metachromatic leukodystrophy, Krabbe disease), peroxisomal disorders (e.g.,

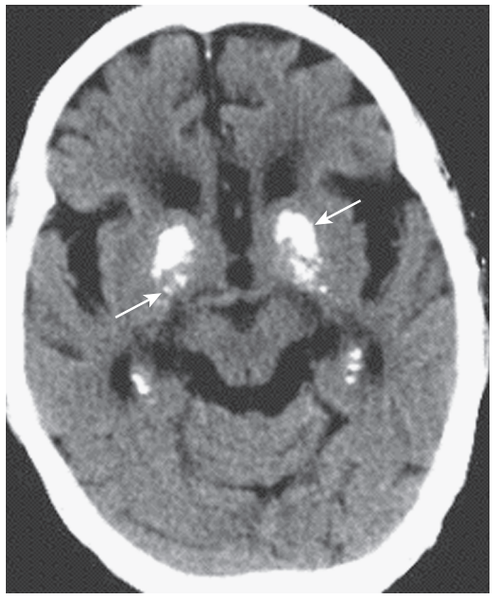

FIGURE 8-99. Fahr disease with basal ganglia calcifications (*arrows*) on CT scan.

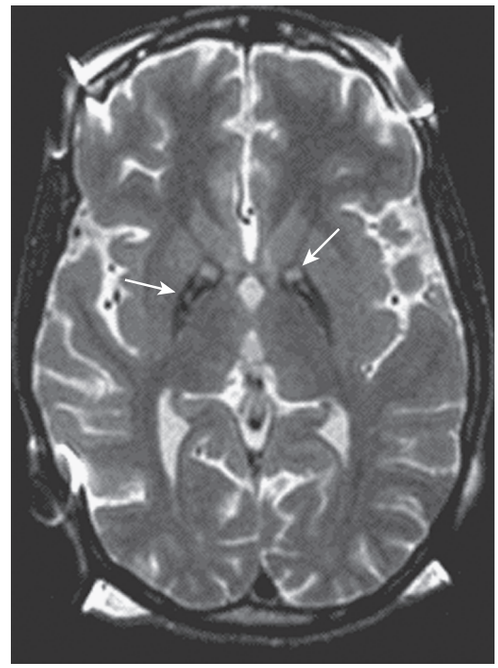

FIGURE 8-101. Pantothenate kinase-associated neurodegeneration with characteristic bilateral high- and low-intensity globus pallidus lesions (*arrows*) on axial GRE MR image.

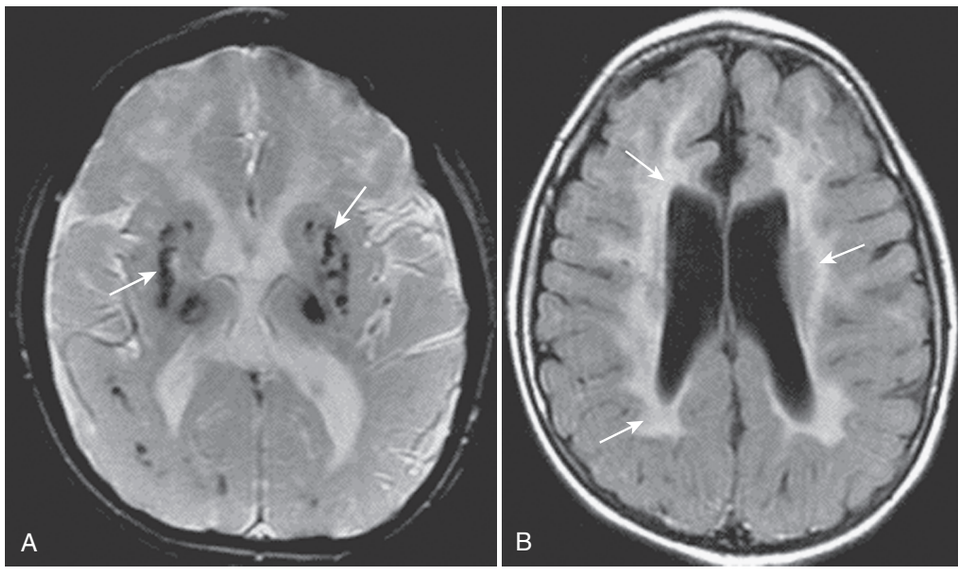

FIGURE 8-100. Cockayne syndrome with basal ganglia mineralization (*arrows*) on axial GRE MR image (**A**) and white matter disease (*arrows*) on axial FLAIR MR image (**B**).

adrenoleukodystrophies [ALDs]), and other diseases of white matter (e.g., Pelizaeus-Merzbacher disease, Canavan disease, Alexander disease, and Cockayne syndrome; see Fig. 8-100).

Certain patterns may be characteristic. Alexander disease is characterized by predominant frontal involvement, and ALD by an occipital distribution. Early subcortical white matter involvement may suggest Alexander disease (frontal U fiber involvement, macrocephaly), Canavan disease (macrocephaly and capsular involvement), galactosemia, or infantile-onset leukoencephalopathy with swelling (macrocephaly), cysts, and mild clinical course (Fig. 8-104). Early central white matter disease may suggest Krabbe disease (also, abnormal thalami), a peroxisomal disorder (e.g., ALD with brainstem involvement), metachromatic leukodystrophy, phenylketonuria, maple syrup urine disease (Fig. 8-105), or Lowe syndrome. The lack of myelination (hypomyelination) may suggest Pelizaeus-Merzbacher or Menkes disease.

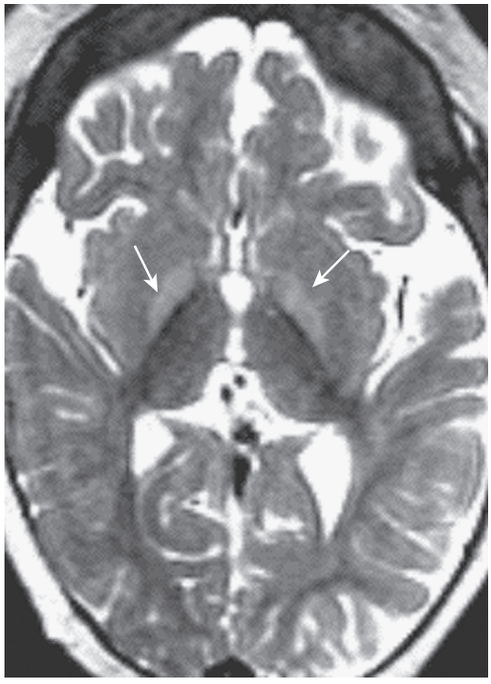

Figure 8-102. Kernicterus with bilateral globus pallidus lesions (*arrows*) and atrophy on axial T2-weighted MR image.

In myelinoclastic (e.g., demyelinating) disorders, the intrinsically normal myelin sheath is damaged by exogenous or endogenous myelinotoxic factors. The cerebral pattern is often asymmetric and sharply defined, and may involve the arcuate U fibers. There may be asymmetric cerebellar, brainstem, and basal ganglia/thalamic involvement. This pattern is seen with infectious and postinfectious demyelinating diseases (e.g., HIV, CMV, ADEM [see Fig. 8-42], PML, and SSPE), chemotherapy (e.g., methotrexate, cyclosporin), radiotherapy, vasculitis (e.g., systemic lupus erythematosus), and multiple sclerosis.

Nonspecific white matter abnormalities may be seen with a variety of metabolic, neurodegenerative, infectious, postinfectious, toxic, and vascular processes. In this situation, the clinical findings must be relied upon. An important example is posterior reversible leukoencephalopathy, which may be seen in a number of conditions associated with hypertension (e.g., cyclosporine therapy in transplant recipients, renal disease [Fig. 8-106]). Also, it is important to remember that the most common causes of cerebral white matter abnormalities (particularly periventricular) and prominent Virchow-Robin spaces in children with developmental delay are static leukoencephalopathies (e.g., maldevelopmental, undermyelinated, post-inflammatory, postischemic, idiopathic).

Disorders Affecting White Matter and Cortical Gray Matter

Disorders affecting both white matter and cortical gray matter include lysosomal disorders such as the lipidoses and mucopolysaccharidoses (associated skeletal dysplasia), and mitochondrial disorders (e.g., Alpers syndrome, Menkes disease). If a diffuse cortical dysgenesis (e.g., lissencephaly, polymicrogyria) is associated with white matter abnormalities, peroxisomal disorders such as Zellweger syndrome should be considered along with congenital infections (e.g., CMV; see Fig. 8-20), and the congenital muscular dystrophies (e.g., Fukuyama syndrome, Walker-Warburg syndrome [see Fig. 8-19], and Santavuori disease).

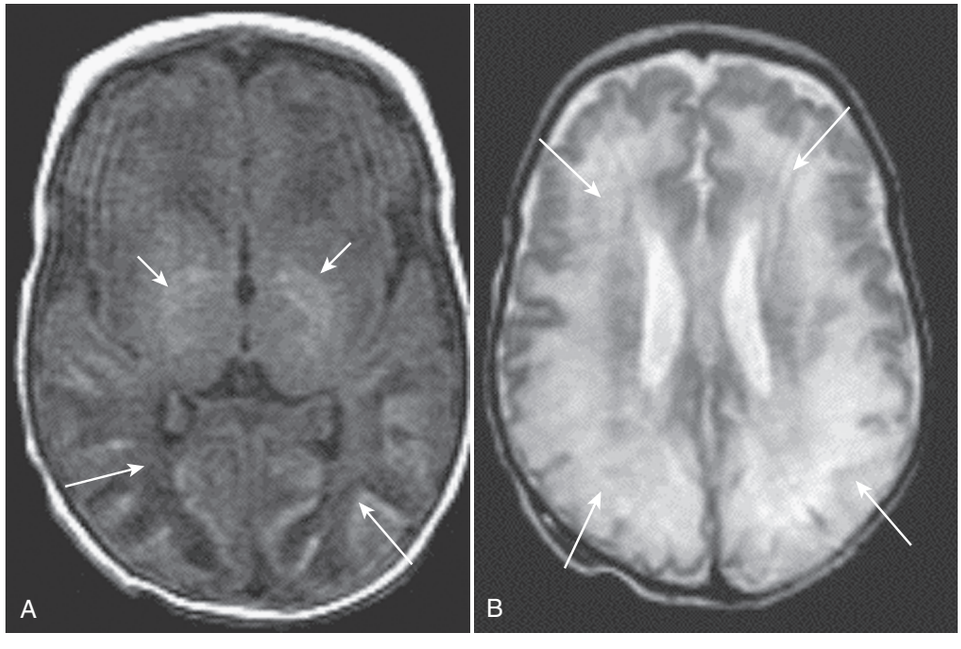

Figure 8-103. Sulfite oxidase deficiency with thalamic (*short arrows* on **A**) and diffuse white matter involvement (*long arrows*) on axial T1-weighted (**A**) and T2-weighted (**B**) MR images.

Disorders Affecting White Matter and Deep Gray Matter

Disorders affecting both white matter and deep gray matter include those with primarily caudate and putaminal involvement (Leigh syndrome [see Fig. 8-97], MELAS syndrome, Wilson disease, Cockayne syndrome [see Fig. 8-100]), predominant thalamic abnormalities (Krabbe disease, GM2 gangliosidosis), or primarily globus pallidus involvement (Canavan disease, maple syrup urine disease [see Fig. 8-105], methylmalonic/propionic acidopathy, Kearns-Sayre disease). More common causes are profound hypoxia-ischemia, osmolar myelinolysis, kernicterus (see Fig. 8-102), toxic exposure (e.g., carbon dioxide, methane, cyanide, radiation, chemotherapy), and infectious or postinfectious processes (e.g., TORCH diseases, HIV, ADEM).

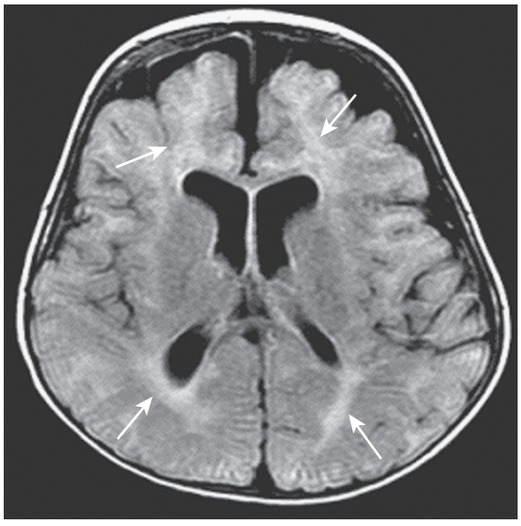

FIGURE 8-104. Infantile leukoencephalopathy (*arrows*) with macrocephaly on axial FLAIR MR image.

Magnetic Resonance Spectroscopy in Metabolic Disorders

Proton MRS is being increasingly used, including in patients with metabolic disorders. Although a number of the metabolic and neurodegenerative disorders have specific biochemical or genetic markers, some may have no differentiating features, even on MRS. Nonspecific MRS abnormalities are those that reflect brain destruction and reactive changes, including delayed maturation, neuronal loss, axonal degeneration, demyelination, and gliosis. In disorders with primary, or predominant, neuronal degeneration, there is loss of cell bodies and their projections (axons and dendrites) and myelin sheaths. Atrophy is the main pathologic result with minimal, or no, white matter changes or gliosis. The primary MRS abnormality in these disorders is a decrease in *N*-acetyl-aspartate (NA), which is proportional to the severity of atrophy but may be evident before atrophy is apparent. In disorders in which demyelination primarily, or predominantly, occurs there is loss of myelin sheaths with secondary axonal degeneration. Pathologically, there is loss of white matter and a reactive gliosis. Atrophy is usually not apparent unless the demyelination is severe and chronic. Active demyelination is characterized by elevated lipids and choline (Ch; increased membrane lipid turnover with increased myelin breakdown products), variable increases in lactate and glutamate/glutamine (Glx; active tissue degeneration and inflammation), and elevated inositols (gliosis). Associated neuronal damage is indicated by a decrease in NA.

More specific MRS abnormalities may be seen in a number of disorders. Abnormal MRS spectra have been reported with some of the lysosomal defects such as Niemann-Pick disease (abnormal lipid peak at 1.2 ppm), the mucopolysaccharidoses (decreased NA late), and metachromatic leukodystrophy (decreased NA, Ch, and creatine [Cr]; increased inositols and lactate). MRS abnormalities have been observed with a number of the peroxisomal disorders, including adrenoleukodystrophy (decreased NA with increased Ch, Glx, inositols, lipids, and lactate) and Zellweger syndrome (decreased NAs with increased lipids and Glx). Other leukodystrophies associated with observed MRS findings are Canavan disease (increased NA with decreased Ch and Cr plus increased inositols and lactate), Alexander disease (decreased NA with increased lactate), and Pelizaeus-Merzbacher disease (normal levels early; decreased NA and increased Ch late).

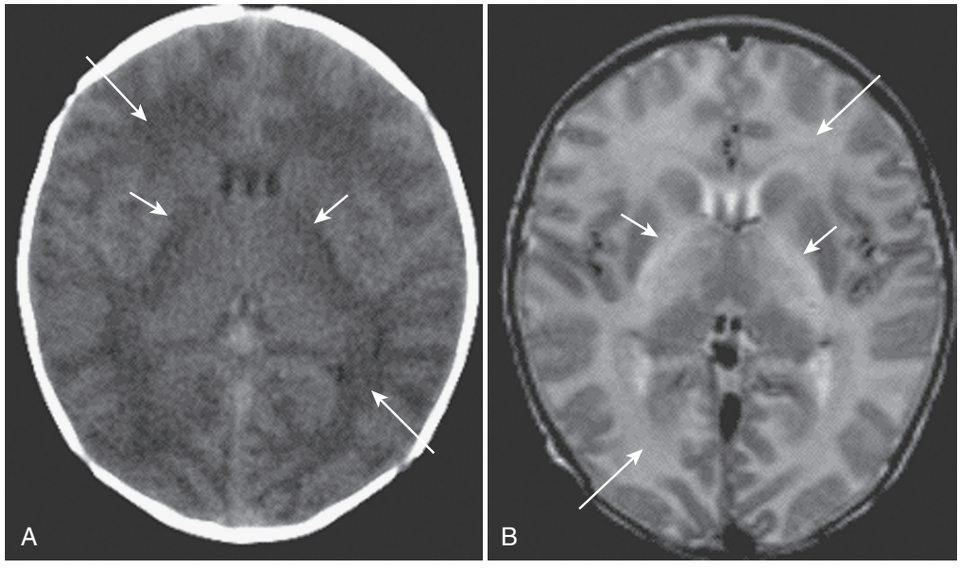

FIGURE 8-105. Maple syrup urine disease in neonate with edema of the globus pallidus (*short arrows*) and white matter (*long arrows*) on an axial CT scan (**A**) and an axial T2-weighted MR image (**B**).

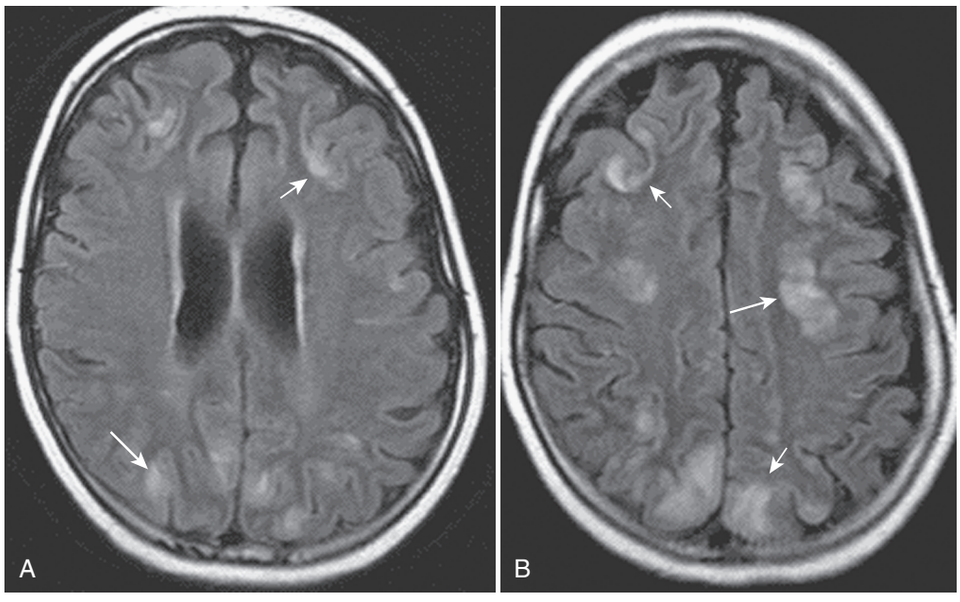

Figure 8-106. **A** and **B**, "Reversible" leukoencephaly (*long and short arrows*) on axial FLAIR MR images.

Disorders of energy metabolism have been associated with MRS findings of decreased NA and increased lactate, including mitochondrial disorders such as Leigh disease (see Fig. 8-97) and MELAS syndrome. Similar findings, however, are present with acute/subacute hypoxia-ischemia (plus elevated Glx, decreased Cr, and increased lipids). Aminoacidopathies with reportedly abnormal spectra include phenylketonuria (increased phenylalanine peak at 7.37 ppm), maple syrup urine disease (elevated leucine, isoleucine, and valine with abnormal peak at 0.9 ppm), and nonketotic hyperglycinemia (elevated glycine peak at 3.55 ppm). Other metabolic disorders associated with abnormal MRS findings include the creatine deficiencies (decrease or absence of Cr), hepatic encephalopathy (increased Glx with decreased inositols and Ch), and hyperosmolar states (increased inositols, Cr, and Ch).

Suggested Readings

Ball W Jr: Pediatric Neuroradiology. Philadelphia, Lippincott-Raven, 1997.
Barkovich A: Pediatric Neuroimaging, ed 4. Philadelphia, Lippincott-Raven, 2005.
Blaser SI, Illner A, Castillo M, et al: Peds Neuro: 100 Top Diagnoses. (Pocket Radiologist.). Philadelphia, WB Saunders, 2003.
Harwood-Nash D, Fitz CR: Neuroradiology in Infants and Children. St. Louis, Mosby-Year Book, 1976.
Kirks DR: Practical Pediatric Imaging, ed 3. Philadelphia, Lippincott-Raven, 1998.
Kuhn JP, Slovis TL, Caffey J, Haller JO: Caffey's Pediatric Diagnostic Imaging, ed 10. New York, Elsevier Mosby Saunders, 2003.
Levine D: Atlas of Fetal MRI. Boca Raton, FL, Taylor and Francis Group, 2005.
Swischuk LE: Imaging of the Newborn, Infant, and Young Child. ed 5. Philadelphia, Lippincott Williams & Wilkins, 2003.
Tortori-Donati P, Rossi A: Pediatric Neuroradiology. New York, Springer, 2005.
van der Knaap MS, Valk J: Magnetic Resonance of Myelination and Myelin Disorders. ed 3. New York, Springer, 2005.
Volpe JJ: Neurology of the Newborn, ed 4. Philadelphia, WB, Saunders, 2001.
Wolpert S, Barnes P: MRI in Pediatric Neuroradiology. St. Louis, Mosby-Year Book, 1992.
Zimmerman RA, Gibby WA, Carmody RF (eds): Neuroimaging: Clinical and Physical Principles, New York, Springer, 2000.

Articles and Monographs

Barkovich AJ, Naidich TP (eds): Pediatric Neuroradiology. Neuroimaging Clin North Am 1994;4(2).
Barnes PD (ed): Imaging of the Developing Brain. Top Magn Reson Imag 2007; 18(1).
Barnes PD, Krasnokutsky M: Imaging of the central nervous system in suspected or alleged nonaccidental injury, including the mimics. Top Magn Reson Imaging 2007;18:53-74.
Edwards-Brown MK, Barnes PD (eds): Pediatric Neuroradiology. Neuroimaging Clin North Am 1999;9(1).
Mukherjee P (ed): Advanced Pediatric Imaging. Neuroimaging Clin North Am 2006;16(1).
Mukherji SK (ed): Pediatric Head and Neck Imaging. Neuroimaging Clin North Am 2000;10(1).